



**DOCTORAL THESIS IN
BUSINESS, INTERNET, AND COMMUNICATION TECHNOLOGIES**

**IDENTIFICATION OF NOSEMA CELLS USING
MICROSCOPIC IMAGES**



PhD SOUMAYA DGHIM

SUPERVISOR CARLOS MANUEL TRAVIESO GONZÁLEZ

UNIVERSITY OF LAS PALMAS DE GRAN CANARIA

SPAIN

2023

Identification Of Nosema Cells Using Microscopic Images

Identification Of Nosema Cells Using Microscopic Images

CONTENTS

1 CHAPTER I: INTRODUCTION	1
1.1 MOTIVATION.....	1
1.2 STATE OF THE ART	3
1.2.1 <i>Nosema disease and its negative complications</i>	3
1.2.2 <i>Biological diagnosis of Nosema disease</i>	7
1.2.3 <i>Diagnosis of Nosema disease using technical and microscopic image analysis methods</i>	8
1.3 HYPOTHESIS	11
1.4 OBJECTIVE	11
1.5 METHODOLOGY	12
1.6 CONTRIBUTIONS AND RESULTS	14
1.7 STRUCTURE OF THE THESIS	15
2CHAPTER II : DATASET ANALYSIS AND SEGMENTATION OF MICROSCOPIC IMAGES	17
2.1 INTRODUCTION	17
2.2 EXTRACTION.....	17
2.2.1 <i>Problems with the used microscopic images</i>	17
2.2.1.1 Cantwell's method and related problems	18
2.2.1.2 Noise problem of microscopic images.....	20
2.2.2 <i>Building of dataset from sub-images extracted from microscopic images.</i> ..	21
2.2.3 <i>Automatic segmentation and features extraction: building of dataset with extracted features:</i>	23
2.2.3.1 Extracting the shape of the object.....	23
2.2.3.1.1 Classic edge extraction techniques	24
2.2.3.1.1.1 Gradient approach	24
2.2.3.1.1.2 Laplacian approach	26
2.2.3.1.1.3 Active edges	27
2.2.3.1.1.4 Binary mathematical morphology	27
2.2.3.1.2 Contour extraction using mathematical and binary morphology tools	27
2.2.3.1.2.1 Grayscale representation.....	28
2.2.3.1.2.2 Binarisation	28
2.2.3.1.2.3 Populating regions and holes in the image.....	29
2.2.3.1.2.4 Using the dilation method	29
2.2.3.1.2.5 Contour calculation.....	30
2.2.3.2 Automatic segmentation and Features extraction	31
2.2.3.2.1 Geometric features	31
2.2.3.2.2 Statistic Features.....	33
2.2.3.2.3 Automatic segmentation and feature extraction from the texture of the color image:	34

Identification Of Nosema Cells Using Microscopic Images

2.2.3.2.3.1 Extracting the characteristics of the color channels (six characteristics)	34
2.2.3.2.3.2 Feature extraction using the GLCM: (four characteristics).....	36
2.3 CONCLUSION	38
3 CHAPTER III: NOSEMA RECOGNITION	41
3.1 INTRODUCTION	41
3.2 ARTIFICIAL INTELLIGENCE, MACHINE LEARNING, AND DEEP LEARNING	42
3.3 PRINCIPLES OF CLASSIFICATION.....	46
3.3.1 Concepts	46
3.3.2 Supervised learning	47
3.4 USING OF ARTIFICIAL NEURAL NETWORKS AND SUPPORT VECTOR MACHINE FOR THE IDENTIFICATION PROBLEM.....	48
3.4.1 Identification using artificial neural network.....	48
3.4.1.1 Concepts	48
3.4.1.2 Activation functions.....	50
3.4.1.3 Multi-layers perceptron	51
3.4.1.4 Number of hidden layers.....	53
3.4.1.5 Radial Based Function	53
3.4.1.6 Experimental methodology for artificial neural networks.....	54
3.4.2 Identification using SVM	56
3.4.2.1 Concepts	56
3.4.2.2 Experimental methodology for SVM	59
3.5 USING OF DEEP LEARNING TOOLS.....	59
3.5.1 Concepts	59
3.5.2 Convolutional Neural Network.....	61
3.5.2.1 Concepts and history	61
3.5.2.2 Experimental methodology:.....	65
3.5.3 The use of Transfer learning architectures.....	66
3.5.3.1 Concepts	66
3.5.3.2 Transfer learning resolves deep learning problems.....	68
3.5.3.2.1 Using pre-trained models as feature extractors	68
3.5.3.2.2 Adjusting pre-trained models	69
3.5.3.3 Application of transfer learning in the real world	70
3.5.3.3.1 Fine-tuning AlexNet transfer learning model	71
3.5.3.3.1.1 Concepts.....	71
3.5.3.3.1.2 Experimental methodology for fine-tuned AlexNet model.....	73
3.5.3.3.2 Fine-tuning VGG16 and VGG19 transfer learning models.....	74
3.6 RECOGNITION RESULT	77
3.6.1. RESULTS OF CLASSIFICATION WITH ANN AND SVM: THE USE OF DS1	77
3.6.2. RESULTS OF CLASSIFICATION WITH CNN AND TRANSFER LEARNING: THE USE OF DS2	78
3.6.2.1. CNN result	78
3.6.2.2. Transfer learning results	80
3.6.2.2.1. Result for AlexNet.....	80

Identification Of Nosema Cells Using Microscopic Images

3.6.2.2.2. Results for VGG16 and VGG19	80
3.7 DISCUSSION	83
3.8 FINE-TUNED MODELS WITHOUT DATA AUGMENTATION	86
3.8.1 Methodology	86
3.8.2 Experiment results.....	89
3.9 FINE-TUNING VGG16 WITH DATA AUGMENTATION.....	90
3.10 CONCLUSION	96
4 CHAPTER IV: AUTOMATIC ALGORITHM FOR NOSEMA IDENTIFICATION & COUNTING.....	99
4.1 INTRODUCTION	99
4.2 THE AUTOMATIC ALGORITHM.....	99
4.2.1 Used libraries.....	101
4.2.2 Variables configuration	102
4.2.3 Load the pretrained model: VGG16	103
4.2.4 Pyramid Function.....	104
4.2.5 Sliding window function	105
4.2.6 Record Results	107
4.3 RESULTS AND DISCUSSION	107
4.3.1 Experimental results.....	107
4.3.2 Discussion	111
4.4 CONCLUSION	113
5 CHAPTER V: CONCLUSIONS.....	115
5.1 SYNTHESIS	115
5.2 FUTURE WORKS	116
6 BIBLIOGRAPHY	117
7 RESUMEN EN ESPAÑOL.....	129

LIST OF FIGURES

Figure 1.1 <i>Apis Ceranae</i> (A), and <i>Apis Mellifera</i> (B)	3
Figure 1.2 Honeybee colony collapsed by <i>Nosema Ceranae</i> (Higes, Meana, Bortolomé, Botias & Martín, 2013)	4
Figure 1.3 Example of sampling zones in Spain: Castilla-La Mancha (Buendia & al., 2018).....	5
Figure 1.4 Sampling <i>Nosema</i> disease in several ecoregions of north Asia (Ostroverkhova, Konusova, Kucher, Kireeva, & Rosseykina, 2020).....	6
Figure 1.5 Detailed views of ventricular epithelial cells parasitized at 7 days p.i. at 33°C. <i>N. apis</i> -infected cells (A) displayed similar quantities of immature and mature stages (red), while <i>N. ceranae</i> -infected cells (B) exhibited a higher proportion of immature stages (Pink) at this time (Martín & al., 2009)	9
Figure 1.6 An example of used microscopic images from every infection level: from (a) to (d): very mild, mild, moderate, semi-strong, and strong	13
Figure 2.1 Blocks used for spores counting in a hemocytometer.....	18
Figure 2.2 Actual image of the hemocytometer used in capturing of microscopic images.	19
Figure 2.3 A microscopic image with the red color of the Counting Grid.	19
Figure 2.4 Example of cells overlapping the counting grid	20
Figure 2.5 Example of the change in cell shape during the preprocessing phase.....	20
Figure 2.6 Image obtained by the microscope: (A) a whole image and (B) a part of the image that shows the existing noise.	21
Figure 2.7 Example of spores hidden behind or superimposed on other objects: <i>Nosema</i> spores in the red circle.....	21
Figure 2.8 Instance of dataset extraction of <i>Nosema</i> cells and other existing objects in the microscopic images.	22
Figure 2.9 Construction of the image dataset contains both types of objects <i>Nosema</i> (N) and none <i>Nosema</i> (n-N).....	23
Figure 2.10: Gradient of a given point belonging to a given boundary	24
Figure 2.11 Calculating a gradient with multiple filters.....	25
Figure 2.12 Contour search with the Laplacian.....	26
Figure 2.13 Approved approach to detect the shape (border) of an object.	28
Figure 2.14 Steps to Remove Unwanted Objects	29
Figure 2.15: Used Matrix for dilation	30
Figure 2.16 Edge Detection	30
Figure 2.17 The preprocessing steps for automatic contour extraction: (a) RGB image, (b) gray image, (c) binarization and hole filling, (d) dilation, and (e) contour extraction	31

Identification Of Nosema Cells Using Microscopic Images

Figure 2.18 Histograms describing the distribution of distances that flow from an object's centroid to each pixel of its shape in both cases Nosema and non-Nosema object for two examples of each type: this shows the large difference between the two types.....	33
Figure 2.19 Extracting an object from its background.....	35
Figure 2.20 used images for entropy measurements for both Nosema cell and non-Nosema cell: (a) extracted RGB object, (b) Red mask, (c) Green Mask, (d) Blue Mask, (e) yellow mask, (f) hue channel, and (g) saturation channel.	36
Figure 2.21 DS2 Features Dataset stored files.	39
Figure 3.1 The Implemented Methodology for Identification.....	42
Figure 3.2 A Venn diagram showing how deep learning is a kind of representational learning, which is in turn a kind of machine learning, used for many, but not all, approaches to artificial intelligence	43
Figure 3.3 For a given learning problem, an object $o \in O$ representative of this problem is described by a vector of attributes $x \in X$ and is identified by the oracle o as a class $y \in Y$. In this diagram, f_d and f_o represent respectively the procedure performing the description of an object o and the decision-making process of the oracle o . The learner's objective is to choose a hypothesis $f \in H$ whose predictions are as close as possible to the oracle.....	47
Figure 3.4 Artificial neuron.....	49
Figure 3.5 Different neural network topologies. (a) multilayer networks, (b) local connections, (c) with recurring connections, and (d) full connections	50
Figure 3.6 Multi-Layer Perceptron with a Single Hidden	52
Figure 3.7 Implemented ANN for Nosema recognition.....	56
Figure 3.8 Basic principle of SVM (Russell & Norvig, 2011). (a) nonlinearly separable problem, the equation of the separator plane is $x_1^2 + x_2^2 \leq 1$ (7); (b) projection of the data in a three-dimensional space ($x_1^2, x_2^2, \sqrt{2x_1} x_2$) (3.12).....	57
Figure 3.9 Notion of maximum margin, for a set of linearly separable points, there are an infinite number of separator hyperplanes; the optimal hyperplane (in yellow) with the maximum margin, the surrounded samples represent the supporting vectors.....	58
Figure 3.10 A diagram of the convolutional neural network. (The depth of the matrices represents the number of used filters. The size of the output vector is determined after flattening the matrices of the previous layer and concatenating the resulting vectors.	62
Figure 3.11 A conceptual diagram of the convolutional neural network using three filters.....	63
Figure 3.12 Implemented CNN for Nosema Recognition	65
Figure 3.13 Traditional approach vs. Transfer learning approach.....	67
Figure 3.14 Deep transfer learning approach	69
Figure 3.15 AlexNet Architecture	72
Figure 3.16 Fine-tuned AlexNet Model for DS1 images classification	73
Figure 3.17 VGG16 Architecture.....	75

Identification Of Nosema Cells Using Microscopic Images

Figure 3.18 The Fine-Tuned VGG16 Model for Nosema Recognition.....	76
Figure 3.19 The Fine-Tuned VGG19 Model for Nosema Recognition.....	76
Figure 3.20 Best result accuracy given by the implemented ANN	78
Figure 3.21 Example of the output of the first layer	79
Figure 3.22 Best simulation results for VGG16 (a) and VGG19 (b): 70% of data for training and 30% of data for validation with 6 epochs.	81
Figure 3.23 Best simulation result of VGG16 (a) and VGG19 (b): for 80% for training and 20% for validation and with 20 epochs for VGG16 and 25 epochs for VGG19.	81
Figure 3.24 Best simulation result of VGG16 (a) and VGG19 (b): for 90% for training and 10% for validation, with 6 epochs for VGG16 and 30 epochs for VGG19.....	82
Figure 3.25 Best succès accuracy (96.25%) given by VGG16 fine-tuned model.....	83
Figure 3.26 Pipeline of fine-tuned models.....	87
Figure 3.27 Prepared Input Images for fine-tuned models	88
Figure 3.28 9 first augmented images with 30-degree rotation.....	92
Figure 3.29 Experiment setting for VGG16	92
Figure 3.30 Accuracy and loss models for best precision given with 2-fold cross validation strategy.....	93
Figure 3.31 Confusion matrix for best accuracy (99.70%) given by VGG16 with Augmentation Data.	94
Figure 3.32 The increment of VGG16 precision accuracy from the first to the last experiment.....	95
Figure 3.33 An example of a misclassified Nosema image	96
Figure 4.1 Pipeline of the proposed algorithm for the automatic detection.	100
Figure 4.2 Used libraries.....	101
Figure 4.3 Sliding window in green color moving through the microscopic image	106
Figure 4.4 Sliding window Details	106
Figure 4.5 Record results description	107
Figure 4.6 Detection and counting results on an input image of mild level	108
Figure 4.7 Detection and result on an input image of moderate level	108
Figure 4.8 Detection and counting result on an input image of semi-strong level.....	108
Figure 4.9 Detection and counting result on an input image of strong level.....	109

LIST OF TABLES

Table 3-1: Some common transfer functions, x is the input vector.....	49
Table 3-2: Experiments for Nosema recognition using a vector of 15 features/19 features: the initial number of neurons in the hidden layer is 15/19 equals to the number of features and the final number is 1800 equal to the maximum number of training data	55
Table 3-3: CNN experiment Values for an 80×80 input image.....	66
Table 3-4: Experimental setting for retrained AlexNet model	74
Table 3-5: Experiment for VGG16 and VGG19 fine-tuned models.....	77
Table 3-6: Best recognition results given by ANN and SVM.....	77
Table 3-7: Best classifications results for AlexNet fine-tuned classifier	80
Table 3-8: Best classifications results for VGG16 and VGG19 fine-tuned classifiers	80
Table 3-9: Comparison of proposed method with existed method in the literature using different image processing tools (%)	83
Table 3-10: Experiment results for fine-tuned models with 50 epochs.....	89
Table 3-11: Experiment results of fine-tuned models with 100 epochs	90
Table 3-12: Experiment results for fine-tuned VGG16 model with Augmentation Data	93
Table 3-13: Comparison between proposed methods	95
Table 4-1: Experiment results for the Automatic Algorithm	109
Table 4-2: Performance of the automatic algorithm in predicting infection level.....	110
Table 4-3: Comparison of the automatic Algorithm with previous works in the literature (%).....	112

LIST OF ACRONYMS AND ABBREVIATIONS

ML	MACHINE LEARNING
DL	DEEP LEARNING
AD	AUGMENTATION DATA
N. APIS	NOSEMA APIS
N. CERANAE	NOSEMA CERANAE
HDS	HIVE DEPOPULATION SYNDROM
A. CERANAE	APIS CERANAE
A. MELLIFERA	APIS MELLIFERA
PCR	POLYMERASE CHAIN REACTION
DNA	DEOXYRIBONUCLEIC ACID
RT PCR	RELATIVE POLYMERASE CHAIN REACTION APPROACH
CCD	COLONY COLLAPSE DISORDER
ANN	ARTIFICIAL NEURAL NETWORK
SVM	SUPPORT VECTOR MACHINE
CNN	CONVOLUTIONAL NEURAL NETWORK
CINAT	CENTRO DE INVESTIGACIÓN NACIONAL DE APICULTURA TROPICAL
DS1	DATASET 1
DS2	DATASET 2
NN	NEURAL NETWORK
MLP-BP	MULTI-LAYER PERCEPTRON TRAINED BY BACK PROPAGATION ALGORITHM

Identification Of Nosema Cells Using Microscopic Images

ROI	REGION OF INTEREST
GPU	GRAPHICS PROCESSING UNITS
CPUS	CENTRAL PROCESSING UNITS
RGB	RED-GREEN-BLUE
AI	ARTIFICIAL INTELLIGENCE
GLCM	GREY LEVEL COOCCURRENCE MATRIX
GPU	GRAPHICS PROCESSING UNIT
ASM	ANGULAR SECOND MOMENT
DNN	DEEP NEURAL NETWORK
MLPS	MULTI-LAYER PERCEPTRONS
RBF	RADIAL BASIS FUNCTION
FNNS	FUZZY NEURAL NETWORKS
RELU	RECTIFIED LINEAR UNIT
HMM	HIDDEN MARKOV MODEL
MSE	MEAN SQUARED ERROR
PK	POLYNOMIAL KERNEL
RBFK	RADIAL BASIS FUNCTION KERNEL
IDL	INSTITUTE OF DEEP LEARNING
TDNN	TIME DELAY NEURAL NETWORK
NLP	NATURAL LANGUAGE PROCESSING
FCN	FULLY CONNECTED LAYER
FFT	FAST FOURRIER TRANSFER
POS TAGER	POST OF-SPEECH TAGGER

ABSTRACT

Research in the field of computer vision and intelligent systems has become increasingly vast and extensive to meet the needs and conditions of all users. Additionally, new machine learning architectures have shown profound results and made the interpretation and analysis of media more robust and efficient. The robustness and efficiency of these new architectures, coupled with technology development, have made a new area of application and opened the door for new research more beneficial for the end-user. Indeed, in the field of biology, microscopic image analysis has led to an important evolution in terms of the creation of new diagnostic support systems. The purpose of the latter is to provide practitioners with an automatic interpretation of microscopic images to allow an exploitation of the cells of such a studied disease.

Different segmentation approaches have been proposed in the literature, but a method has yet to be deemed optimal for only a specific application. Therefore, it can be admitted that there is no universal method for segmentation; rather it depends on the type of knowledge sought. This thesis is articulated around the axis of segmentation methods, highlighting the crucial dependence on the specific type of knowledge being sought. The main objective of this work is to propose methods and algorithms to help recognize the cells of Nosema disease in microscopic images and make the diagnosis. These methods are very helpful in many fields and present an important pre-work for many applications. To achieve the objectives outlined in this thesis, various approaches such as: Machine Learning (ML), Deep Learning (DL, the newest and most efficient algorithm in machine learning techniques), and Augmentation Data (AD) are implemented and explored. As such, in this thesis, image processing tools will be used to calculate interesting features of Noema cells, and computer vision techniques, ML, DL, and AD techniques will be employed to recognize them. Finally, an automatic algorithm for cell identification and counting will be implemented. The automated system performs well in the diagnosis task, demonstrating high accuracy across four Nosema infection levels.

Resumen

La investigación en el campo de la visión informática y los sistemas inteligentes se ha vuelto cada vez más amplia y extensa para satisfacer las necesidades y las condiciones de todos los usuarios. Además, las nuevas arquitecturas de aprendizaje automático han mostrado resultados profundos y han hecho la interpretación y el análisis de los medios más robustos y eficientes. La robustez y la eficiencia de estas nuevas arquitecturas, junto con el desarrollo tecnológico, se han convertido en una nueva esfera de aplicación y han abierto la puerta a nuevas investigaciones más beneficiosas para el usuario final. De hecho, en el campo de la biología, el análisis de imágenes microscópicas ha conducido a una importante evolución en términos de la creación de nuevos sistemas de apoyo diagnóstico. El propósito de este último es proporcionar a los profesionales una interpretación automática de imágenes microscópicas para permitir una explotación de las células de una enfermedad estudiada. En la literatura se han propuesto diferentes enfoques de segmentación, pero ningún método ha sido considerado óptimo para una aplicación específica. Por lo tanto, se puede admitir que no existe un método universal para la segmentación; más bien, depende del tipo de conocimiento buscado. Esta tesis se articula en torno al eje de los métodos de segmentación, destacando la dependencia crucial sobre el tipo específico de conocimiento que se busca. El objetivo principal de este trabajo es proponer métodos y algoritmos para ayudar a reconocer las células de la enfermedad de Nosema en imágenes microscópicas y hacer el diagnóstico. Estos métodos son muy útiles en muchos campos y presentan un importante trabajo previo para muchas aplicaciones. Para alcanzar los objetivos establecidos en esta tesis, se implementarán y explorarán Aprendizaje Automático (AA), Aprendizaje Profundo (AP) (el algoritmo más nuevo y eficiente en técnicas de aprendizaje automático) y Aumento de Datos (AD). Como tal, en esta tesis, se utilizarán herramientas de procesamiento de imágenes para calcular características interesantes de las células de Noema, y se emplearán técnicas de visión por ordenador, y técnicas de AA, AP y AD para reconocerlas. Por último, se implementará un algoritmo automático para la identificación y el conteo de células. El

Identification Of Nosema Cells Using Microscopic Images

sistema automatizado se desempeña bien en la tarea de diagnóstico, demostrando una alta precisión en cuatro niveles de infección de Nosema.

Acknowledgments

I would like to express my sincere gratitude to my thesis advisor, Carlos Manuel Travieso-González, for his invaluable guidance and unwavering support throughout my PhD journey. His expertise and mentorship have been instrumental in shaping this research. I extend my heartfelt thanks to my thesis committee members.

I would also like to thank Prof. Mourad Zaied, full Professor at Gabès Engineering School and head of the RTIM -Lab, Department of Electronic Engineering, University of Gabès, Tunisia, for accepting me as a trainee in his laboratory, as well as for his high availability, constructive precision, dedication, and for their helpful comments.

Special thanks to Jaime Roberto Ticay Rivas and Alejandro Pian Roescher, engineers from the University Institute for Technological Development and Innovation in Communications (IDeTIC), for their assistance and support with the software used in this thesis. They were always eager to share their expertise and experience with me.

Also, I would like to express my profound gratitude to Maria Cristina Carmona Duarte, Associate Professor at ULPG and a valued IDeTIC member, for her unwavering encouragement and support throughout this journey.

A heartfelt thank you to Dr. Walid Bouamra, a doctor in Business, Internet, and Communications Technologies from the University of Las Palmas. Assistant Professor in Computer Science at the University of Tebessa, Algeria, his constant encouragement and insights have been invaluable to my endeavors.

I would like to express my heartfelt gratitude to Marcos del Pazo Banos, a senior lecturer at Swansea University's medical school; Tobias Kutzner, an academic staff member from the Economics, Computer Science, and Law (WIR), TH Wildau, Germany; Walid Bouamra, a doctor in Business, Internet, and Communications Technologies from the University of Las Palmas and Assistant Professor in Computer Science at the University of Tebessa, Algeria; and finally, Soufiane Boudabous, Assistant Professor at Hassiba Ben Bouali University, Algeria, for spending their valuable time reading my thesis and supporting it.

Identification Of Nosema Cells Using Microscopic Images

I want to express my deepest thanks to my husband, Fekri Laatar, doctor of polymer chemistry at the University of Tunis, Tunisia, the hours spent reviewing the manuscript, for his flawless support and listening, his fresh and sincere gratitude, and his great patience.

Finally, I want to thank my parents, Samira and Dghim, my brother Nejib, and my sisters for their continuous support and understanding throughout this difficult road. Their love and support kept me going through the ups and downs of this venture. I am grateful for their assistance; this work is dedicated to them and my two children.

1 Chapter I: Introduction

1.1 Motivation

In microbiological studies focused on diseases, researchers frequently employ direct observation methods to gain a deeper understanding of the behaviors exhibited by diseased microorganisms or cells within specific conditions. This observation can take place at different scales, offering insights into the characteristics and dynamics of the microbial entities under investigation. At the level of a colony, researchers often engage in counting procedures. This involves quantifying the number of microorganisms present within a collective group, providing a macroscopic view of their population and distribution. Colony-level observation is particularly useful for assessing overall health, growth patterns, and interactions among microorganisms.

Conversely, observation at the cellular level involves scrutinizing individual microorganisms or cells. This finer-scale approach aims to unravel intricate details about the morphology and structure of individual entities. Researchers focus on parameters such as the shape, size, and texture of cells, seeking to discern patterns or irregularities that could be indicative of specific characteristics or behaviors.

In the case of Nosema, it is a disease known to cause degeneration of the digestive tissue in honeybees, leading to acute starvation and, consequently, early mortality. This degeneration can also affect the flying behavior of bees, resulting in a reduced population of bees (Eiri, Suwannapong, Endler, & Neih, 2015). The impact of Nosema extends beyond the bees themselves; it has adverse effects on plant species diversity and crop productivity. This, in turn, leads to pollination shortages and substantial economic losses in honey production (Gisder, Schuler, Horchler, Groth, & Genersch, 2017), impacting both honey production and pollination efficiency.

The motivation behind undertaking this thesis is rooted in the recognition of significant deficiencies and losses stemming from the impact of infectious illnesses on food-producing animals, particularly bees. The identified deficiencies and losses serve as a driving force for the research conducted herein. Pollination is a fundamental ecological process that facilitates the reproduction of flowering plants, contributing to biodiversity

Identification Of Nosema Cells Using Microscopic Images

and overall ecosystem health. The potential consequences of a breakdown in the pollination process extend beyond the immediate impact on bees. If effective diagnostic measures are not in place to identify and combat infectious illnesses in bees, crucial actions to treat the affected bees and hives may not be implemented. This failure in diagnosis and subsequent treatment has the potential to exacerbate the spread of lethal diseases among bee populations. The repercussions of such a scenario could be severe, not only for the bees themselves but also for the broader ecosystem, agriculture, and food production systems that rely on the pollination services provided by these vital pollinators.

In summary, the study of Nosema is crucial not only for understanding the health of honeybee colonies but also for assessing its broader ecological and economic ramifications, including effects on plant species, crop productivity, and the pollination ecosystem.

In essence, this thesis seeks to address these critical issues by contributing to the development of effective diagnostic tools and strategies for combating infectious diseases in bees. By doing so, it aims to mitigate the potential losses and deficiencies in pollination processes, safeguarding the health of ecosystems and the essential role played by pollinators in sustaining biodiversity and food production. Furthermore, in earlier research endeavors, there has been a notable gap in effectively addressing this disease from a technological perspective. To address this deficiency, the present thesis aims to leverage a comprehensive set of tools in microscopic image processing alongside advanced machine learning methods. The intention is to enhance the identification of this disease through the application of robust and innovative technological approaches.

This thesis introduces a novel automatic algorithm designed to detect and count Nosema cells within microscopic images. The primary objective is to identify and quantify these cells to assess the level of infection, thereby providing valuable support for diagnosing the associated disease.

Identification Of Nosema Cells Using Microscopic Images

1.2 State of the art

1.2.1 Nosema disease and its negative complications

Two species of the genus *Apis* (the true honeybees) have long attracted man's special attention. These are the European honeybee, *Apis Mellifera* (Figure 1. 1, A), and the physically smaller but very similar Asian honeybee, *Apis Ceranae* (Figure 1.1, B). These species have been of particular interest to man because they produce large amounts of honey and can be kept as “domesticated animals” in movable nests or hives. Throughout the past centuries, the European honeybee has been transported all over the world and widely distributed. The Asian honeybee, however, is restricted only to Southeast Asia, China, eastern Russia, and Japan. Due to this restriction, *Apis Ceranae* is to some extent being actively replaced by *A. Mellifera*. Honeybees are well studied insects. Many detailed descriptions of the honeybee’s biology can be found in literature, such as (Seely, 1995) and (Winston, 1987).

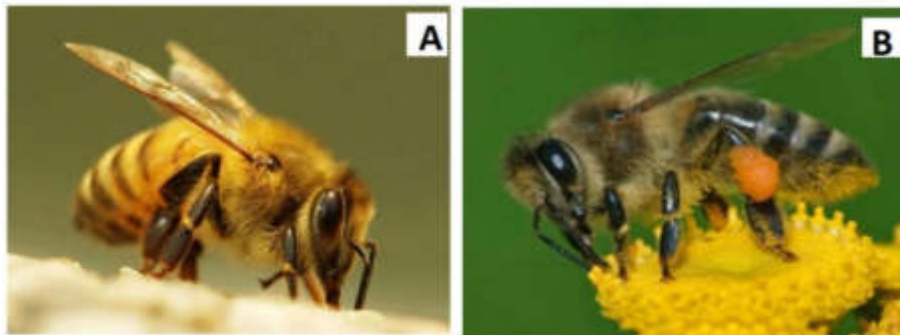


Figure 1.1 *Apis Ceranae* (A), and *Apis Mellifera*(B)

Apis Mellifera and *Apis Ceranae* (figure 1.1), the European and Asian honeybees, support biodiversity and are also of considerable agricultural relevance. These bee species have been the topic of several recent research because they are critical pollinators of human-maintained crops. According to the research of (Klein et al, 2006), honeybees account for 90% of commercial pollination. Originally introduced by Europeans for crop management, many honeybees are now kept in heavily farmed areas. As a result, honeybee health is inextricably tied to agricultural success and sustainability. Pathogenic research is being prioritized to preserve the health of the honeybee.

Despite new breakthroughs, populations are dropping all around the world, from France to the United States. If the current population reduction continues, many agriculturally

Identification Of Nosema Cells Using Microscopic Images

developed countries may face a large-scale environmental problem. If not addressed appropriately, such a calamity will exacerbate the world's food crisis. Researchers have been working hard on uncovering because honeybee colonies are dying all around the world, thanks to donations from agriculturally based economies and huge environmental corporations. *Hive depopulation syndrome (HDS)*

The depopulation syndrome is characterized by the decrease in the number of bees in a colony, without apparent cause. In depopulation, the surviving bees cannot maintain the basic tasks of the colony, causing it to collapse and disappear without presenting any symptoms that allow one to pinpoint the origin of the problem (see Figure1.2)



Figure 1.2 Honeybee colony collapsed by *Nosema Ceranae* (Higes, Meana, Bortolomé, Botías & Martín, 2013)

Honeybee colonies collapse due to various causes, including a lack of resources, predation, sickness, and environmental variables. Changes in nest temperature, for example, disrupt brood rearing circumstances, which has the potential to reduce organism count and biodiversity within a colony (Klein et al, 2006). Any of the aforementioned loads might be critical in promoting catastrophic hive collapse. The detection and understanding of the fungal diseases *Nosema Ceranae* and *Nosema Apis* is one area of focus for halting the tremendous loss of world honeybee populations. Pathogenic elements are a health risk for every colony, and infection of tiny organisms can cause sickness inside the hive.

The so-called hive depopulation syndrome is not a new phenomenon. It was detected in Spain, in the late 90's and early 2000, although with a lower diffusion than the current one. There are several possible causes of depopulation, which were investigated until

Identification Of Nosema Cells Using Microscopic Images

the real cause was found. Such possible reasons ranged from a depopulation hypothesis due to the treatment of sunflower seeds with insecticides to parasitic diseases of bees (Matt, Wall, & Zamir, 2014). The latter will be the real cause and the object of our interest. (See Figure1.3 and Figure 1.4)

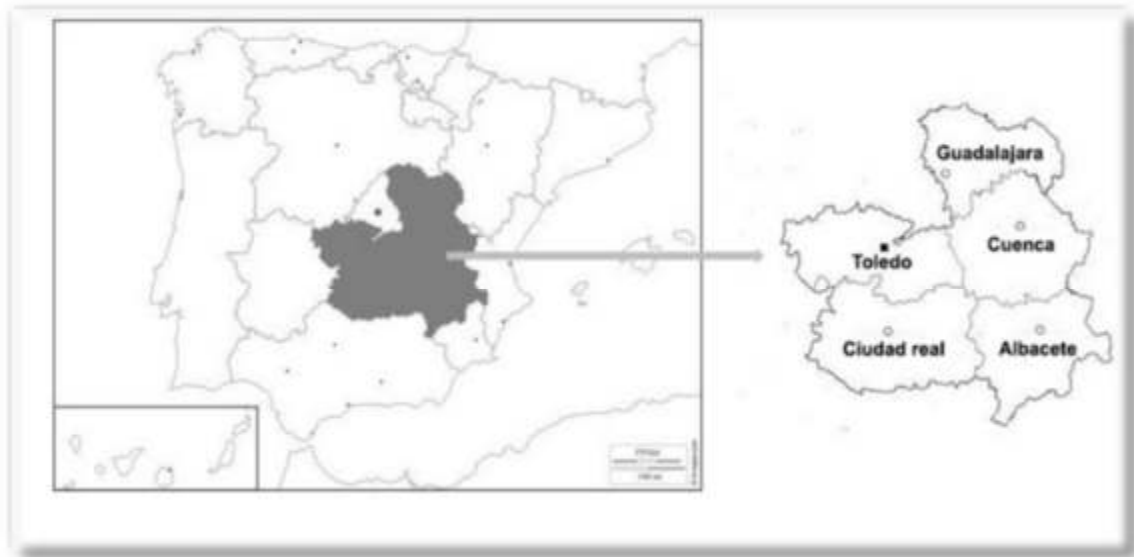


Figure 1.3 Example of sampling zones in Spain: Castilla-La Mancha (Buendia & al., 2018)

Identification Of Nosema Cells Using Microscopic Images

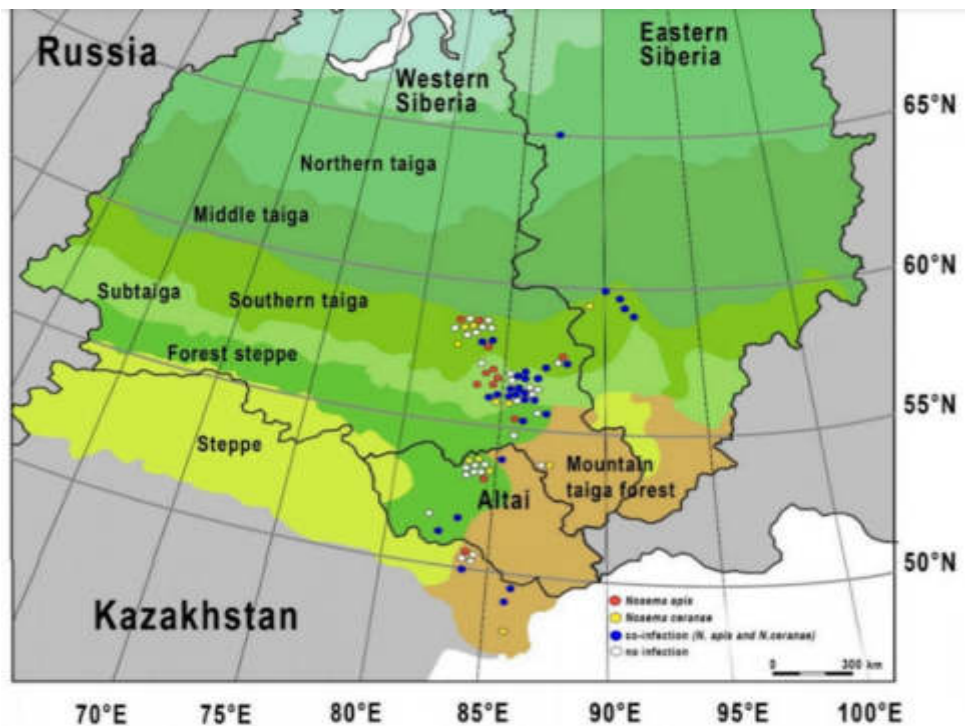


Figure 1.4 Sampling *Nosema* disease in several ecoregions of north Asia (Ostroverkhova, Konusova, Kucher, Kireeva, & Rosseykina, 2020)

Nosemosis, a degenerative gut illness, is caused by the microsporidia *Nosema ceranae* and *Nosema Apis*. Nosemosis is a disease that causes organism death, which can result in fast colony loss. Both parasitic and fungal research is quite recent and innovative. One of these fungi, *Nosema ceranae*, is thought to be more dangerous than *N. Apis* with important agricultural value. The transfer of its pathogenicity from its native host, *A. Ceranae*, to *A. Mellifera*, however, poses a difficult scenario for infectious disease prevention. The dual infection of *Nosema ceranae* in different bee species could potentially lead to colony collapse on a global scale if it continues to spread rapidly across all bee populations. Of particular concern is the European bee species, *A. mellifera*, which is widely used in commercial agriculture. If *Nosema ceranae* becomes more generalized and infects *A. mellifera* extensively, it could result in millions of dollars lost in the agricultural industry. There are few treatments for combating parasitic fungus, although approaches are constantly developing. To effectively protect bee populations, a thorough examination of these parasitic species is required. Understanding their behavior and developing effective control measures is crucial for the conservation of bee populations worldwide.

Identification Of Nosema Cells Using Microscopic Images

Several works on the impact of Nosema disease on commerce, society, and food have been published, as shown in (Sinpo, Paseton, Disayathanoowat, Krongdang, & Chantawannakul, 2018) and (Paneka & al., 2018), and the disease is now of major economic importance globally (Calderón & Ramirez, 2010). Biologists are particularly interested in the health of the two kinds of bees, not only because of their importance in the economy and food production, but also because of the critical function they play in pollinating agricultural and horticultural crops.

1.2.2 Biological diagnosis of Nosema disease

Detecting spores of Nosema spp. using microscopic analysis has historically been used to diagnose Nosema's illness (Slimanuki & Kanox, 2000).

However, given the recent discovery that both Nosema Ceranae and Nosema Apis harm western honeybees (*Apis mellifera*), genetic approaches are needed to distinguish between two various types of microsporidia. This is important since the spores of the two Nosema species cannot be consistently recognized based only on their shape (Fries, Hernandez, Meana, Plencia, & Higes, 2006). Furthermore, microscopic investigations are not as sensitive as molecular approaches, such as PCR, at detecting low levels of Nosema infection.

There are several biological descriptions of its DNA and behavior in the literature, including (Higes, Hernández, Bailón, Palencia, & Meana, 2008) and (Higes, Martn, & Meana, 2010).

Furthermore, microscopic inspection of Nosema spores is not only expensive, but also time-consuming and difficult. Previously, the first molecular approaches used to distinguish Nosema spp. required PCR followed by sequencing like in (Higes, Martn, & Meana, 2006) and (Chen, Evans, Smith, & Pettis, 2008) or the use of restriction analysis of PCR products like in (Klein & al., 2006). Although effective, some approaches require extra steps beyond simple amplification.

In (Martín et al., 2007), a simplified approach for identifying *N. Apis* and *N. Ceranae* was established. They developed a duplex PCR-based approach for amplifying the 16S rRNA sections of *N. Apis* or *N. Ceranae* in a single reaction with two sets of primers, allowing them to identify both microsporidians in tandem.

Identification Of Nosema Cells Using Microscopic Images

More recently, a real-time duplex PCR assay that amplified the same 16S rRNA regions as *N. Apis* and *N. Ceranae* in a single reaction was devised (Bourgeois, Renderer, Beaman, & Danka, 2010).

Real-time PCR thermocyclers and techniques, on the other hand, are not widely accessible in many laboratories and are more expensive than normal PCR thermocyclers and procedures. As a result, an enhanced multiplex-PCR approach is used to differentiate and quantify *Nosema* spp. in honeybees in a single reaction. This method combines Martin-Hernández et al.'s (Martn & al., 2007) duplex PCR-based method with the relative RT-PCR strategy (Dean, Goodwin, & Hasiang, 2002), which incorporates a house-keeping gene of the host in each reaction for relative quantification based on PCR band intensity. Using a conventional PCR thermocycler, this semiquantitative approach may assess *Nosema* infection levels.

A new DNA extraction procedure was also used to improve the amount of DNA retrieved from honeybee samples. The newly enhanced approach offers significant advantages over previously reported conventional PCR-based tests, as demonstrated in this work. Indeed, this novel technology allows for the detection and quantification of *Nosema* spores in honeybee samples. A multiplex PCR test will be used to diagnose and quantify *Nosema* infections in honeybees (*Apis Mellifera*) using the approach described in (Bailey & Ball, 1991). The precise identification of the microsporidia species, namely *Nosema apis* and *Nosema ceranae*, holds paramount importance in both comprehending and managing *Nosema* disease within honeybee (*Apis mellifera*) populations.

1.2.3 Diagnosis of *Nosema* disease using technical and microscopic image analysis methods

Diagnosing parasitic diseases in bees continues to rely on traditional microscopic analysis methods. However, studies focusing on the life history detection phase of microsporidia *N. Apis* and *Ceranae* (Martín & al., 2009) employ image processing techniques. These techniques are utilized to monitor temperature variations, which are then analyzed to determine potential temperature-dependent influences on the life cycle (refer to Figure 1.5).

Identification Of Nosema Cells Using Microscopic Images

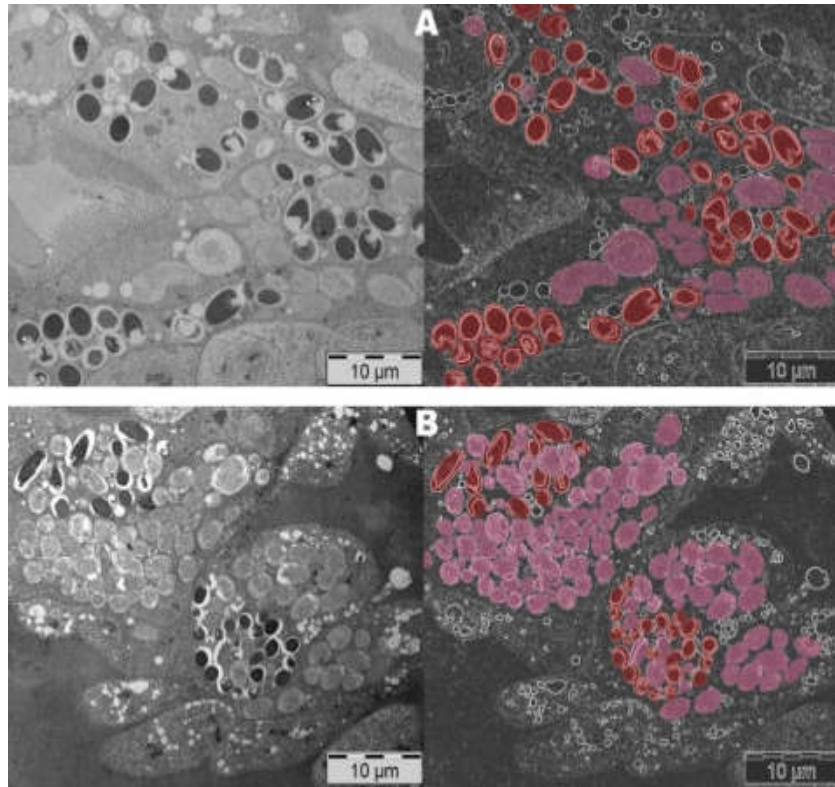


Figure 1.5 Detailed views of ventricular epithelial cells parasitized at 7 days p.i. at 33°C. *N. apis*-infected cells (A) displayed similar quantities of immature and mature stages (red), while *N. ceranae*-infected cells (B) exhibited a higher proportion of immature stages (Pink) at this time (Martín & al., 2009)

Furthermore, numerous recent studies, like (Suannapong, Maksong, Phainchajoen, Benbow, & Mayack, 2008) and (Mura & al., 2020), attempt to cure this condition by chemical modeling.

In addition, honeybees are important in computer science. Several efforts have included observing bees and manipulating their behavior. For example, (Tu, Hansen, Kryger, & Ahrendt, 2016) observed bee behavior to assist beekeepers in managing their honey colonies. The key finding of this study was the identification of bee disruption induced by a disease, Colony Collapse Disorder (CCD), or colony health assessment.

Similarly, numerous image analysis approaches were investigated in (Giuffre, Lubkin, & Tarpy, 2017) to research honeybee auto grooming behavior. Chemical and gas sensors were employed to collect data. To identify illness, Destructor infestations were introduced into the honeybee colony.

Identification Of Nosema Cells Using Microscopic Images

In (Szczurek, Maciejewska, Bak, Wilde, & Siuda, 2019), during a 12-hour experiment, the researchers measured the environment of six beehives using six different types of solid-state gas sensors.

There are now numerous notable pieces of research accessible in image processing relating to the study of Nosema's illness.

The Scale Invariant Feature Transform was used to extract features from cell pictures in (Alvarez-Ramos, Nio, & Santos, 2013). Image data is converted into scale-invariant coordinates with respect to local features using this approach. On the obtained microscopic pictures, a segmentation approach and a support vector machine algorithm were used to perform automatic categorization of *N. Apis* and *N. Ceranae* microsporidia.

In (Patricio-Nicolas, Mauro-German, Sergio-Damián, Paola-Verónica, & Hector-Luis, 2016), the authors used the Open CV library to do the identification of Nosema cells in microscopic images. To achieve the task of identifying the contours of each spore, we utilized the `findContours` function from the OpenCV library, as described in the ("Structural Analysis and Shape Descriptors OpenCV 2.4.13.0 documentation," n.d.-b). This function made use of the Suzuki algorithm. As the Nosema cells exhibit an elliptical form, we employed the `fitEllipse` function, also detailed in the ("Structural Analysis and Shape Descriptors OpenCV 2.4.13.0 documentation," nd-a) to implement Fitzgibbon's ellipse detection algorithm. Finally, considering the shape elliptical measurements in a range of approximately $5-7\mu\text{m} \times 3-4\mu\text{m}$, it was assumed that any preselected elliptical shape with width and length measurements of the ellipse within the mentioned range, would correspond to a Nosema spore.

In (Prendas-Rojas, Figueroa-Mata, Ramírez-Montero, Calderón-Fallas, Ramírez-Bogantes, & Travieso-González, 2018), the authors implement an automatic infection diagnosis system. Image processing tools were employed to effectively segment the images and compute the three most significant descriptors of Nosema spores: size, eccentricity, and circularity. Once the Nosema cells were characterized within the microscopic images, the researchers proceeded to quantify the spores and ascertain the extent of infection. The accuracy of success of the system has been considered high (84%).

Identification Of Nosema Cells Using Microscopic Images

The authors of (Dghim, Travieso-Gonzales, Dutta, & Hernández, 2020) employed image processing approaches to extract the most valuable information from Nosema microscopic pictures. Following that, they used an Artificial Neural Network (ANN) for recognition, which was statistically evaluated using the cross-validation approach.

1.3 Hypothesis

By leveraging advanced tools in microscopic image processing, machine learning methodologies including transfer learning and deep learning, this thesis aims to develop an automatic algorithm for the detection and counting of Nosema cells. It is hypothesized that the proposed algorithm will not only surpass traditional methods in accuracy and efficiency but will also contribute significantly to the diagnosis of Nosema disease. The successful implementation of this algorithm is expected to enhance the understanding of the disease, providing valuable support for biologists, and contributing to the preservation of honeybee populations and overall ecosystem health. Moreover, the automatic algorithm is anticipated to streamline the detection and diagnosis process, saving time and effort for biologists involved in Nosema disease recognition and contributing to more efficient and timely interventions.

1.4 Objective

Due to the high costs and complexity of manual and commercial disease detection systems, this investigation strays from traditional systems and takes a newer approach. Beyond the many advantages of image analysis, these newer methods automate the intricate process of detecting and distinguishing diseased cells from other cell types present within the same microscopic image.

The fundamental goal of this research is to develop an algorithm capable of automated identification and cell counting, which will allow biologists to measure infection levels and provide accurate diagnoses. A number of consecutive tasks or objectives must be performed in order to reach this overarching goal:

1. Creation of Image Dataset: Generate a comprehensive dataset of images by cropping individual shots of Nosema cells and other coexisting objects from the primary microscopic images.

Identification Of Nosema Cells Using Microscopic Images

2. Feature Investigation of Nosema Cells: Thoroughly investigate the distinctive features of Nosema cells and compute them. This investigation involves meticulously assessing various tools in image processing and pattern recognition within computer vision. The aim is to either select an existing methodology or formulate a new one and compile a dataset of features.
3. Testing with Diverse Machine Learning Techniques: Utilize the constructed two datasets to test a diverse array of machine learning, deep learning, and transfer learning models to know the most proficient method for identifying Nosema cells. This process aims to establish a streamlined, rapid, and reliable model for spore recognition.
4. Model Creation and Implementation: Implement an automatic algorithm for Nosema counting and diagnosis using the model established in the previous step.

While the methodology proposed in this project applied to images of Nosema disease, its foundational principles remain versatile and applicable to other image categories, as long as they conform to the same statistical criteria. This adaptability underscores the potential broader impact of the proposed approach in image analysis and pattern recognition.

1.5 Methodology

The primary aim of this study is to introduce a robust method capable of recognizing and identifying cells afflicted by Nosema disease. While certain prior efforts have delved into the analysis of microscopic images of Nosema, the methodologies proposed therein are often confined to the application of specific morphological tools for image investigation. In a solitary instance, a support vector machine was employed to process extracted features. Although these undertakings are intriguing, they fall short of delivering comprehensive solutions. This means that with the development of technologies and human needs to deal with computer vision, processing more methods under this axe becomes a necessity. One of our main contributions of this thesis started from this point; how to exploit proposed techniques in image processing, computer vision, and machine learning to establish a system capable of analyzing the microscopic images of Nosema and detect the cells' disease.

Identification Of Nosema Cells Using Microscopic Images

This work combines two disciplines: microbiology and image processing. The aim of this project is to devise a methodological protocol customized for detecting and identifying Nosema disease cells in microscopic images. This will be achieved by employing innovative image processing tools. The implementation of a coherent analysis strategy is crucial, covering each stage from image acquisition to the extraction of relevant information.

The dataset used in this research was obtained from “Centro de Investigación Nacional de Apicultura Tropical” (CINAT), belonging to Universidad Nacional de Costa Rica.

Initially, the dataset of images intended for study (including its origin, data, and structure) is introduced. We used a total of 400 microscopic photos that were arranged in files of five and labeled by the specialists with the severity of the infection (very mild, mild, moderate, semi-strong, severe). Figure 1.6 shows an example of every group.

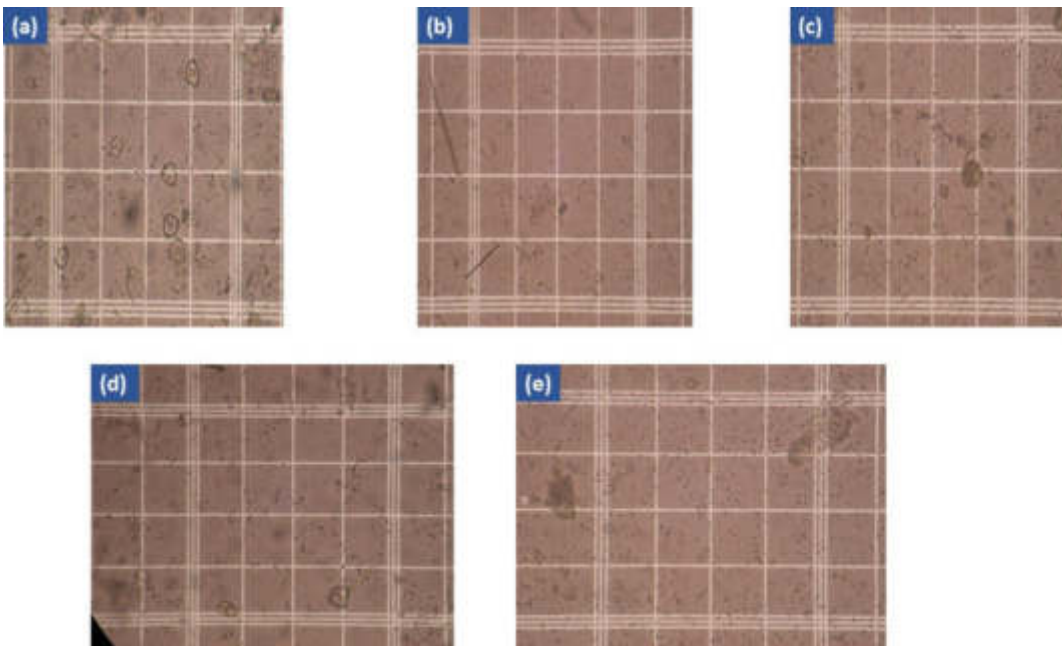


Figure 1.6 An example of used microscopic images from every infection level: from (a) to (e): very mild, mild, moderate, semi-strong, and strong

Second, the construction of a DS1 sub-images dataset derived from the original dataset, Subsequently, this dataset is utilized for calculating image features. Techniques involving image segmentation and object characterization are applied, leading to the creation of a new feature dataset known as DS2.

Identification Of Nosema Cells Using Microscopic Images

Third, ANN and SVM classification systems will be automatically reproduced and applied to the dataset of features (DS2) for the recognition of Nosema spores. Furthermore, a CNN will be implemented and reproduced to DS1 for the task of recognition. Also, several models of transfer learning will be fine-tuned and applied, the experiments will be conducted according to different training conditions, the data augmentation tool is approved to push the results to get the maximum accuracy that can be achieved in this work.

Fourth, an automatic algorithm will be developed performing the pre-trained model with the highest accuracy to count the cells within the image and identify the infection level.

The stages, the experiments as well as the results will be detailed in the chapters of this thesis.

1.6 Contributions and results

During the course of this doctoral thesis, three publications were produced: a book chapter, a conference paper, and a journal paper. All these publications delve into the implementation of microscopic image segmentation approaches, merging them with classification and recognition systems to achieve the detection and identification of Nosema cells.

We will present a summary of the two papers.

A summary of the conference Paper: “Nosema Pathogenic Agent Recognition Based on Geometrical and Texture Features Using Neural Network Classifier.”

The dataset utilized in this paper comprises 30 microscopic images. From these images, all the existing objects were cropped with a semi-automatic program to obtain a second dataset of 185 sub-images. The implemented approach extracted a number of 9 features: geometric and texture parameters which are the most useful in the definition of our Nosema cell. The choice of these parameters was based on the good role played by the preprocessing block in defining the perimeter of Nosema cells. Subsequently, a Multi-Layer Perceptron NN trained by the Back Propagation algorithm (MLP-BP) has been configured to do the classification of images between Nosema and non-Nosema.

Identification Of Nosema Cells Using Microscopic Images

The measure quality is based on the binary confusion matrix, the methodology was based on a supervised recognition approach, and the training and test samples were randomly separated according to a cross-validation strategy to be retained until getting the optimum result.

A summary of the journal paper: “Analysis of the Nosema Cells Identification for Microscopic Images”

Several techniques are used in this study to recognize and locate Nosema cells among other existent objects in a microscopic picture. 400 microscopic pictures were utilized as the primary dataset. From this dataset, we constructed DS1, a new dataset containing 2000 sub-images. Subsequently, we employed two main strategies for the recognition of Nosema images. The initial strategy involves using image processing techniques to extract useful information and attributes from a collection of microscopic images. The first dataset used comprises 400 microscopic images, from which we extracted 2000 sub-images to construct the second dataset. Following this, machine learning methods like neural networks (ANN) and support vector machines (SVM) are employed for the detection and classification of Nosema disease cells. The second strategy investigates deep learning and transfers learning. Multiple algorithms were investigated, including a convolutional neural network (CNN) classifier and multiple transfer learning methods (Alex Net, VGG-16, and VGG-19), which were fine-tuned and used to the object sub-pictures to distinguish the Nosema images from the other object images.

1.7 Structure of the Thesis

Throughout this thesis, our endeavor has been to encompass an extensive array of details while striving to maintain completeness and rigor in presenting essential information. Most of the high-level details are explained in the five chapters that make up this thesis. The chapters are organized as follows:

Chapter 2 details the methodology developed for the construction of the datasets ranging from image processing to feature calculation.

Chapter 3 describes the approved classification systems and details the methods implemented, the experiments carried out, and the recognition results provided.

Identification Of Nosema Cells Using Microscopic Images

In Chapter 4, the procedures for performing the automated algorithm for Nosema cell counting and diagnosis are detailed. The automatic algorithm detects the cells, counts their number, and determines the infection level (the diagnosis). The algorithm was tested on a variety of microscopic images and produced the most effective outcomes.

The report ends with the overall conclusion, outlining the findings and future works.

2 Chapter II : Dataset analysis and segmentation of microscopic images

2.1 Introduction

Following the presentation of this project's motivations, hypothesis, objectives, and state of the art in Chapter 1, Chapter 2 will describe the first part of the method utilized in this study to recognize Nosema cells. This first part consists in extracting of objects that exist in microscopic images to:

1. Build the dataset of sub-images of objects extracted from the primary images and which are in RGB format. These sub-images will be used in the identification of Nosema using deep learning and transfer learning techniques (in Chapter 3).

2. Preprocess and segment the collected dataset of images to calculate the most significant features which can characterize and define an object in a microscopic image and thus build a second dataset in Excel file form to be used later in the recognition of Nosema basing on ANN and SVM classifiers (in Chapter 3).

The preprocessing and preparation of the extracted sub-images for segmentation, as well as the basic principles of segmentation of these images (in grayscale level and in RGB color), are detailed in this chapter. More specifically, as will later be discussed in this chapter, the segmentation of these images is conditioned by criteria of brightness and texture of the studied microscopic images. As such, this thesis will propose and employ a segmentation algorithm that is self-adapting to the context of the used images. Indeed, this algorithm is quite original due to its genericity, flexibility, and adaptability to variable contexts.

2.2 Extraction

2.2.1 Problems with the used microscopic images

Microscopic images used in this study were acquired using Cantwell's method, as employed by biologists.

Identification Of Nosema Cells Using Microscopic Images

2.2.1.1 Cantwell's method and related problems

Cantwell's method is described in (Molina & al., 1990). The process followed in this project was to collect 30 adult bees per sample and place them on absorbent paper. The bees' abdomens were then separated and put in a mortar to macerate. Each abdomen received 1.0 ml of distilled water, for a total of 30 ml. The mash was stirred for a minute to be homogenized, then a drop of the mixture was placed on a blade. The macerated abdomens were ready to be imaged under a microscope at a magnification of 40x at the end of this operation. This method was applied to 75 samples, which is comparable to 2,250 adult bees. This approach requires the counting of all *Nosema* spores framed by double lines, including those that contact the double lines on the left and top sides of each block, but not those that touch the bottom double lines or those on the right side of the block. This is done in just five of the twenty-five center blocks (see Figure 2.1 and Figure 2.2), specifically the four corner blocks and the center block.

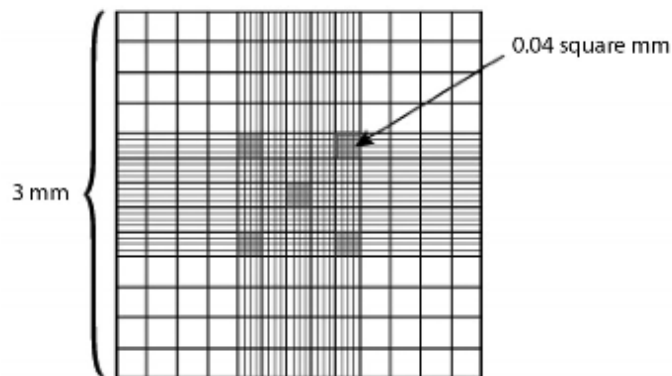


Figure 2.1 Blocks used for spores counting in a hemocytometer.

Identification Of Nosema Cells Using Microscopic Images

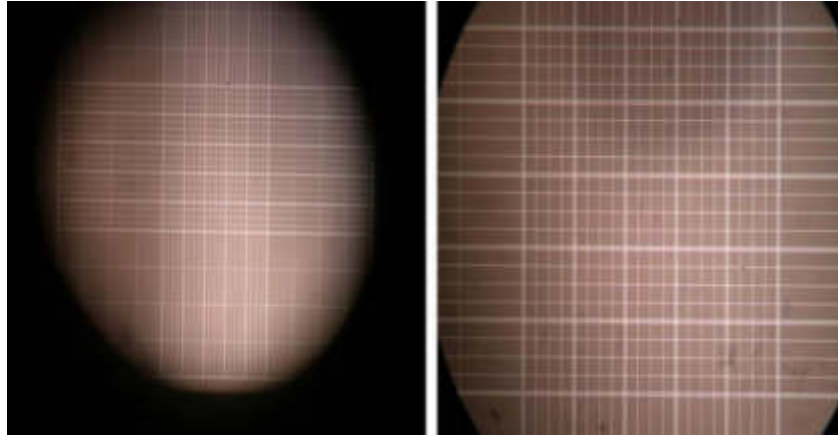


Figure 2.2 Actual image of the hemocytometer used in capturing of microscopic images.

Positioning the Nosema cells within the photos presents a challenge in its own right, as they might sometimes be obscured by other objects or located on the grid or blocks utilized by biologists for spore counting. The grid is also an object occupying a large part of the image (Figure 2.3) and in the case of cell counting, it can be considered as an artifact, especially in case of overlap.

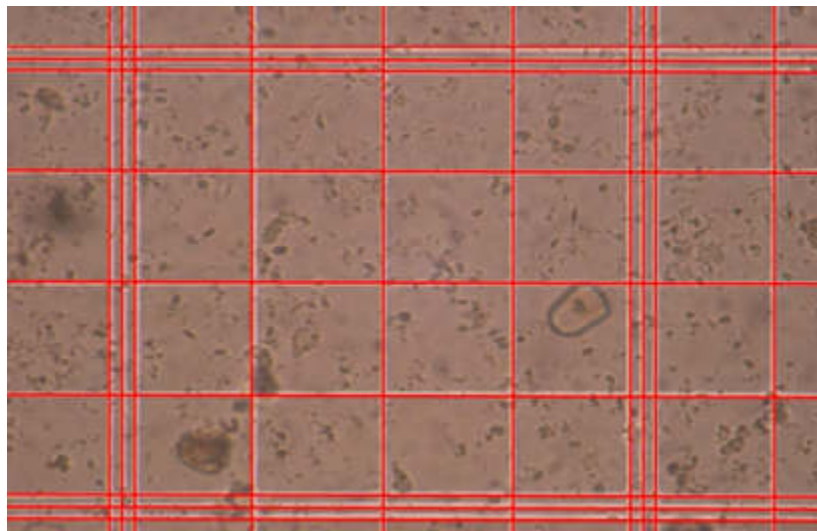


Figure 2.3 A microscopic image with the red color of the Counting Grid.

The artifact itself is a big problem because its brightness level is too high in the images, this poses a problem when transforming the image into grayscale, more precisely when detecting the elliptical shape of the Nosema cell (see Figure 2.4). This problem affects

Identification Of Nosema Cells Using Microscopic Images

the shape of the cell, it gets smaller or bigger or completely changes its shape (Figure 2.5).

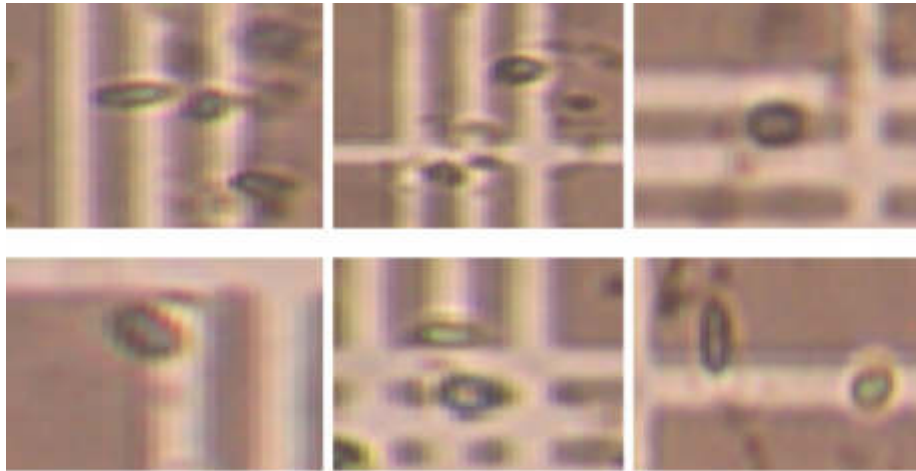


Figure 2.4 Example of cells overlapping the counting grid



Figure 2.5 Example of the change in cell shape during the preprocessing phase

2.2.1.2 Noise problem of microscopic images

Figure 2.6 illustrates a representative photograph obtained under a microscope using the Cantwell method. It is evident that a considerable amount of noise is present, with numerous elements in the image not corresponding to Nosema spores. Moreover, there is a lot of similarity between the spores' color and the background color.

Identification Of Nosema Cells Using Microscopic Images

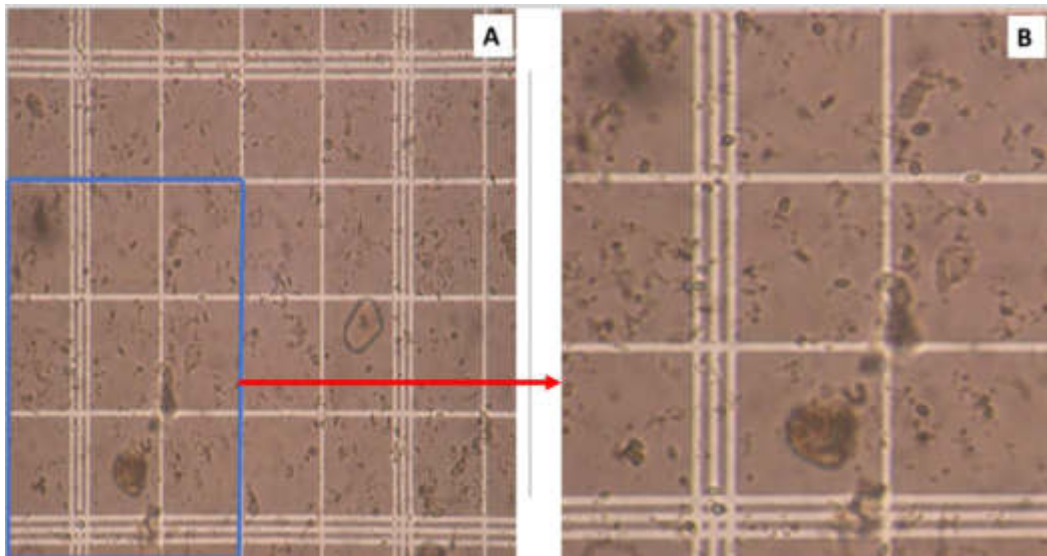


Figure 2.6 Image obtained by the microscope: (A) a whole image and (B) a part of the image that shows the existing noise.

Figure 2.7 clearly describes the noise that affects the spores of Nosema. In such instances, the sole identification of Nosema spores becomes unfeasible, as they would be perceived as distinct objects.

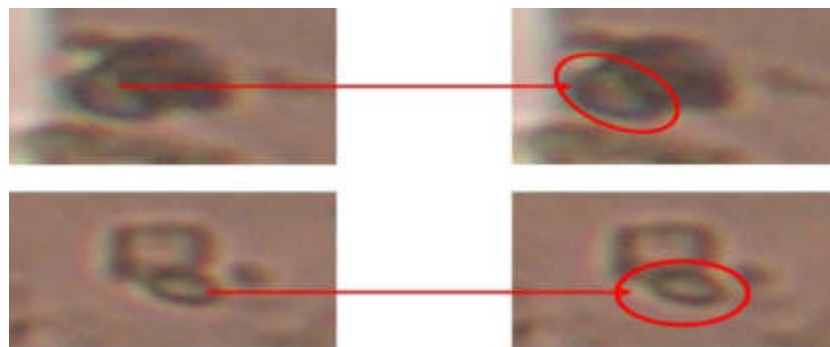


Figure 2.7 Example of spores hidden behind or superimposed on other objects: Nosema spores in the red circle.

2.2.2 Building of dataset from sub-images extracted from microscopic images

Based on the problems detailed before, the processing of the complete microscopic image is likely to lead to the disappearance of numerous Nosema cells or their misidentification as noise. Furthermore, objects that have a shape close to that of

Identification Of Nosema Cells Using Microscopic Images

Nosema will be considered as Nosema cells. Due to this reason, the decision was made to initially analyze the characteristics of these cells by isolating them through cropping from the original digital image (Figure 2.8).

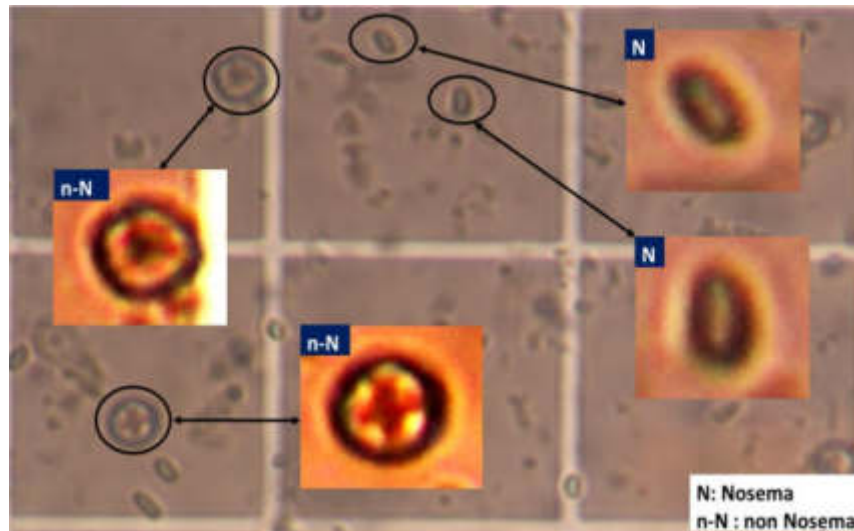


Figure 2.8 Instance of dataset extraction of Nosema cells and other existing objects in the microscopic images.

The procedure begins by selecting the region of interest (ROI), followed by the development of a simple semi-automatic algorithm to capture and crop the cell's image within the chosen ROI. Subsequently, automated preprocessing is applied to ascertain the cell's shape. The used microscopic images are loaded by several objects, they are quite unclear and noisy. To mitigate this, we involve Nosema cells that are distinctive from other items, ensuring that only pertinent information is extracted for analysis. Our preference is for a minimally sized, isolated cell area (see Figure 2.9). Thus, each Nosema cell subpicture contains only one clear cell. The same work is applied to objects that are not considered Nosema cells. Based on the preceding phases, a DS1 database was built that contains a total of 2000 sample images. DS1 consists of 1000 sample images of Nosema cells and 1000 images of non-Nosema cells (that is, any different object that

Identification Of Nosema Cells Using Microscopic Images

exists in the microscopic images). Figure 2.9 below depicts the process of building DS1.

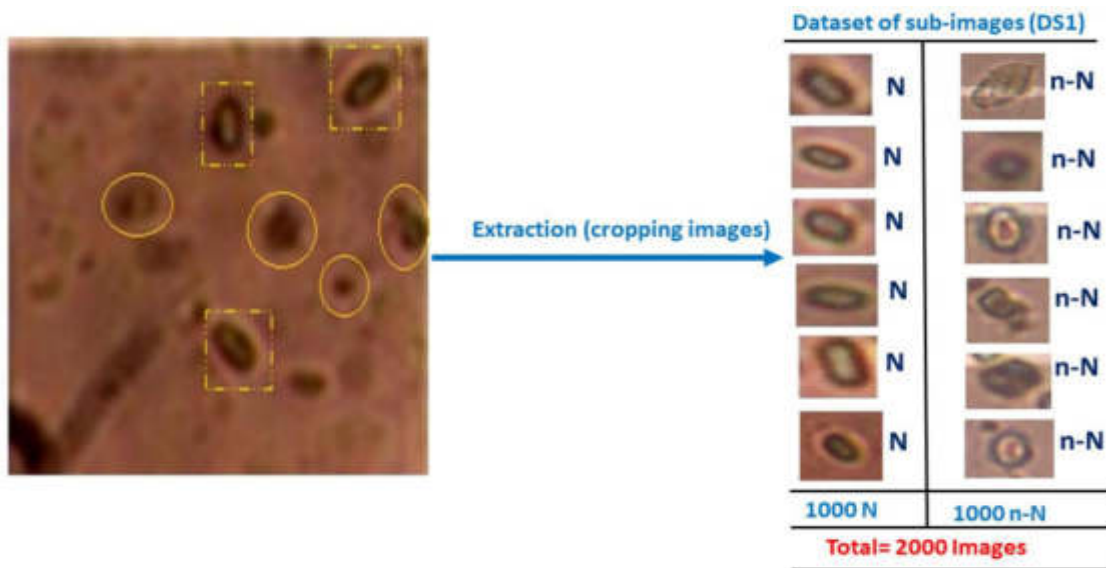


Figure 2.9 Construction of the image dataset contains both types of objects Nosema (N) and none Nosema (n-N)

In this chapter, the method involves collecting the Nosema cells and the coexisting objects (ROIs) in the studied microscopic images and investigating and analyzing these ROIs automatically. The next chapter details the detection of Nosema cells among other non-Nosema items.

2.2.3 Automatic segmentation and features extraction: building of dataset with extracted features:

The aim of this part of the chapter is to propose a method that prepares objects for extracting semantic information. To achieve this objective, this approach has been proposed:

Step 1: Contour detection of the extracted objects: the goal of this step is to extract and calculate the most relevant and reliable geometric features that characterize an object.

Step 2: Extract the objects from their background: The aim of this second step is to study the object color: color channels as well as texture.

2.2.3.1 Extracting the shape of the object

During the extraction of the cell shape, the following objectives must be achieved:

- the outline must be thin: the ideal thickness of the outline must be one pixel,

Identification Of Nosema Cells Using Microscopic Images

- the shape must correspond to the cell wall.

The technique for contour extraction needs to be in alignment with the rest of the processes, as the significance and accuracy of the extracted contours play a crucial role in distinguishing between the cells and obtaining their measurements.

There are two viable approaches for object identification: using regions or contours. However, we find the contours approach to be more appropriate. It is the contours of the cells that will be scrutinized to facilitate their identification. The contour or shape can be appreciated as the edge or border of two regions (objects). Detecting the edges of objects is equivalent to detecting changes in gray levels, or discontinuities at the boundary of two regions. The cells are distinct from the image's background, which is defined by a lower gray scale level.

2.2.3.1.1 Classic edge extraction techniques

Different approaches are used, we will mention derivative approaches, surface methods and, more recently, active contours.

2.2.3.1.1.1 Gradient approach

The gradient, in one pixel of a digital image, is a vector characterized by its modulus and direction. The module is directly related to the amount of local grayscale variation. The direction of the gradient is orthogonal to the boundary that passes at the point considered (Figure 2.10) and is oriented from the light part to the dark part.

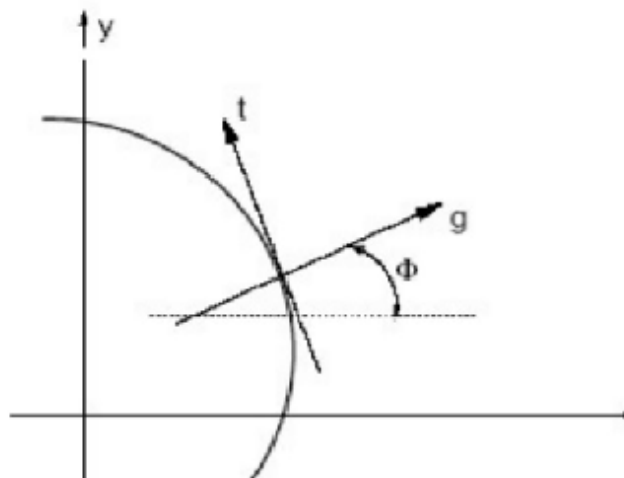


Figure 2.10: Gradient of a given point belonging to a given boundary

Identification Of Nosema Cells Using Microscopic Images

By considering $f(x, y)$ the grayscale function of the image, the gradient is used to measure the rates of change of this function values with respect to the distances in the direction x and y , by the maximum of the first derivative or by the passage to zero of the second derivative.

The study of an image behaves like the study of a function. To make the discontinuities appear in a signal, it is necessary to work on the differences between neighboring pixels, a difference that relates to the gray level. Figure 2.11 shows the calculation of the gradient using the filter of Sobel and Prewitt for two images, A and B. A is a Nosema cell image, and B is a non-Nosema image.

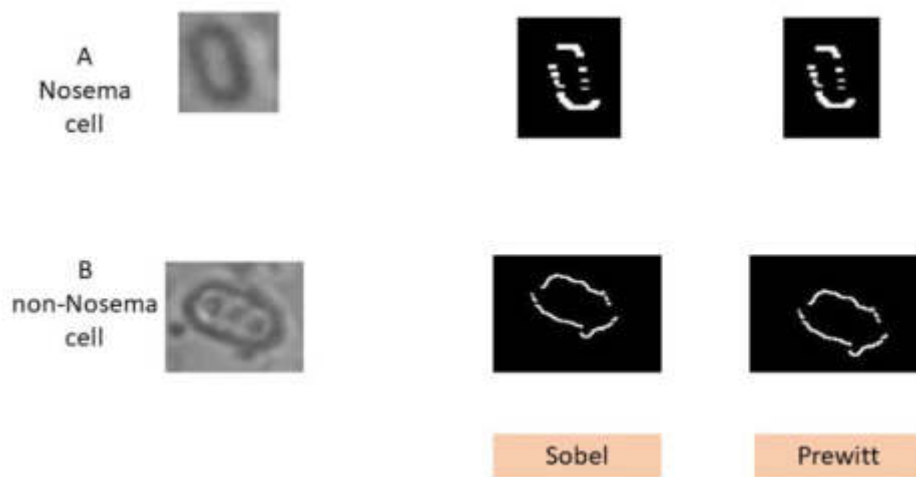


Figure 2.11 Calculating a gradient with multiple filters

The results are quite comparable for both filters they both produced open results. Additionally, the contours were relatively thick, exceeding two pixels in width. Knowing that the size of the matrix used for the calculation of the gradient was of size 3×3 there's a potential for closed contours. However, such an operation would generate an outline that might not align precisely with the concave region's wall. Moreover, this contour would not be an accurate representation of the wall for the identification of objects. The objective is to have the thinnest possible outline (one pixel). Unfortunately, gradient usage falls short in delivering fine contours, despite producing closed contours for all cells.

Identification Of Nosema Cells Using Microscopic Images

2.2.3.1.1.2 Laplacian approach

The maximums of the first derivative correspond to the zero passages of the second derivative, signifying locations with substantial grayscale variations. Since the first derivative is very sensitive to noise, the second derivative of the signal is then calculated. The second derivative, in the direction of the gradient, passes through 0 by changing the sign on an outline point. This causes the Laplacian to:

$\nabla^2 f = \frac{\partial^2 f}{\partial x^2} + \frac{\partial^2 f}{\partial y^2}$ equal to 0 in these points. The passages by zero, between the dark areas and the light areas are thus localized. The principle is to calculate the Laplacian of the image and look for the zeros.



Figure 2.12 Contour search with the Laplacian

The results are almost the same for both image types (Figure 2.12). The contour of the cell seems to decompose into two internal and external "contours". The ideal contour is between the two contours obtained. The thickness of the contour, thus obtained, is about 5 to 6 pixels in these examples. The resulting contours are all closed but the disadvantage of this method is that the resulting contours are too far from the actual contours of the object; the difference is estimated at about 5 pixels. Thus, the Laplacian cannot allow a good extraction of the contour of a cell, more precisely of the wall of a cell.

Identification Of Nosema Cells Using Microscopic Images

2.2.3.1.1.3 Active edges

An active edge is a set of points that we will try to move, to make them fit a shape. The idea of this method is to move the points to bring them closer to the areas of high gradient, while retaining characteristics such as the curvature of the contour or the distribution of the points on the contour, other constraints related to the arrangement of the points. Active contours were also used in this study and proved to be as effective as gradient or Laplacian methods, but the disadvantage of this method is that it is costly in terms of calculation time and operations since we will repeat the work for 2000 images.

2.2.3.1.1.4 Binary mathematical morphology

The well-known tools of binary mathematical morphology were also tested in this study and proved to be more effective than the previously cited methods.

2.2.3.1.2 Contour extraction using mathematical and binary morphology tools

Since the contour methods cited have not been validated and the contours calculated by mathematical and binary morphologies were the most appropriate, we will quote and explain the steps for calculating the contour of an object.

The analysis of images by mathematical morphology dates to the 1960s. This theory was initially introduced in materials science by J. Serra to analyze objects through their texture (Serra, 1982). Over the past two decades, it has undergone many developments, both theoretically and practically. It now covers a wide range of fields of application, particularly in robotics and machine vision, medical imaging and even multimedia (Soile,2004). Originally developed for the study of porous materials, mathematical morphology now finds its applications in many areas of image processing, both 2D and 3D, in biology and quantitative cytology, in medical imaging, in aerial imaging and satellite, robotics and computer vision, non-destructive industrial testing, studies of documents and works of art. Outside the field of image processing, we find applications for example in data analysis, on data represented by graphs, hypergraphs, fuzzy sets, etc., in logic, or even in game theory. To detect the contour of an object, the procedure described in Figure 2.13 was followed. The steps taken will be set out in the following paragraphs.

Identification Of Nosema Cells Using Microscopic Images

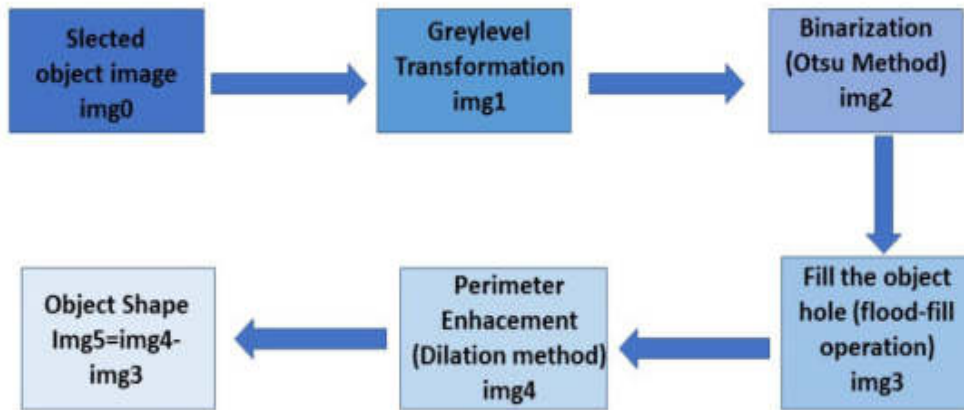


Figure 2.13 Approved approach to detect the shape (border) of an object.

2.2.3.1.2.1 Grayscale representation

For edge detection, the grayscale representation of the color was used. Images are converted to grayscale for manipulation, where image data consists of a single channel representing the intensity, brightness, or density of the image. In most cases, positive values are those that make sense (e.g., the intensity of light). Typically, a grayscale image uses 8 bits (1 byte) per pixel and the range of intensity values is from [0-255], where the minimum range value represents the minimum brightness (Black), and the maximum value represents the maximum brightness.

2.2.3.1.2.2 Binarisation

This step is carried out to create a binary image where all cell contours are enclosed. Otsu's method (Miss, Vola, & Baxi, 2013) was used to perform automatic thresholding from the shape of the image's histogram, or reduce a grayscale image to a binary image. The algorithm assumes that the image to be binarized contains only two classes of pixels, (that is, the foreground and the background) and then calculates the optimal threshold that separates these two classes so that their intraclass variance is minimal. The name of this method comes from the name of its initiator, Nobuyuki Otsu.

Some cells are complete entities, while others have points in common with the edge of the image. To overcome the bias in the treatments and measurements that will result, a mathematical morphology operation, called "bwareaopen" (an operation that removes all connected components (objects) that have fewer P pixels of the binary

Identification Of Nosema Cells Using Microscopic Images

image, producing another binary image), is applied to eliminate connected objects that are very close to the cell and that have a smaller size (see Figure 2.14).

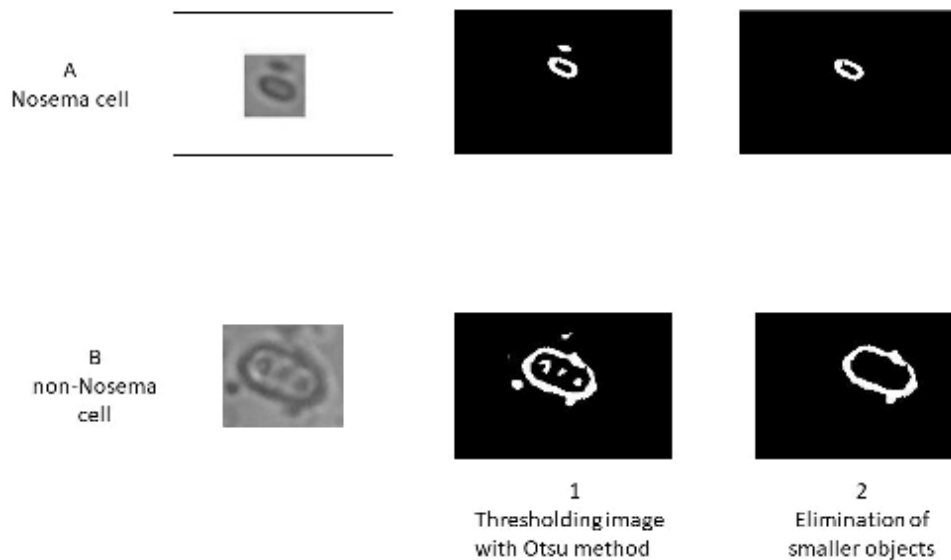


Figure 2.14 Steps to Remove Unwanted Objects

2.2.3.1.2.3 Populating regions and holes in the image

A flood filling operation was used. This method conducts a fill operation on the background pixels of the input binary image to fill the item's hole from its precise positions before discarding any small existing objects in the image of the desired object.

2.2.3.1.2.4 Using the dilation method

The dilation calculates the maximum of the neighbors of each pixel and removes holes inside the object that are smaller than the structuring element (Gonzalez & Woods, 2017). If we want to calculate an expansion of an image B by a structuring function A such that Z is the grayscale, the mathematical equation can be defined as follows:

$$B \oplus A = \{z | A_z \cap B \neq \emptyset\} \tag{2.1}$$

It is the boundary of the object using a matrix consisting of 0 and 1. A matrix 3×3 (see Figure 2.15) was used in such a way that it did not greatly widen the boundary of the object by adding only one pixel to the boundary.

Identification Of Nosema Cells Using Microscopic Images

0	1	0
1	1	1
0	1	0

Figure 2.15: Used Matrix for dilation

2.2.3.1.2.5 Contour calculation

Following dilation, the contour of the object is recognized by computing the difference between the two pictures before and after expansion, as shown in Figure 2.16 below:

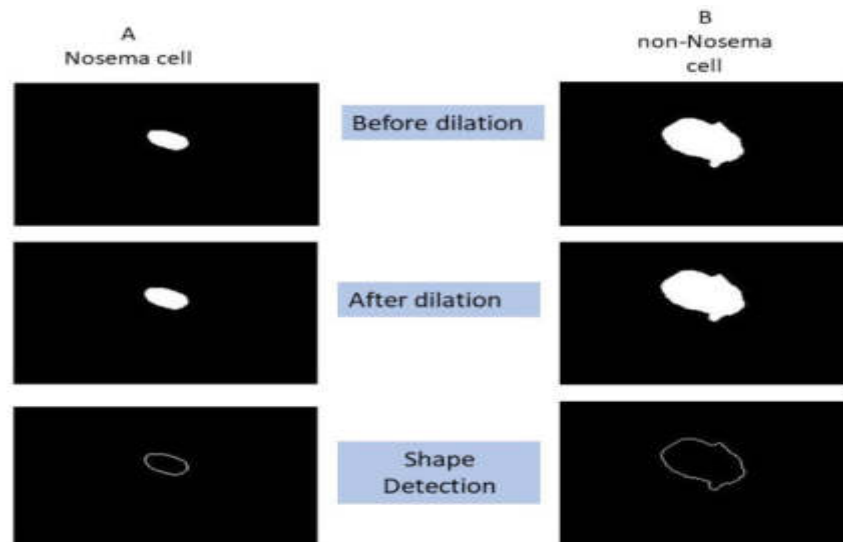


Figure 2.16 Edge Detection

The method offers the advantage of being computationally efficient and operationally cost-effective, thus yielding closed contours for each cell. Furthermore, the provided contours are outside the cell and with a thickness of 1 pixel.

Figure 2.17 illustrates the detailed approach to detecting the contour of an ROI.

Identification Of Nosema Cells Using Microscopic Images

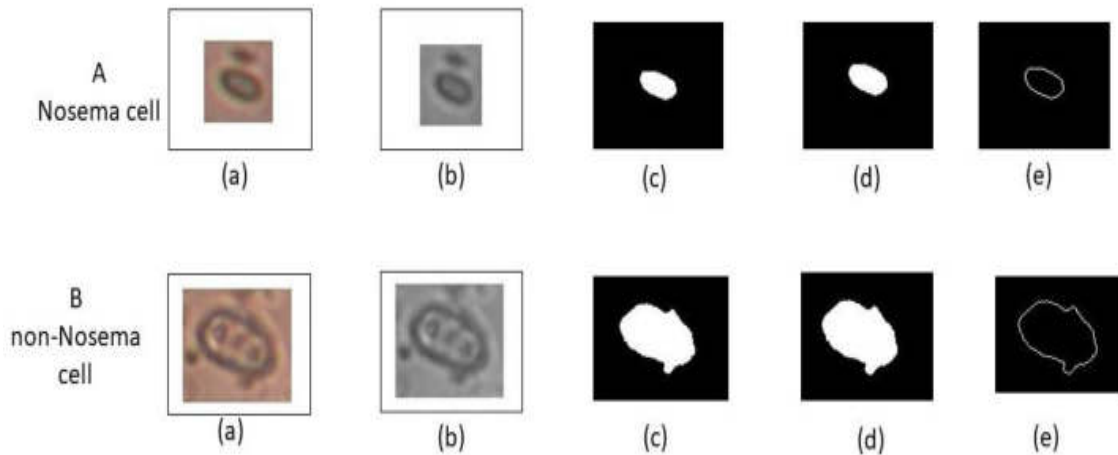


Figure 2.17 The preprocessing steps for automatic contour extraction: (a) RGB image, (b) gray image, (c) binarization and hole filling, (d) dilation, and (e) contour extraction

2.2.3.2 Automatic segmentation and Features extraction

After presenting the contour extraction algorithm developed within this document, this section demonstrates its application in extracting features. The latter will be employed for identifying and characterizing the region of interest within an image. The goal of the segmentation method proposed in this chapter is to keep separately the information of each object (regardless its kind: Nosema or non-Nosema. Consequently, upon completing the segmentation, a vector encompassing all computed or extracted features is obtained.

From the calculated shape/contour, two types of features were extracted:

- Geometric features (six features)
- Statistical features (three features)

2.2.3.2.1 Geometric features

The geometric aspects define the fundamental qualities of geometric shape. Their significance lies in the fact that, through numerous experiments, we have found them to consistently yield the best results. These parameters were used and defined in our work (Dghim, Travieso-González, Dutta, & Hernández, 2020) respectively:

Identification Of Nosema Cells Using Microscopic Images

- Size/Perimeter provided that the Nosema cell has an elliptical shape, and the other items have distinct spherical forms. This elliptical perimeter calculation is based on the a and b variables, where a is the semi-major axis and b is the semi-minor axis. The following equation gives the perimeter P:
- The formula for Area A is as follows:

$$P = \pi \cdot \sqrt{2 \cdot (a^2 + b^2)} \quad (2.2)$$

$$A = \pi \cdot a \cdot b \quad (2.3)$$

- The Relation R is the quotient of the shape's height (H) and width (W):

$$R = H/W \quad (2.4)$$

- Equivalent diameter (D) is the diameter of a circle that has the same area as the item:

$$D = \sqrt{4 \times \frac{A}{\pi}} \quad (2.5)$$

- Solidity (S) is the fraction of the convex region contained in the item:

$$S = \frac{A}{\text{convex area}} \quad (2.6)$$

- Eccentricity (E) is defined as the ratio of the distance between the ellipse's foci to its major axis length: Let a be the semi-major axis and b be the semi-minor axis of the ellipse:

$$E = 1 - \frac{b^2}{a^2} \quad (2.7)$$

Identification Of Nosema Cells Using Microscopic Images

$$E = \sqrt{f \times (2 - f)} \quad (2.8)$$

2.2.3.2.2 Statistic Features

The remaining features 7, 8, and 9 were determined using the object's polar coordinates, namely the polar coordinates of a Cartesian point (x, y) (Dghim, Travieso-González, & Burget, 2021). Assume that a point M is located at such a distance (r) and in such a direction (θ) from the reference points. It is a boundary projection or one-dimensional representation. This is determined by calculating the distances from the object's centroid (center of "mass") to the border as a function of angles in any selected increment. When appropriately scaled, the resulting set of distances was the vector required as angle distances to the border pixel. Figure 2.18 shows the distribution of this distance for Nosema and non-Nosema object.

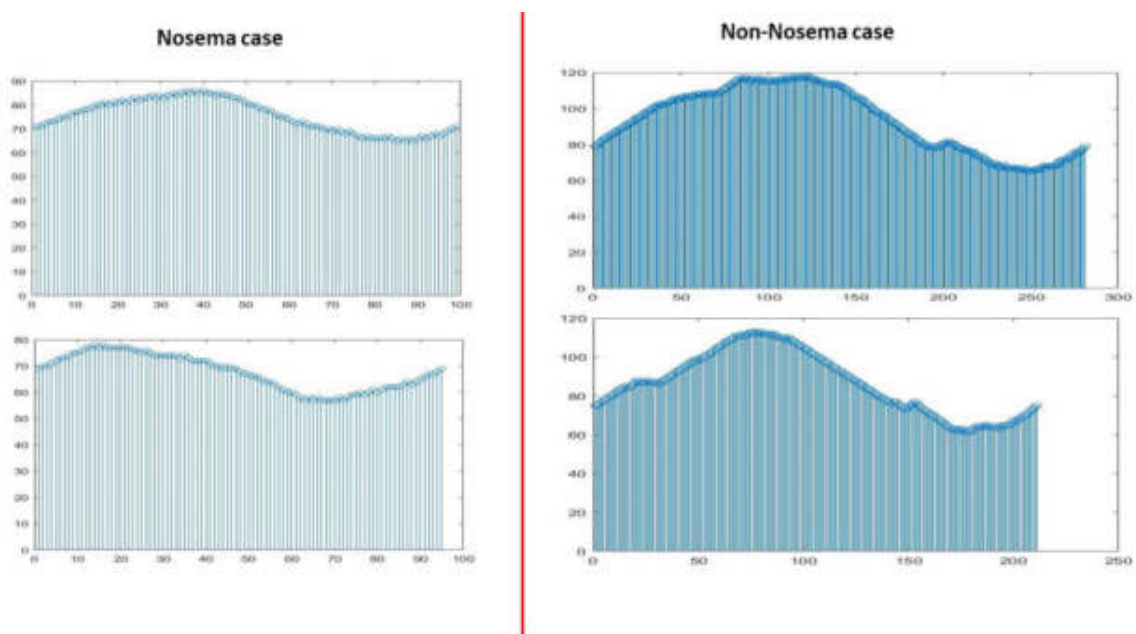


Figure 2.18 Histograms describing the distribution of distances that flow from an object's centroid to each pixel of its shape in both cases Nosema and non-Nosema object for two examples of each type: this shows the large difference between the two types

Following that, a value for these distances is shortened, and the nearest integers to a value are used to determine the three following respective parameters.

- The standard deviation of these distances has been determined, resulting in feature number 7. Standard deviation is a measure of variability that

Identification Of Nosema Cells Using Microscopic Images

successfully normalizes the elements of N through the first array dimension whose size does not equal one; where P can be an array or a matrix and in this case is a vector of the radius values of the studied object's polar coordinates, and E is its mean. It is provided by Equation:

$$\text{Std. deviation } (\sigma) = \sqrt{\frac{1}{N} \cdot \sum_{j=1}^N (P_{ij} - E_i)^2} \quad (2.9)$$

- Variance deviate computes the difference and the closest derivative of the variance (X) for a vector X, which is [X (2) X(1) X(3) X(2)... X(n) X(n1)]. It is provided by the following equation:

$$\sigma^2 = \frac{(x_1 - \mu)^2 + (x_2 - \mu)^2 + (x_3 - \mu)^2 + \dots + (x_n - \mu)^2}{n} \quad (2.10)$$

2.2.3.2.3 Automatic segmentation and feature extraction from the texture of the color image:

2.2.3.2.3.1 Extracting the characteristics of the color channels (six characteristics)

The RGB object image is then used to extract further information regarding texture and color (Dghim, Travieso-González, & Burget, 2021). However, first, the item must be separated from its background in the image; to do so, follow these steps:

1. The bounding box image was extracted based on shape characterization (calculated in the section of shape extraction).
2. After converting the picture from RGB to HSV color space, individual Hue (V), Saturation (S), and Value (V) channels were retrieved.
3. Use the V mask to find the vibrant color.
4. Concatenate the three new HSV channels by setting the H and S masks to 0 and the V mask to 1.

Identification Of Nosema Cells Using Microscopic Images

5. Finally, transform the image back to RGB color to remove the object's backdrop, as illustrated in Figure 2.19:

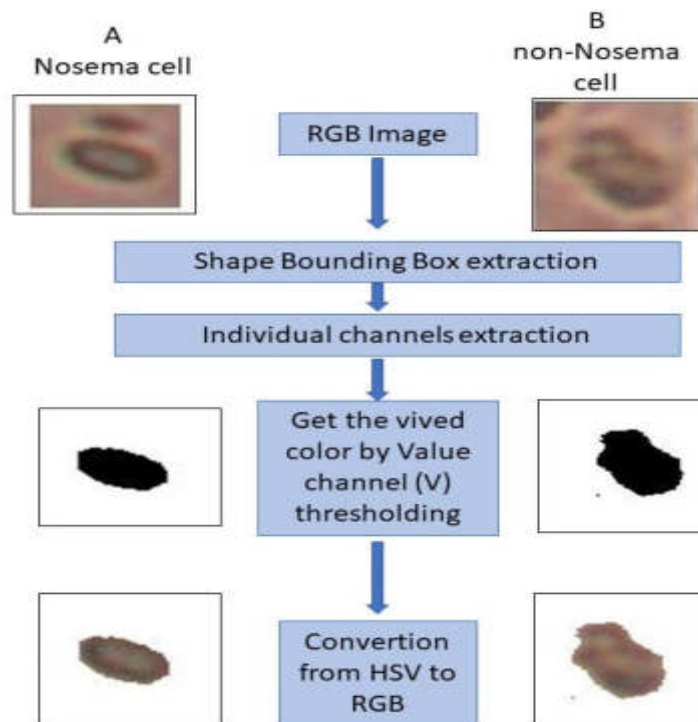


Figure 2.19 Extracting an object from its background.

The texture parameters are 6 in number and quantify the entropy of the RGB and HSV channels; it may be characterized as a logarithmic measurement of the number of states having a substantial likelihood of being occupied. The blue, red, green, and yellow channels are the input intensity images. Furthermore, the randomization of the Hue and saturation masks is determined. The value/lightness channel was removed because it provides no further information.

Figure 2.20 shows the extracted channels for features calculation.

Identification Of Nosema Cells Using Microscopic Images

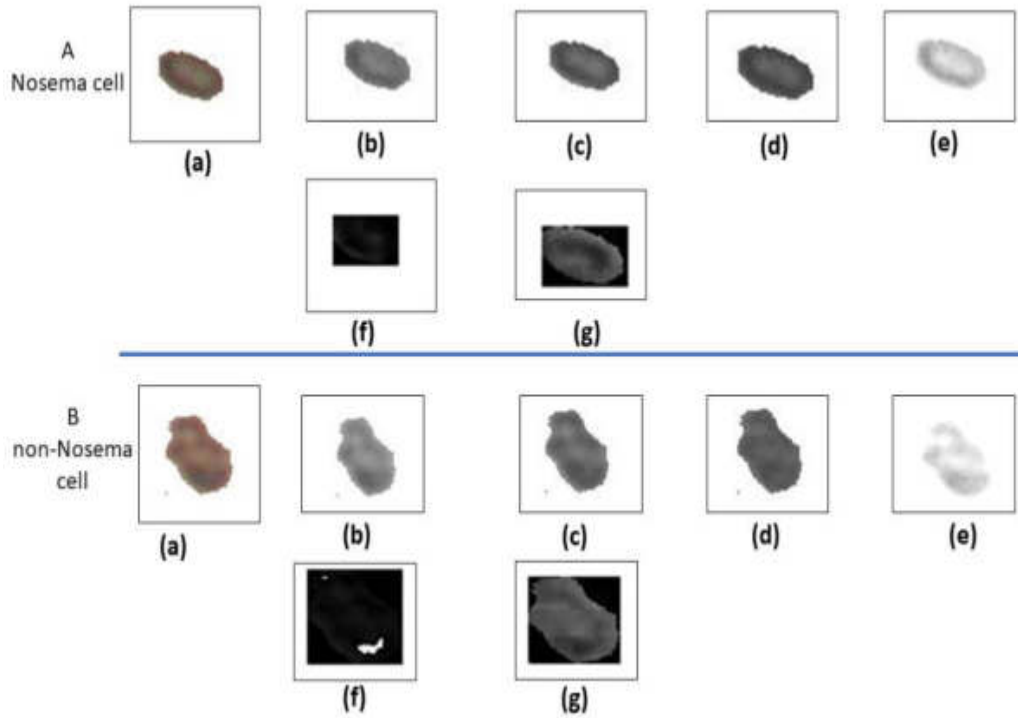


Figure 2.20 used images for entropy measurements for both *Nosema* cell and non-*Nosema* cell: (a) extracted RGB object, (b) Red mask, (c) Green Mask, (d) Blue Mask, (e) yellow mask, (f) hue channel, and (g) saturation channel.

Assume x_i is the set of pixels in the image with the color/channel i , and $p(x_i)$ represents its probability. The following equation 11 is used to determine the six entropy parameters:

$$E(x_i) = \sum_{i=1}^N P(x_i) \cdot \log_2(p(x_i)). \quad (2.11)$$

2.2.3.2.3.2 Feature extraction using the GLCM: (four characteristics)

A) Concepts

As mentioned before, (Dghim, Travieso-González, & Burget, 2021) *Nosema* cells tend to exhibit a more pronounced yellow hue internally. This observation prompted the utilization of a Grey Level Co-occurrence Matrix (GLCM) used on the yellow mask. This approach was employed to calculate additional texture information specific to the yellow color. The GLCM is a popular statistical approach for extracting textural features from microscopic images. It was employed in numerous feature extraction operations, such as feature skin extraction (Kolkur & kalbande, 2016) or plant disease feature extraction (Al-Hiary, Ahmed, Reyalat, Braik, & Alrahameh, 2011). As shown be (Rundo

Identification Of Nosema Cells Using Microscopic Images

et al., 2020), a novel strategy to compute the GLCM called HaraliCU can offload the computations into the Graphics Processing Units (GPU) cores, allowing to drastically reduce the running time required by the execution on Central Processing Units (CPUs). In (Rundo et al., 2021), an invented method called CHASM uses the previously mentioned HaraliCU method, a GPU-enabled approach capable of overcoming the issues of existing tools by efficiently computing the mappings of features for high-resolution images with their full dynamics of grayscale levels, and CUDA-SOM, a GPU-based execution of the SOMs for recognizing of clusters of pixels in the image. The statistical texture calculator's main rule states that they are determined from the statistical distribution of intensities measured at defined points relative to each other in the picture. Statistics are classified into first-order, second order, and higher-order statistics based on the number of pixels in each pair. The GLCM approach collects the statistical texture properties of the second order. Third and higher-order textures are theoretically conceivable but are seldom used because of the computational time requirements and difficulties in interpreting them (Mohanaiah, Sathyanarayana, & Gurukumar, 2013).

B) Extracted features with GLCM

The GLCM is a greyscale picture that I defined in Z. The grey level co-occurrence matrix is a square matrix Gd of size N, where N is the total number of grey levels in the picture. Gd's (i, j)th entry specifies the number of instances a pixel X with intensity value i splits from a pixel Y with intensity value j at a certain distance k in a specific direction d. Where k is a non-negative integer and d is described by $d = (d_1, d_2, d_3, \dots, d_n)$, where $d_i \in \{0, k, -k\}$, $i = 1, 2, 3, \dots, n$ (Sebastian, Unnikrishnan, & Balakrishnan, 2012). The Haralick GLCM was used to extract four characteristics from the picture of the yellow channel. The GLCM's most important qualities are contrast, correlation, energy, and homogeneity.

$$Contrast = \sum_{n=0}^{Ng-1} n^2 \cdot \left[\sum_{i=1}^{Ng} \sum_{j=1}^{Ng} p(i, j) \right] \quad (2.12)$$

Correlation quantifies the linear relationship between the grey levels of surrounding pixels:

$$Correlation = \frac{1}{(\sigma_i \cdot \sigma_j)} \cdot \sum_i \sum_j (i - \mu_i) \cdot (j - \mu_j) \cdot P_{i,j} \quad (2.13)$$

It is also known as the Angular Second Moment (ASM), and it is highly useful when two neighbor pixels are quite similar:

$$Energy = \sum_{i=0}^{Ng-1} \sum_{j=0}^{Ng-1} p(i,j)^2 \quad (2.14)$$

When a local grey level is homogeneous, homogeneity is strong:

$$Homogeneity = \sum_i \sum_j P(i,j) \cdot \frac{1}{1 + (i - j)^2} \quad (2.15)$$

2.3 Conclusion

In this chapter, we introduced our segmentation algorithm. The general strategy of our method is to accomplish the final segmentation in two essential steps:

1-Extract the clear and isolated objects that exist in the microscopic images: In this step we built our first DS1 database that contains the sub-images of Nosema objects and non-Nosema objects. DS1 contains a total of 2000 RGB images: 1000 Nosema cells samples image and 1000 non-Nosema samples image.

2-From the images of DS1: we calculated the attributes or features most relevant to the identification of its objects: these features are in the form of a vector of size 19 for each object; and we have built the DS2 features dataset. Features calculation was done by the following two steps:

2.1- Extract the contour of the object derived from the grayscale image and calculate its most relevant geometric and statistical characteristics. From this contour 9 characteristics were calculated.

2.2- Extract the RGB object from its background and calculate its texture and color characteristics. 10 features were extracted from the texture of the studied objects. Figure 2.21 shows a backup extract of 19 calculated

Identification Of Nosema Cells Using Microscopic Images

features for both types of objects as an Excel file.

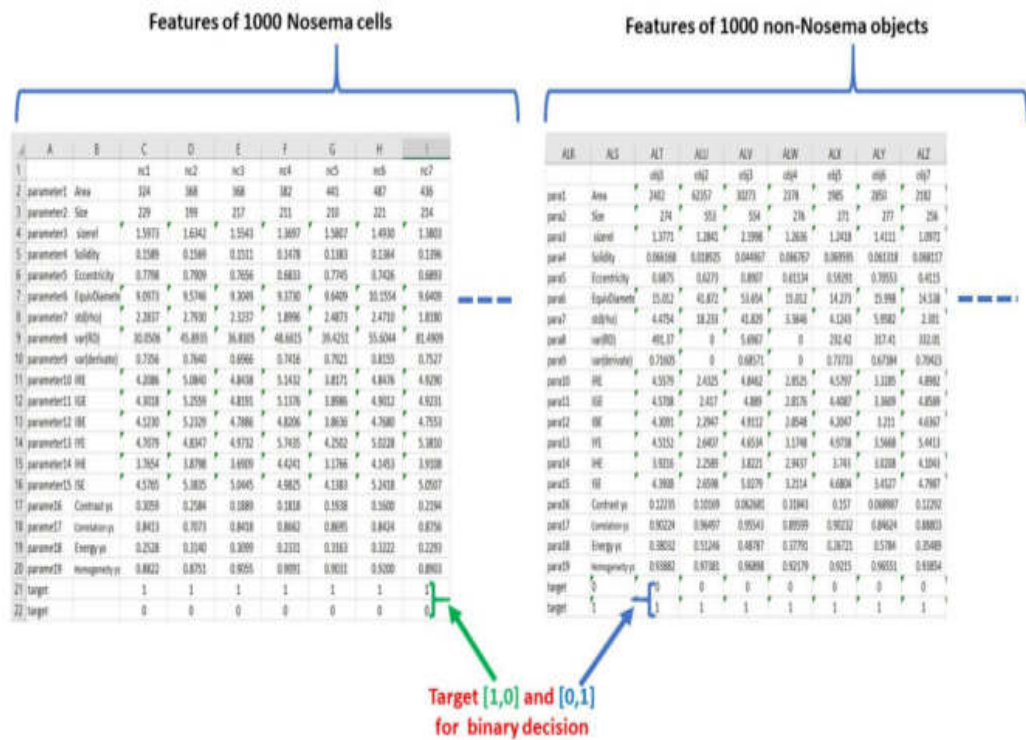


Figure 2.21 DS2 Features Dataset stored files.

The two datasets DS1 and DS2 built will be used in Chapter 3 for the recognition of Nosema cells following different strategies.

The details of using these datasets for Nosema identification will be explained in the upcoming chapter.

Identification Of Nosema Cells Using Microscopic Images

3 Chapter III: Nosema recognition

3.1 Introduction

In the previous chapter, our research strategy focused on image segmentation, laying the groundwork for effective feature extraction. This chapter presents an approach specifically designed to identify Nosema cells and distinguish them from coexisting objects within the same microscopic image. The subsequent section directs attention to cell classification, exploring traditional object classification methods and their efficacy in categorizing cells. This analysis is then contrasted with the effectiveness of modern object classification techniques, including the application of classic methods such as Artificial Neural Networks (ANN) and Support Vector Machines (SVM), as well as contemporary techniques like Convolutional Neural Networks (CNN) and transfer learning, which have emerged within the domain of object classification.

Moreover, the chapter involves testing and validating various architectures of transfer learning models for object recognition. The model demonstrating the highest accuracy will undergo retraining with Augmentation Data to enhance its precision in object recognition. Notably, ANN and SVM will leverage feature vectors extracted from the studied objects, while the second category of methods will employ RGB images of the objects under examination.

This chapter emphasizes that cell recognition can be achieved through several methods. However, for comparison, we will unveil the most effective method for application identification. The strategy pursued for recognition is elucidated in Figure 3.1, providing a visual representation of the proposed approach.

Identification Of Nosema Cells Using Microscopic Images

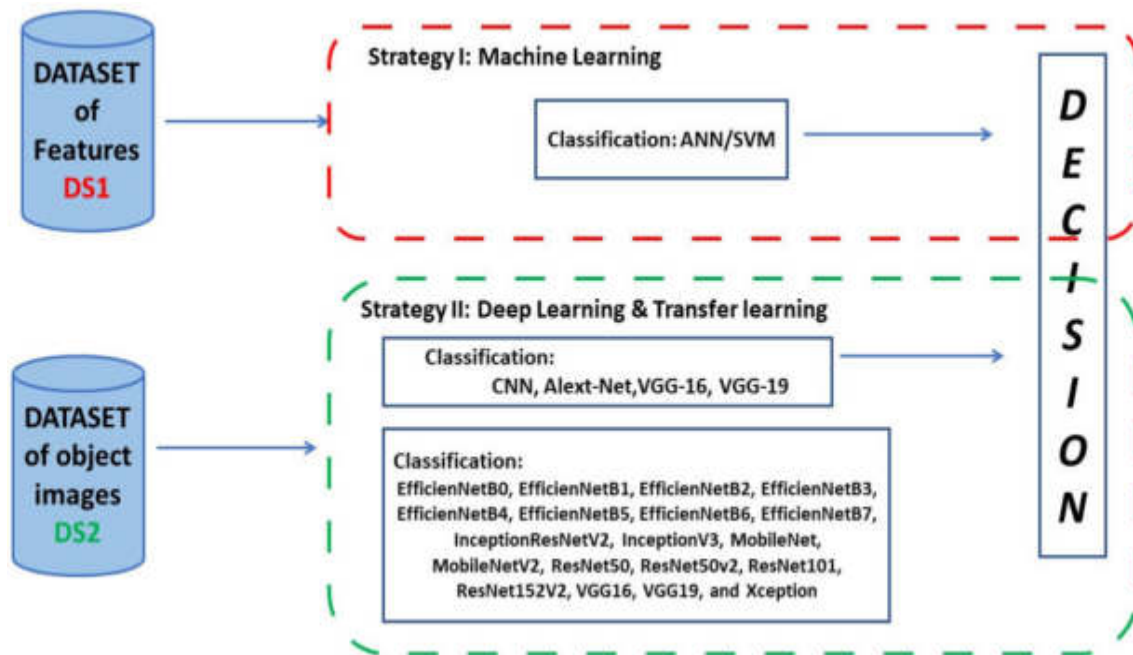


Figure 3.1 The Implemented Methodology for Identification

3.2 Artificial intelligence, machine learning, and deep learning

In 2021, artificial intelligence continues to bring daily benefits to people: music recommendation systems, Google Maps, Uber, and many other applications are powered by artificial intelligence. However, there is confusion between the terms "artificial intelligence," "machine learning," and "deep learning." One of Google's most popular queries is, "Are artificial intelligence and machine learning the same thing?". Let us get it straight: Artificial intelligence, machine learning, and deep learning are three different things (Figure 3.2):

- Artificial intelligence is a science like mathematics or biology. It studies ways to build intelligent programs and machines to solve problems creatively, which has always been considered a human prerogative.
- Machine learning is a field of artificial intelligence that allows systems to learn and improve from experience without being explicitly programmed automatically.

Identification Of Nosema Cells Using Microscopic Images

- Deep learning is a sub-domain of machine learning, which uses neural networks to analyze different factors with a structure similar to the human neural system.

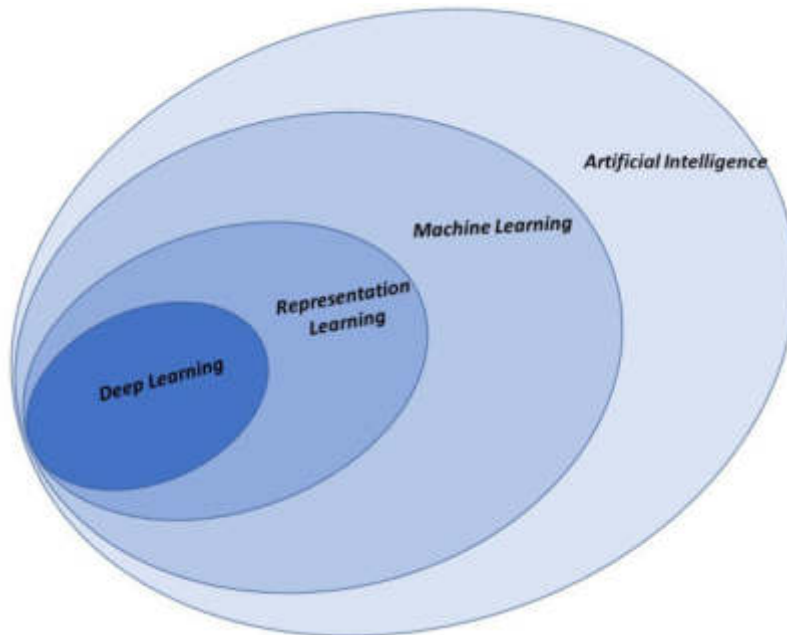


Figure 3.2 A Venn diagram showing how deep learning is a kind of representational learning, which is in turn a kind of machine learning, used for many, but not all, approaches to artificial intelligence

Many of artificial intelligence's early breakthroughs occurred in somewhat antiseptic and formal contexts, with computers having little awareness of the world. For example, IBM's Deep Blue chess engine defeated world champion Garry Kasparov in 1997 (Campbell, Hoane, & Hsu, 2002). Chess is a fairly basic game. It only has sixty-four spaces and thirty-two pieces that can move restrictedly. Creating a good chess strategy is a fantastic accomplishment but not very difficult. In truth, there is minimal difficulty in expressing computer-related topics. Failures can be fully characterized by a very short number of perfectly formal rules, which the programmer can simply specify in advance.

Ironically, the abstract and formal tasks that are among the most difficult mental tasks for a human being are among the easiest for a computer. While computers have long been able to beat even the best human chess player, it is only recently that they have reached a level of recognition of objects or speech comparable to that of a human being. A person's daily life necessitates a vast understanding of the globe. Much of this information is subjective and intuitive, making formal expression problematic. To act

Identification Of Nosema Cells Using Microscopic Images

intelligently, computers must capture this same knowledge. One of the main challenges of artificial intelligence is how to bring this informal knowledge into a computer.

Several artificial intelligence projects have sought to hard-code knowledge about the world in formal languages. A computer can automatically reason about utterances in these languages by using logical inference rules. This is called the knowledge-based artificial intelligence approach. The difficulties faced by systems based on hard-coded knowledge suggest that artificial intelligence systems must be able to acquire their knowledge by extracting models from raw data. This capability is known as machine learning. Machine learning has enabled computers to solve challenges using real-world information and make judgments that appear subjective. A basic machine learning technique known as logistic regression can indicate whether a caesarean section should be recommended (Mor-Yousef et al., 1990). Another basic machine learning method, naive Bayes, may distinguish between valid and unwanted emails.

The performance of these rudimentary machine learning algorithms is strongly dependent on the data representation provided to them. When logistic regression is used to propose a caesarean section, for example, the artificial intelligence system does not physically assess the patient. Instead, the doctor sends the system various relevant pieces of information, such as the existence or absence of a uterine scar. A characteristic is any piece of information contained in the patient's depiction. Logistic regression is used to discover how each of these patient features corresponds with different outcomes. It can, however, have no effect on how the qualities are specified.

Many AI challenges may be accomplished by defining the correct collection of features to extract for that job and then feeding those characteristics into a basic machine learning algorithm. However, for many tasks, it is difficult to know what features need to be extracted. Assume someone wants to create software that detects vehicles in photos. We all know that autos have wheels; thus, the existence of a wheel might be employed as a feature. Unfortunately, describing the appearance of a wheel in terms of pixel values is challenging. Although a wheel has a simple physical shape, its picture may be complex. It is necessary to take into account, when describing the wheel, the shadows that fall on the wheel, the sun that glistens on the metal parts of the wheel, the wing of the car or an object in the foreground that obscures part of the wheel, etc.

Identification Of Nosema Cells Using Microscopic Images

One solution to this problem is to use machine learning to discover not only the correspondence between the representation and the output but also the representation itself. This approach is known as representational learning. The representations learned often give much better performances than those obtained with hand-designed representations. They also allow intelligent systems to quickly adapt to new tasks with minimal human intervention. A representation learning algorithm can discover a good set of characteristics for a simple task in a few minutes, while for a complex task, it can take a few hours or even a few months, depending on the complexity of the task. Designing features for a hard task by hand takes a long time and a lot of human labor; it might take decades for an entire community of scientists.

Many aspects of variation impact every piece of data that may be seen, which is a primary source of difficulty in many real-world artificial intelligence (AI) applications. Individual pixels in a photograph of a red automobile, for example, can be extremely close to black at night. The shape of the car's silhouette is determined by the angle of vision. Most applications need to unravel the sources of variation and eliminate those that are irrelevant. In fact, extracting such high-level abstract qualities from raw data might be challenging. Many of these factors of variation, such as the accent of the speaker, can only be identified using a sophisticated understanding of the data at the human level. When obtaining a representation is nearly as complex as solving the actual problem, understanding representation does not appear to help us at first glance.

Deep learning (DL) solves this central problem of learning representation by introducing representations that are expressed in terms of other simpler representations. DL allows the computer to construct complex concepts from simpler concepts. The prime example of a deep learning model is the Deep Neural Network (DNN) or Multilayer Perceptron (MLP). An MLP is just a mathematical function that maps a set of input values to output values. The function is formed by the composition of many simpler functions. It can be considered that each application of a different mathematical function provides a new representation of the input.

Identification Of Nosema Cells Using Microscopic Images

Deep learning is a machine learning approach that allows systems to improve with experience and data. It is the only viable approach to building intelligent systems that can operate in complex real-world environments. Indeed, DL is a special type of machine learning that achieves great power and flexibility by learning to represent the world as a nested hierarchy of concepts and representations, with each concept defined against simpler concepts and more abstract representations calculated based on less abstract concepts.

3.3 Principles of classification

3.3.1 Concepts

Classification makes a direct use of computer-based learning methods. In artificial learning, there are usually several types of learning:

- Unsupervised learning
- Supervised learning
- Semi-supervised learning

For all these learning methods, there is a set of observations $\{x_1, \dots, x_n\} \in X$ and a number of classes to be discriminated against by the classifier. Each observation is described by several characteristics. Unsupervised learning seeks to build a model directly from the data. The goal is to describe how the data is organized and to extract homogeneous subsets from the data. Unsupervised methods include hierarchical classification (Cormuégols & Michet, 2002), self-organizing maps (Dreyfus & al., 2004), k-means (Mitchell, 1997), etc. In supervised learning, in addition to observations, there are target values (or labels or membership classes) $\{y_i\} \in Y$ associated with these observations, where Y designs the set of possible classes. A model is then built that allows to estimate the dependencies between the sets X and Y . Supervised learning is called supervised learning because the elements of Y are used to guide the estimation process. Supervised methods include k-ppv (Kuncheva, 2014), neural networks (Dreyfus & al., 2004), support vector machines (SVM) (Abe, 2005), (Vapnik, 1995), and (Cristianini & Shawe-Taylor, 2000), decision trees (Quinlan, 1994), etc. As part of a semi-supervised learning (Zhou & Schokopf, 2004) and (Chapelle, Schölkopf, & Zien, 2006), among the

Identification Of Nosema Cells Using Microscopic Images

observations, only a small number of them have a label $\{y_i\}$. The objective is then to seek to classify unlabeled observations. In this work, particular attention is put on supervised methods. As such, below more details will be given about the principles of supervised methods.

3.3.2 Supervised learning

The generalization power of an artificial learning algorithm is dependent on the inductive process it performs and the space of H hypotheses. This space corresponds to the set of feasible decision functions. The inductive principle makes it possible to select in space hypotheses, from a set of data, those that best explain these data. These concepts represent the learning bias used by the artificial learner to produce a decision function with the best generalization capabilities (Cormu ejols & Michet, 2002). Let O be a population of objects, X the description space associated with these objects and o an oracle capable of performing a categorization of objects from O , denoted by the function $f_o: O \rightarrow Y$. Let $f_d: O \rightarrow X$ a function that determines, for an object $o \in O$ gives, its description x . From O, Y, f_d and f_o it is possible to define the space of the examples Z . An example $z \in Z$ corresponding to an object $o \in O$ is a pair of data (x, y) such that $(x, y) = (f_d(o), f_o(o))$. In supervised learning, it is important to look for a function $f: X \rightarrow Y$ which allows one to estimate the class y associated with x . f belongs to the hypothesis space H . The ideal case corresponds to $f_o = f_d \circ f$. Figure 3.3 summarizes all these notions.

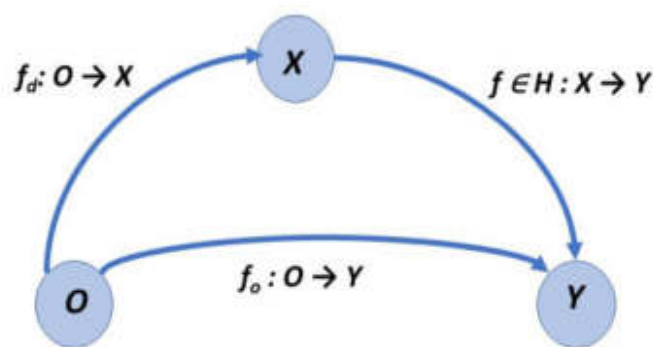


Figure 3.3 For a given learning problem, an object $o \in O$ representative of this problem is described by a vector of attributes $x \in X$ and is identified by the oracle o as a class $y \in Y$. In this diagram, f_d and f_o represent respectively the procedure performing the description of an object o and the decision-making process of the oracle o . The learner's objective is to choose a hypothesis $f \in H$ whose predictions are as close as possible to the oracle

3.4 Using of artificial neural networks and support vector machine for the identification problem

3.4.1 Identification using artificial neural network

3.4.1.1 Concepts

In recent decades, ANN has emerged as an active area of study. To construct a "standard" neural network, neurons must create real-value activations, and the neural networks must react as predicted by modifying the weights. However, depending on the nature of the issue, the process of developing a neural network might include lengthy causal chains of computing operations. Retro-propagation is a fast gradient descent approach that has been used in neural networks since 1980. It enables supervised learning to be used to train ANNs. Although the training accuracy is good, the performance of backpropagation on test data may be inadequate. Because retro-propagation is reliant on local gradient information with a random beginning point, the algorithm frequently gets stuck in local optima. Furthermore, if the amount of the training data is insufficient, neural networks will experience over-learning.

A formal neuron can be considered as an elementary modeling of a biological neuron (Figure 3.4). The neuron receives as input a vector of numerical attributes presenting the description of an observation \mathbf{x} , the elements of this vector x_i are weighted by synaptic weights w_i , a bias w_0 is also added. The y-output of the neuron is obtained by applying a transfer function also called activation function:

$$z = \sum_i^d w_i x_i + w_0, \quad y = f(z) \quad (3.1)$$

Identification Of Nosema Cells Using Microscopic Images

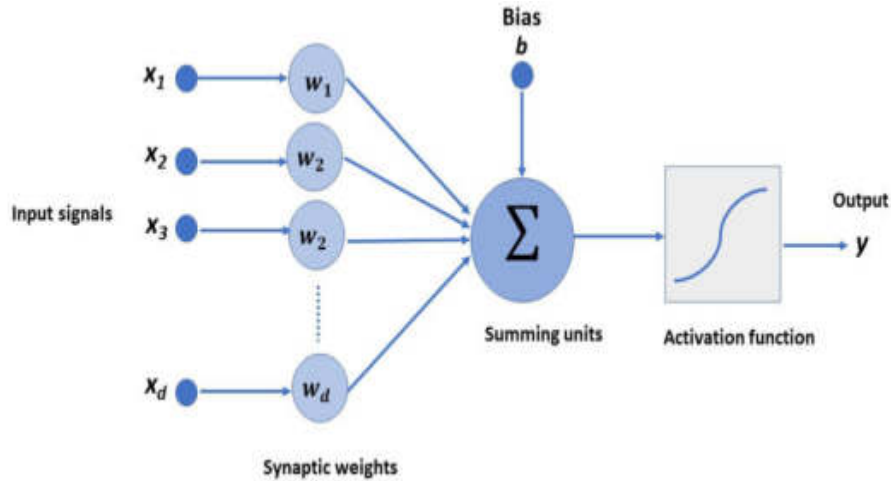


Figure 3.4 Artificial neuron

The artificial neural network (ANN) is a highly connected network of elementary processors (neurons) operating in parallel and having in layers. All neurons in the same layer have the same activation function. The learning of an ANN is most often done iteratively, by backpropagation of the error gradient, this very efficient learning algorithm gives an important boost to this classifier. The types of ANN are as numerous as their definition is general, they are distinguished globally by the function of activation of neurons (table 3-1), the architecture of the network (organized or not in layers, with or without cycles) and the mode of connectivity (fully or locally connected) (see Figure 3.5). In the next part, we will quickly introduce the two most popular types of activation function: the Multi-Layer Perceptron (MLP) and the Radial Basis Function (RBF) network.

Other types such as: convolutional networks, Kohonen map and polynomial networks are well described in (Touzet, 1992) and (Cheriet, Kharma, Lui, & Suen, 2007). An overview of the uses of Fuzzy Neural Networks (FNNs) in image processing is described in (Victor, 2020).

Table 3-1: Some common transfer functions, x is the input vector

Linear function	$\sum_i w_i \cdot x_i + w_0$	(3.2)
Sigmoid function	$\frac{1}{1+e^{-\lambda x}}$	(3.3)

Identification Of Nosema Cells Using Microscopic Images

Tanh function	$\frac{e^{2x}-1}{e^{2x}+1}$	(3.4)
Softmax function	$\frac{e^x}{\sum_i e^{x_i}}$	(3.5)
Radial basis function with center x_c	$exp\left[-\frac{\ x-x_c\ ^2}{2\sigma^2}\right]$	(3.6)

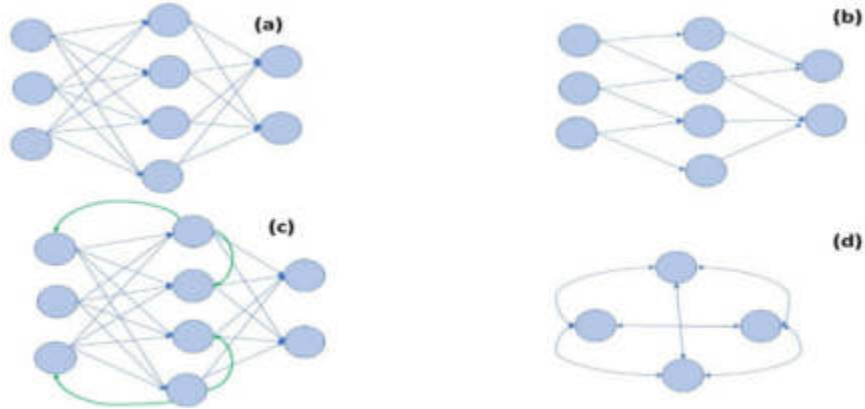


Figure 3.5 Different neural network topologies. (a) multilayer networks, (b) local connections, (c) with recurring connections, and (d) full connections

3.4.1.2 Activation functions

The activation function of a single-layer network may be used to push each neuron's output towards a binary rank. However, in multi-layer neural networks, the activation function is even more essential. Even a massive multilayer neural network with a nonlinear activation function would only have the representational capability of a linear classifier, given the composition of linear functions is a linear function. As a result, the activation function f is a nonlinear function applied to a neuron's output to enable multilayer networks to learn complicated nonlinear functions.

$$z = \sum_i^d w_i x_i + w_0, \quad y = f(z) \quad (3.7)$$

Where w_i is the input x_i weight, f is an activation function, and w_0 is the bias. This is commonly written more succinctly in matrix notation, where each neuron is made up of an input vector $\mathbf{x} = (x_0, \dots, x_N)$, a weight $\mathbf{w} = (w_0, \dots, w_N)$, and a bias $\mathbf{b} = w_0$, the output of which is,

Identification Of Nosema Cells Using Microscopic Images

$$y = f(w^T x + b) \quad (3.8)$$

Traditionally, in the study of neural networks, activation functions have been selected as sigmoid functions, that is, functions that translate negative inputs to negative outputs and positive inputs to positive outputs with a smooth transition around $a = 0$. This is a useful quality to have since the function still drives the network's outputs towards a binary ordering, the function is nonlinear (so the function's composition is not straightforward), and the function has well-defined gradients. The logistic function is an example of a regularly used sigmoid function:

$$f(a) = \frac{1}{1 + e^{-a}} \quad (3.9)$$

and the hyperbolic tangent,

$$f(a) = \tanh(a) \quad (3.10)$$

The fact that gradients are quite low in most of the function domain is one issue with sigmoidal activation functions. As a result, and in order to acquire superior empirical findings, current neural networks often employ the rectified linear unit (ReLU) activation function:

$$f(a) = \max(0, a) \quad (3.11)$$

3.4.1.3 Multi-layers perceptron

Multi-Layer Perceptron's (MLPs), also known as Feedforward supervised neural networks, are the quintessence of deep networks. These are parametric functions defined by the composition of many parametric functions. Each of these component functions has multiple inputs and multiple outputs. Multilayer perceptron are the most popular and simple neural networks. These are direct propagation networks without a cycle, with at least one hidden layer (Figure 3.6), the neurons are usually completely

Identification Of Nosema Cells Using Microscopic Images

connected, and the transfer function is sigmoid (value in $[0,1]$), tanh (value in $[-1,1]$) or SoftMax type.

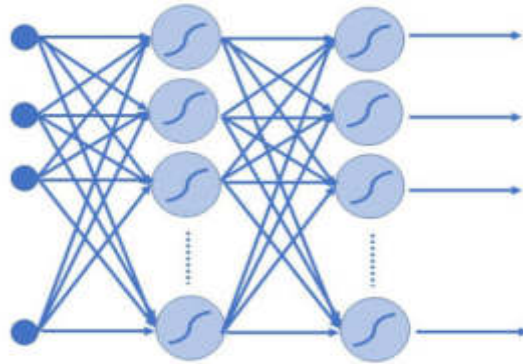


Figure 3.6 Multi-Layer Perceptron with a Single Hidden

In neural network terminology, we refer to each sub-function as a layer of the network, and each scalar output of one of these functions as a unit or sometimes as a characteristic. Even if each unit implements a relatively simple mapping or transformation of its input, the function represented by the entire network can become arbitrarily complex.

This classifier has discovered applications in many areas such as character recognition, face recognition, prediction and more. Its remarkable performance, robust generalization capabilities, and swift decision-making phase have all contributed to its widespread adoption. Nonetheless, its utilization is associated with a set of challenges (over-learning, local minima, etc.). A detailed description of these problems is given in (Parisia, Kemkerb, Part, Kanan, & Wermtera, 2019).

MLPs are also the key technology that underpins most contemporary business applications of deep learning for large data sets. Neural networks allow us to learn new types of non-linearity. Another way of looking at this idea is that neural networks allow us to learn the characteristics provided to a linear model. From this point of view, neural networks allow us to automate the design of features, a task that, until recently, was carried out gradually and collectively, thanks to the combined efforts of a whole community of researchers. MLPs have been among the first and most efficient of nonlinear learning algorithms (Rumelhart, Hinton, & Williams, 1986). These networks learn at least one function defining the characteristics, as well as a (typically linear) function for mapping the characteristics to the output. Layers in the network that match

Identification Of Nosema Cells Using Microscopic Images

characteristics rather than outputs are called hidden layers. This is because the correct values of the characteristics are unknown. The characteristics must be created by the learning algorithm. The input and output of the network are observed in the drive data. It should be noted that in the literature, DNNs can be confused with other deep learning models, but in most cases, DNNs refer to MLPs with more than one hidden layer.

3.4.1.4 *Number of hidden layers*

Research has demonstrated that neural networks with a minimum of one hidden (infinitely wide) layer are universal approximators. This signifies that such neural networks possess the theoretical capability to denote any function (Cybenko, 1989) and (Hornik, Stinchcombe, & White, 1989). This contrasts with the limits of neural networks that lack hidden layers. However, we discover that a network with just one hidden layer, even one with a very wide breadth, may learn to represent complicated functions just as effectively as networks with numerous hidden layers. Indeed, the discovery that networks that have several hidden layers, known as deep networks, continually outperform networks with only a few hidden layers, dubbed as shallow networks, represents a significant step forward in the improvement of neural network learning in recent years (Goodfellow, Bengio, & Courville, 2016).

3.4.1.5 *Radial Based Function*

RBF-like neural networks usually have a single hidden layer. The neurons in this layer are gaussian type and the neurons in the output layer are linear or any other function as for hidden markov model (HMMs). The learning of RBF neural networks is direct (Augustin, 2001), it consists in learning the parameters of the output layer by the gradient descent method. The characteristics of Gaussian neurons are usually estimated at the beginning of the training (most often, by the clustering method) and they will then be frozen. In (Augustin, 2001), Augustine presents a comparison between HMM and RBF networks, he indicates that RBF networks do not always behave well in high-dimensional spaces with redundant and noisy dimensions, a problem that HMM is supposed to solve better. Furthermore, the algorithm for training a Radial Basis Function (RBF) demands a greater number of parameters than that of a Hidden Markov Model (HMM) for achieving equivalent performance. Consequently, a larger dataset is required. Additionally, the

Identification Of Nosema Cells Using Microscopic Images

count of hidden neurons could escalate exponentially in tandem with the increase in dimensions. However, an RBF network models the probability distributions of shapes conditionally to classes, which is more information than modeling the only neighborhood of decision boundaries like does HMM.

3.4.1.6 Experimental methodology for artificial neural networks

In the chapter before, existent items in Nosema illness microscopic pictures were discovered and extracted (both Nosema cells and other kinds of cells present in microscopic images). Their images were automatically segmented for feature calculation (geometric, texture, and statistical features), and the result was given as a vector of the 19 most significant features.

As mentioned in the introduction, this chapter will focus on object classification between Nosema cells and non-Nosema cells, and a multilayer Neural Network system is the first approved tool for this purpose. To do this, the feature dataset DS2 is created once the features of the various objects have been retrieved. The DS2 has 38,000 values that represent 2000 pictures, each with 19 attributes that are distributed evenly between the two types of objects (Nosema objects/images and non-Nosema objects/images). This section of the task was quite computationally difficult, since the extraction of 2000 sub-images, together with the calculation of 19 characteristics for each picture, took several days of calculations on a CPU, namely a PcCom Basic Elite Pro Intel Core i7-9700/8GB/240SSD.

Neural networks were utilized in this part of the study to detect Nosema illnesses in honeybees automatically. The neural networks demonstrated their worth in a variety of real-world applications, including classification tests. A neural network is often composed of two sets of functionalities: the first set is used to train the NN model, while the second set of testing functionality is used to evaluate the correctness or validity of the trained NN model. In the learning phase, computational units are connected to one another through weights, which serve the same role as the strengths of synaptic connections in biological organisms. Each input to a neuron is scaled with a weight, which affects the function computed at that unit. The artificial neural network computes a function of the inputs by propagating the computed values from the input neurons to the output neuron(s) and using the weights as intermediate parameters. The connection

Identification Of Nosema Cells Using Microscopic Images

weights were constantly updated and changed until they achieved the specified repetition number or the tolerable error. Thereby, the ANN model's capacity to respond appropriately was assured by utilizing the mean squared error (MSE) criteria to improve the reliability of the model between input and network output.

As usual, during the experiment, the set of data was separated into two parts: learning and testing/validation of the model. The approved approach consists of conducting two experiments using the extracted features, and the goal of these two tests was to demonstrate the high presence of a yellow hue in Nosema's cell image. In the first one, the model was tested with only the first three kinds of extracted features (geometric, statistical, and texture features); that is, just 15 characteristics were used, not including the four yellow color features estimated using the GLCM. The second experiment was carried out by utilizing all 19 attributes. The studies were performed by varying the accuracy of the data split between training and testing data. The architecture of the applied Artificial Neural Network (ANN) comprised a singular hidden layer, with experimentation conducted on the count of neurons within this layer. Several repeats of the test (at least 30 times) were performed with each authorized hidden layer neuron number to get the ideal value of success recognition accuracy. Overall, the software was evaluated with a number of hidden layer neurons equal to the number of picture input characteristics retrieved (15 or 19), with weights inserted at random. The number of neurons in the hidden layer was then raised to 50 for the second test. The number of neurons was then raised by 50 in each successive trial until it reached 1800. Table 3-2 and Figure 3.7 further clarify the experimentation process.

A 10-cross-validation approach ranging from 10% to 90% for training and testing was used for statistical assessment. The output is a binary decision: [1 0] means a Nosema object, and [0 1] means a non-Nosema object.

Table 3-2: Experiments for Nosema recognition using a vector of 15 features/19 features: the initial number of neurons in the hidden layer is 15/19 equals to the number of features and the final number is 1800 equal to the maximum number of training data

Experiments for (15/19) Features		Number of Neurons in the Hidden Layer	Number of Experiment repetition
Training Data	Test Data		
10%	90%		

Identification Of Nosema Cells Using Microscopic Images

20%	80%	(15 o 19)->50->100->150->200- ----->500----->1000- ----->1700-- --->1750->1800	30 times repetition for every experiment
30%	70%		
40%	60%		
50%	50%		
60%	40%		
70%	30%		
80%	20%		
90%	10%		

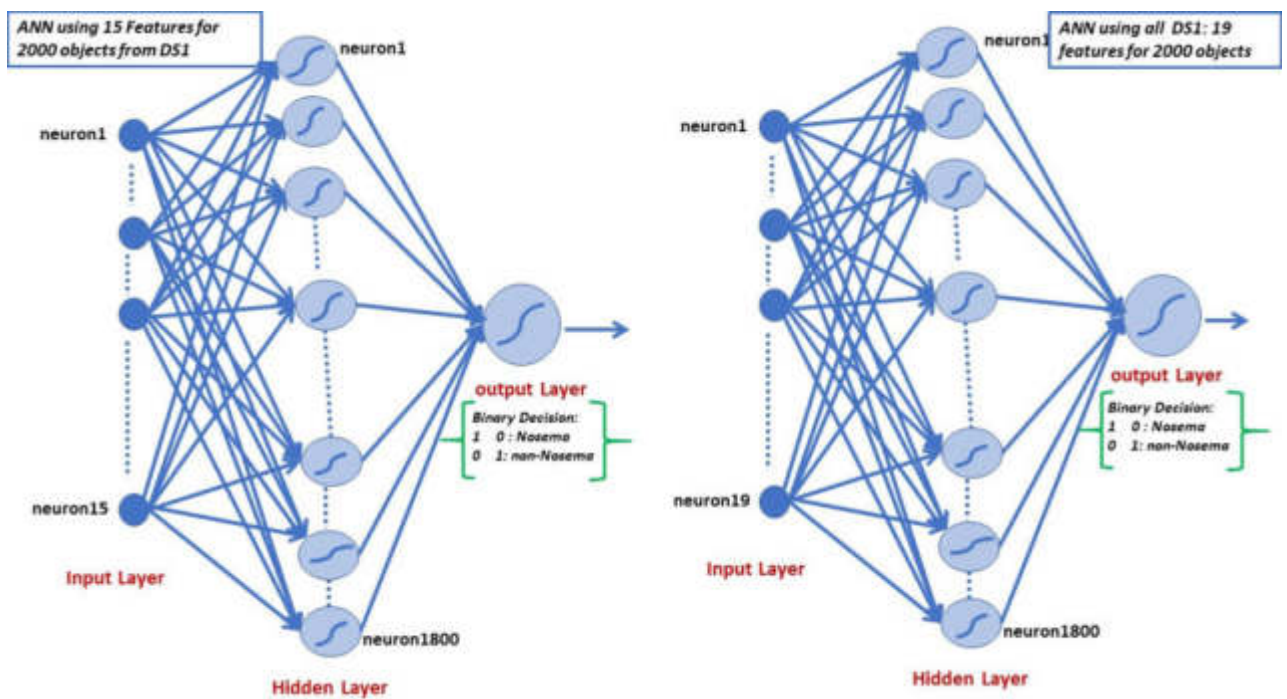


Figure 3.7 Implemented ANN for Nosema recognition

3.4.2 Identification using SVM

3.4.2.1 Concepts

Within the realm of kernel methods, and drawing inspiration from Vladimir Vapnik's statistical learning theory, the most renowned family is that of Support Vector Machines (SVM). (Cortes & Vapnik, 1995). SVMs are binary classifiers by supervised learning

Identification Of Nosema Cells Using Microscopic Images

intended to solve problems of discrimination or regression (prediction). This method relies on using a nonlinear transformation to redescribe the training data in a larger space. Nonlinearly separable data in initial space will therefore be simpler to separate in large space. The objective is thus to ascertain, within the new re-description space, a hyperplane that optimally separates the training data. This concept is referred to as the notion of maximum margin. For simplicity, taking the case of linearly separable data. In SVM, the line used to separate classes is called hyperplane.

The choice of the separator hyperplane is not obvious. There are indeed an infinite number of separator hyperplanes (see Figure 3.8), whose learning performance is identical, but the generalization performance can be very different.

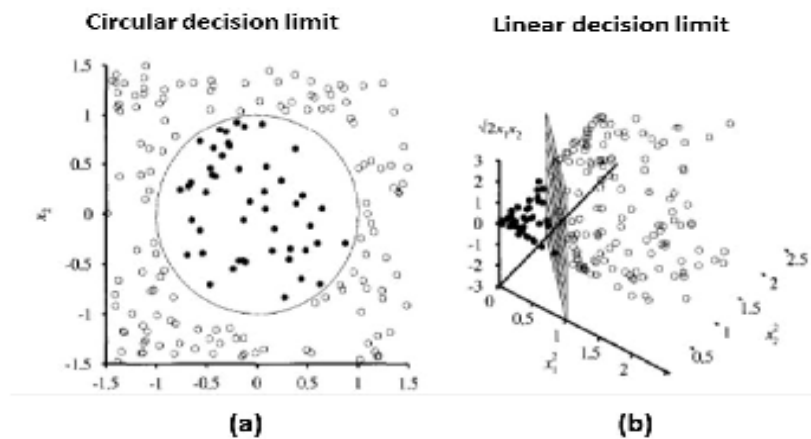


Figure 3.8 Basic principle of SVM (Russell & Norvig, 2011). (a) nonlinearly separable problem, the equation of the separator plane is $x_1^2 + x_2^2 \leq 1$ (7); (b) projection of the data in a three-dimensional space $(x_1^2, x_2^2, \sqrt{2}x_1x_2)$ (3.12)

To address this issue, it has been demonstrated that there is a single optimal hyperplane defined as the hyperplane that maximizes the margin between the samples and the separator hyperplane (Cortes & Vapnik, 1995) (Figure 3.8(b)). For this purpose, only the points located on the hyperplanes of maximum margins called support vectors participate in the definition of the optimal hyperplane (Figure 3.9).

In other words, only a small subset of data is needed for the calculation of the solution, the other samples do not participate in its definition. This is therefore effective in terms of complexity. On the other hand, changing or enlarging the training set has less influence than in Hidden Markov Model (HMM) classifier for example, where all the data

Identification Of Nosema Cells Using Microscopic Images

participates in the solution. Indeed, adding samples to the training set that are not support vectors has no influence on the final solution.

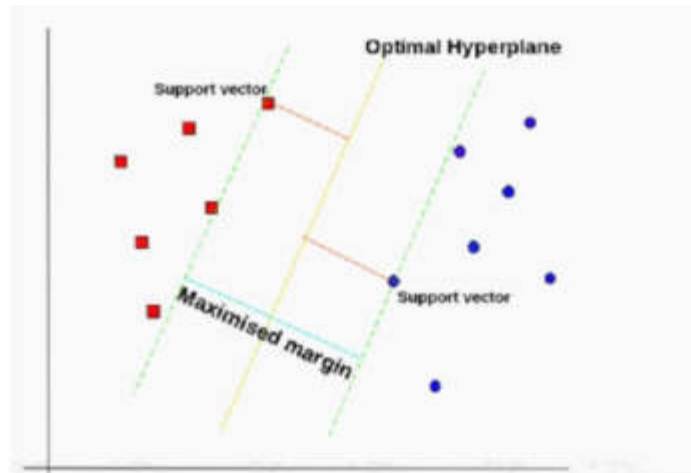


Figure 3.9 Notion of maximum margin, for a set of linearly separable points, there are an infinite number of separator hyperplanes; the optimal hyperplane (in yellow) with the maximum margin, the surrounded samples represent the supporting vectors.

For nonlinearly separable data, the idea of SVMs is to reconsider the problem in a higher-dimensional space, possibly infinite-dimensional. In this new space, it is then likely that there is a linear separation hyperplane. However, the problem that arises is the determination of this hyperplane in a very large space. The solution is to use the "kernel trick" to determine the hyperplane that optimally separates the data in a very large space without the need to redescribe the data in it (Cervantes, Lamont, Mazahua, & Lopez, 2020). This solution is much less expensive than a scalar product in the redescription space. Commonly used kernel functions are:

- linear kernel:

$$k(x, x_i) = x \cdot x_i \quad (3.13)$$

- Sigmoid kernel:

$$k(x, x_i) = \tanh(k \cdot (x \cdot x_i) + \theta) \quad (3.14)$$

- Nucleus polynomial:

$$k(x, x_i) = (k \cdot ((x \cdot x_i) + 1))^p \quad (3.15)$$

- RBF kernel:

$$k(x, x_i) = \exp \left[\frac{\|x - x_i\|^2}{2\sigma^2} \right] \quad (3.16)$$

Identification Of Nosema Cells Using Microscopic Images

K , θ , p , σ are parameters of the kernels, whose determination and the choice of the kernel function are the responsibility of the user because there is no proven guide for any use. However, the polynomial kernel (P_k) and the RBF kernel (RBFK) are listed in (Cheriet, Kharma, Liu, & Suen, 2007) as the most performant kernel types for pattern recognition applications. In (Cervantes, Lamont, Mazahua, & Lopez, 2020), authors compare two combination strategies: "one against one" and "one against all."

3.4.2.2 Experimental methodology for SVM

The SVM method operates based on features and tries to find a decision model. As the complexity of SVM increases with the size of the learning base, its direct application without special precautions is difficult for classification. Indeed, this work's pixel database is extensive and highly redundant due to the similarity of many pixels within the same class. While an SVM can yield favorable classification rates, its decision function will necessitate querying for the classification of a considerable number of pixels when aiming to classify the pixels within a new image. This can become very disabling if we want quick segmentation. Subsequently, the method for constructing decision functions with reduced complexities for object classification was implemented. Each decision function will be optimized independently. To determine the best model θ^* for each binary decision function, incorporating the desired settings for adjustment into this model is a requisite. To perform an object classification by a decision function, we used the data extracted in the previous chapter: 19 features for 2000 objects, which we introduced to our SVM model in the form of 38000 parameters. Then we selected the optimal hyperparameters by choosing the optimal values of C and θ after several tests as follows: $C = 3$ and $\theta = 5 \times 10^{-5}$.

3.5 Using of deep learning tools

3.5.1 Concepts

Deep learning emerged from research on artificial neural networks (ANN) (Geoffrey, Hinton, & Salakhutdinov, 2006). Authors developed a novel learning approach (named layer-wise-greedy-learning) in (Hinton, Osindero, & Teh, 2006), which marked the start of deep learning techniques. This algorithm's fundamental concept is based on unsupervised learning, which must be performed as a network pre-training step before

Identification Of Nosema Cells Using Microscopic Images

subsequent layer-by-layer learning. By extracting characteristics from the inputs, the size of the data is reduced, and a compact representation is obtained. Then, by exporting the characteristics to the next layer, all the samples will be labeled, and the network will be refined with the labeled data.

The popularity of deep learning can be attributed to two main factors: on the one hand, the development of large data analysis techniques indicates that the problem of overlearning of training data can be partially solved; on the other hand, the pre-training procedure before unsupervised learning will assign non-random initial values to the network. Therefore, a better local minimum can be achieved after the training process and a faster rate of convergence can be achieved. So far, deep learning research has received a lot of attention, and a number of intriguing outcomes have been discussed in the literature. Since 2009, the ImageNet competition has drawn a huge number of image-processing research organizations from academia and business across the world. Hinton's research group won the ImageNet competition in 2012 utilizing deep learning algorithms (Krizhevsky, Sutskever, & The, 2006). Hinton's group competed for the very first time, and its scores were 10% greater than those of second place. Google and Baidu have both modified their image search engines to include Hinton's deep learning architecture, which has resulted in significant gains in search accuracy. Baidu also founded the Institute of Deep Learning (IDL) in 2013 and appointed Andrew Ng, a Stanford University associate professor, as its head scientist. In March 2016, Google's deep learning team (named DeepMind) staged a Go Game match in South Korea between the ALPHAGO AI player and one of the world's greatest players, Lee Se-dol (Silver & al., 2016). AlphaGo, which used deep learning algorithms, demonstrated startling strength and defeated Lee Se-dol by a factor of four. Deep learning algorithms have also demonstrated an excellent ability to forecast the activity of new therapeutic compounds as well as the impact of non-coding DNA alterations on gene expression. With the fast growth of computational methods, ANN with deep architectures for supervised learning has given a strong framework. The deep learning method, overall, is made up of a hierarchical design with several layers, each of which is a nonlinear information processing unit. In this chapter, we will go through the deep architectures that we have employed in our research.

Identification Of Nosema Cells Using Microscopic Images

3.5.2 Convolutional Neural Network

3.5.2.1 *Concepts and history*

Convolutional CNNs are deep learning models that have demonstrated excellent performance in the processing of two-dimensional data with grid topologies, such as photos and movies (Arel, Rose, & Karnowski, 2010). CNN architecture is inspired on the arrangement of animal visual cortex. Hubel and Wiesel (Hubel & Wiesel, 1960) introduced the notion of receptive fields in the 1960s. They revealed that the intricate cell configurations were included in the animal visual cortex, which is in charge of detecting light in overlapping and tiny subregions of the visual field. Furthermore, the Neocognitron computational model with hierarchically ordered picture transformations was introduced in (Kunihiko,-Fukishima, & Miyales, 1982). However, the Neocognitron differs from CNN networks in that it does not require a shared weight. The concept of CNN networks is inspired by time delay neural networks (TDNN). In a TDNN network, weights are shared in a time dimension, resulting in a reduction in calculations. In CNN networks, convolution has replaced general matrix multiplication in standard neural networks. In this way, the number of weights is reduced, which decreases the complexity of the network. In addition, the images, as raw inputs, can be imported directly into the network, thus avoiding the procedure of extracting characteristics in the standard learning algorithms. It should be noted that CNN networks are the first truly successful deep-learning architecture thanks to the effective learning of hierarchical layers. CNN network topology exploits spatial relationships to reduce the number of parameters in the network, and performance is therefore improved by using standard backpropagation algorithms. Another advantage of the CNN model is that it requires minimal pre-processing. With the rapid development of computational techniques, GPU-accelerated computing techniques have been exploited to train CNNs more efficiently. Today, CNNs have already been successfully applied to handwriting recognition, face detection, behavior recognition, speech recognition, recommendation systems, image classification, and natural language processing.

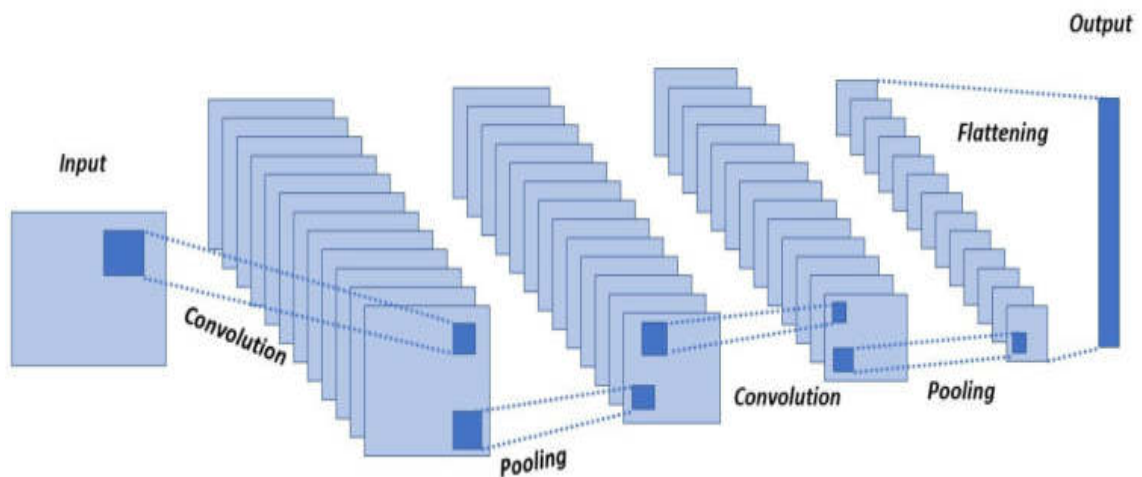


Figure 3.10 A diagram of the convolutional neural network. (The depth of the matrices represents the number of used filters. The size of the output vector is determined after flattening the matrices of the previous layer and concatenating the resulting vectors.)

The absence of contact, the exchange of parameters, and equivocal representation all play important roles in the training process of a CNN (Gonzalez & Wood, 1993). Unlike traditional neural networks where the relationship between input and output units is derived by matrix multiplication, CNN networks reduce computational overhead through low interaction where kernels are made smaller than inputs and used for the entire image. The basic idea of sharing parameters is that instead of learning a separate set of parameters at each location, we only need to learn one set of these parameters, which implies better CNN performance. Parameter sharing has also given CNN an attractive property called equivariance, which means that every time the input changes, the output changes in the same way. As a result, fewer parameters are needed for CNN compared to other traditional neural network algorithms, resulting in a reduction in memory and an improvement in efficiency. A conceptual diagram of a standard CNN is shown in Figure 3.11.

Identification Of Nosema Cells Using Microscopic Images

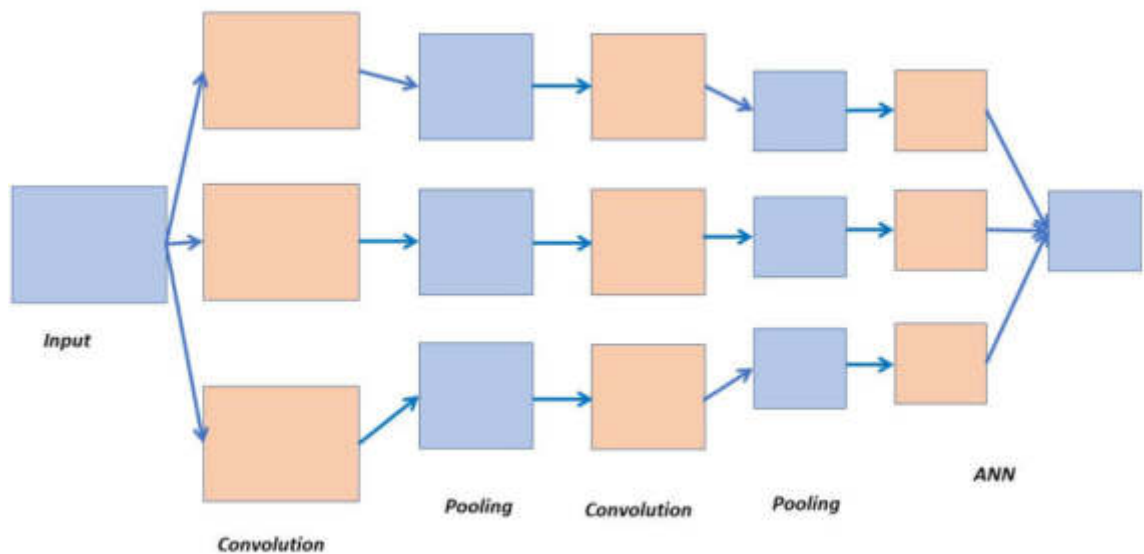


Figure 3.11 A conceptual diagram of the convolutional neural network using three filters.

As shown in Figure 3.11, CNN is a multilayer neural network that consists of two different types of layers, namely convolution layers and pooling layers (Krizhevsky, Sutskever, & The, 2006), (Goodfellow, Bengio, & Courville, 2016), and (Deng, 2012). The convolution and pooling layers are connected alternately and form the central part of the network. In the first convolution layer, the input picture is convoluted using filters that may be learned at all conceivable offsets to yield feature maps, as illustrated in Figure 3.10. Each filter contains a connection weight layer. Typically, four feature map pixels make a group. These pixels generate extra feature maps in the first pooling layer after passing through a sigmoid function. This method is repeated until we have the feature maps in the subsequent convolution and subsampling layers. Finally, the pixels' values are simplified into a single vector that will be used as input to the MLP network (Arel, Rose, & Karnowski, 2010).

Convolution layers are often employed to extract features when the input of each neuron is connected to the preceding layer's local receptive field. After obtaining all of the local features, the position connection between them may be calculated. A subsampling layer is required for feature mapping. These weighted feature mapping layers create a plane. Because of its minor impact on the function's core, the sigmoid function is chosen as the activation function to provide scale invariance. It must

Identification Of Nosema Cells Using Microscopic Images

additionally be mentioned that the filters in this model link a series of overlapping receptive fields and turn the 2D picture batch input into a single unit in the output. However, when the dimension of the inputs is equivalent to the dimension of the filter output, it will be difficult to preserve translation invariance with more filters. Using a classifier might result in over-learning due to the high dimensionality. To address this issue, a pooling procedure known as subsampling is used to minimize the total size of the signal. Subsampling has already been used successfully in audio compression to reduce data size. Subsampling was also employed in the 2D filter to improve position invariance.

A CNN's training technique is identical to that of a normal neural network, which uses retro-propagation. (Bengio, 2009) used an error gradient to generate CNNs. The information is pushed forward through multiple levels in the first stage. By adding digital filters to each layer, the main features are obtained. After that, the output values are computed. The error over the predicted values and the actual value of the output is computed in the second phase. Subsequently, the weight matrix is fine-tuned to minimize this error, leading to the refinement of the network. In contrast to other conventional image classification algorithms, CNNs don't often necessitate pre-processing. It is sufficient to train the filters in CNNs rather than establishing parameters, as is the case with classic neural networks. Furthermore, CNNs are independent of past information and human influence in the extraction of attributes. The max-pooling approach for subsampling was proposed in LeNets in 1998 (Lucun, Bottou, Bengio, & Haffner, 1998). A pooling function is used to substitute the network output at a certain point by summing the statistics of the neighboring outputs. We may acquire the maximum output in a rectangle neighborhood by using the max-pooling approach. The pooling approach can also make the representation insensitive to input translations. Adding a max-pooling layer between convolutional layers now enhances spatial abstraction as feature abstraction grows. Pooling, as indicated in (Boureau, Ponce, & Lecun, 2010), is used to achieve invariance in picture modifications. This method allows for increased noise resilience. It is stated that the performance of the various pooling methods is dependent on numerous parameters, such as the resolution at which the low-level components are retrieved and the linkages between the sample's cardinalities.

Identification Of Nosema Cells Using Microscopic Images

Boureau (Boureau, Le Roux, Bach, Ponce, & Lecun, 2011) discovered that while the traits are highly varied, they may be grouped together as long as their locations are near. Furthermore, it has been observed that doing the pooling before to the pooling phase results in improved performance. It is demonstrated by (Jia, Huang, & Darrell, 2012) that greater pooling performance may be obtained by learning receptive fields in a more adaptable way. Particularly an efficient learning algorithm based on an incremental selection of features is presented to accelerate the training process utilizing the idea of over-skill.

3.5.2.2 Experimental methodology:

The CNN architecture employed consists of three distinct blocks. The first convolutional block comprises two convolutional layers with kernel $3 \times 3 \times 32$ filters, an activation layer ReLU, and a batch normalization layer (batch_normalization) to standardize the inputs. To speed up the training process and improve the performance of the CNN, we applied a 2×2 max_pooling and dropout layers technique to randomly disconnect nodes from the current layer to the next layer to decrease overfitting. As a result, increasing the number of filters deepens the network. The second block contains one convolutional layer with $3 \times 3 \times 64$, followed by ReLU and batch normalization. The third block includes one convolutional layer with $3 \times 3 \times 64$, followed by max_pooling and dropout layers. Table 3-3 shows the architecture utilized for an 80×80 input picture of three RGB channels. This architecture is described in Figure 3.12.

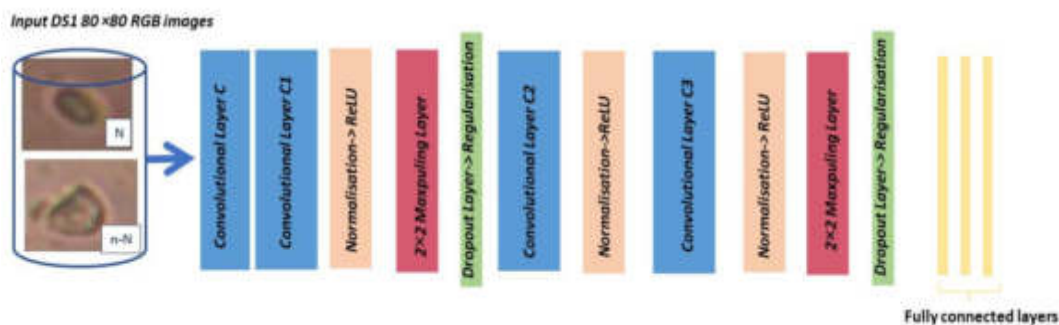


Figure 3.12 Implemented CNN for Nosema Recognition

Table 3-3: CNN experiment Values for an 80 × 80 input image

Layer Type	Output Shape	Number of Parameters
conv2d (Conv2D)	(None, 80, 80, 32)	896
batch_normalization (BatchNo)	(None, 80, 80, 32)	128
conv2d_1 (Conv2D)	(None, 80, 80, 32)	9248
batch_normalization_1 (Batch)	(None, 80, 80, 32)	128
max_pooling2d (MaxPooling2D)	(None, 80, 80, 32)	0
dropout (Dropout)	(None, 80, 80, 32)	0
conv2d_2 (Conv2D)	(None, 80, 80, 64)	18,496
batch_normalization_2 (Batch)	(None, 40, 40, 64)	256
conv2d_3 (Conv2D)	(None, 40, 40, 64)	36,928
batch_normalization_3 (Batch)	(None, 40, 40, 64)	256
max_pooling2d_1 (MaxPooling2)	(None, 40, 40, 64)	0
dropout_1 (Dropout)	(None, 40, 40, 64)	0

3.5.3 The use of Transfer learning architectures

3.5.3.1 Concepts

Transfer Learning refers to the set of methods that allow the transfer of knowledge acquired from the resolution of given problems to deal with another problem.

With the ascent of Deep Learning, Transfer Learning has achieved remarkable success. Frequently, models employed in this domain demand extensive computation time and substantial resources. However, using pre-trained models as a starting point, Transfer Learning makes it possible to quickly develop high-performance models and effectively solve complex problems in Computer Vision or Natural Language Processing, NLP (Lezory & Cardot, 2002).

Transfer learning corresponds to the ability to use existing knowledge, developed for the solution of given problems, to solve a new problem. Transfer Learning is based on a simple idea, that of re-exploiting the knowledge acquired in other configurations (sources) for the solution of a particular problem (target), (Figure 3.13).

Identification Of Nosema Cells Using Microscopic Images

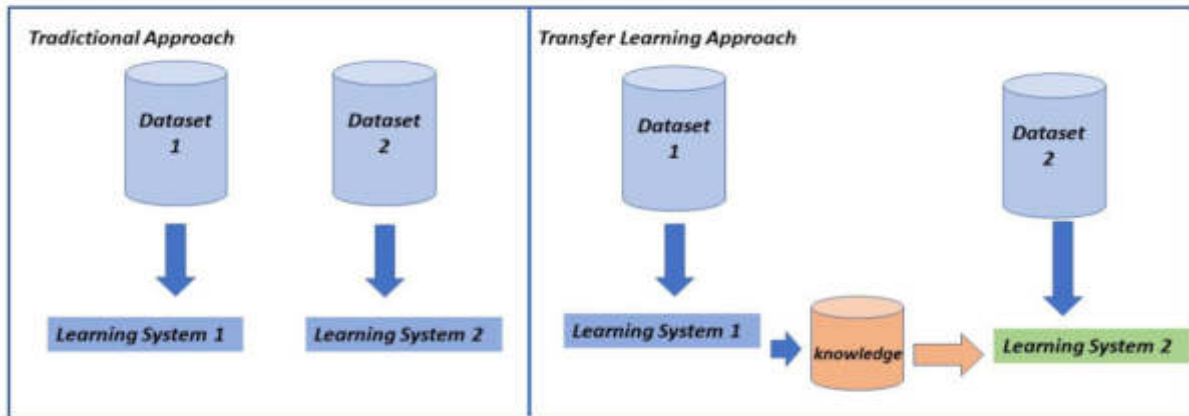


Figure 3.13 Traditional approach vs. Transfer learning approach

A domain D is defined by two parts: a feature space X and a marginal probability distribution $P(X)$, where $X = \{x_1, \dots, x_n\} \in Y$, where Y is the possible features of the space. Let's say D_S is the source domain, D_T is the target domain, T_S is the source task, T_T is the target task, and (f) is the predictive function. Transfer learning improves the target predictive function $(f)_T$ by using the related information from D_S and T_S , where $D_S \neq D_T$ or $T_S \neq T_T$. The single source domain defined here can be extended to multiple source domains. Given the definition of transfer learning, since $D_S = \{Y_S, P(X_S)\}$ and $D_T = \{Y_T, P(X_T)\}$, the condition where $D_S \neq D_T$ means that $Y_S \neq Y_T$ and/or $P(X_S) \neq P(X_T)$. The case where $Y_S \neq Y_T$ concerning transfer learning is defined as heterogeneous transfer learning. The case where $Y_S = Y_T$ concerning transfer learning is defined as homogeneous transfer learning. Heterogeneous transfer learning occurs when the source software project has different metrics (features) than the target software project. Alternatively, homogeneous transfer learning occurs when the software metrics are the same for the source and the target software projects. Continuing with the definition of transfer learning, the case where $P(X_S) \neq P(X_T)$ means the marginal distributions in the input spaces are different between the source and the target domains. Shimodaira (Zhuang et al., 2021) demonstrated that a learner trained with a given source domain will not perform optimally on a target domain when the marginal distributions of the input domains are different.

In this context, many techniques may be identified based on what one desires to transfer, when, and how the transfer should be carried out. Overall, there are three forms of Transfer Learning:

Identification Of Nosema Cells Using Microscopic Images

➤ **Inductive Transfer Learning**

The source and target domains are the same (same data) in this arrangement, while the source and target tasks are different yet nearby. The objective is to leverage current models to minimize the scope of prospective models' applications (model bias).. For example, it is possible to use a trained model for the detection of animals on images to build a model capable of identifying dogs.

➤ **Unsupervised Transfer Learning**

The source and target domains are comparable, as in inductive transfer learning, but the tasks are not. However, neither domain's data is labeled.

It is frequently faster to get huge volumes of unlabeled data, such as through databases and web-based sources, than labeled data. As a result, there is a lot of interest in the notion of combining unsupervised learning with transfer learning.

As an example, self-taught clustering is an approach that allows you to cluster small collections of unlabeled target data, with the help of a large amount of unlabeled source data. This approach is more efficient than the state-of-the-art approaches traditionally used when the target data is labeled in an irrelevant way.

➤ **Transductive Transfer Learning:**

The source and target tasks are comparable in this design, but the related domains differ in terms of data or marginal probability distributions.

For instance, the NLP models used for morpho-syntactic word tagging, Part-Of-Speech Tagger (POS Tagger), are often trained and evaluated using Wall Street Journal news data. They can be tailored to data from social networks, which material differs but is similar to that of newspapers.

3.5.3.2 Transfer learning resolves deep learning problems

These models, in general, relate to high-performance algorithms that have been created and trained on huge databases and are now openly available. We can differentiate two tactics in this context:

3.5.3.2.1 Using pre-trained models as feature extractors

Deep learning models frequently use a tiered stack of neurons as its architecture. Depending on the level at which they are positioned, these layers learn distinct

Identification Of Nosema Cells Using Microscopic Images

properties. In the case of supervised learning, the last layer (typically a fully linked layer) is employed to obtain the final output. As a result, the goal is to reuse a pre-trained network without its final layer. This new network then serves as an extractor of fixed characteristics for the accomplishment of additional tasks. In our case we will use the second strategy that will be described in the following paragraph.

3.5.3.2.2 Adjusting pre-trained models

This is a more complex technique, in which not only is the last layer replaced to perform classification or regression, but other layers are also selectively re-training. Indeed, deep neural networks are highly configurable architectures with various hyperparameters. In addition, while the first layers capture the generic characteristics, the last layers focus more on the specific task at hand.

The concept is thus to immobilize (i.e., fix the weights) of certain layers during training and refine the rest to answer the problem. This strategy makes it possible to reuse knowledge in terms of the overall architecture of the network and to exploit its states as a starting point for training. It therefore makes it possible to obtain better performance with a shorter training time.

The figure below summarizes the main transfer learning approaches commonly used in deep learning.

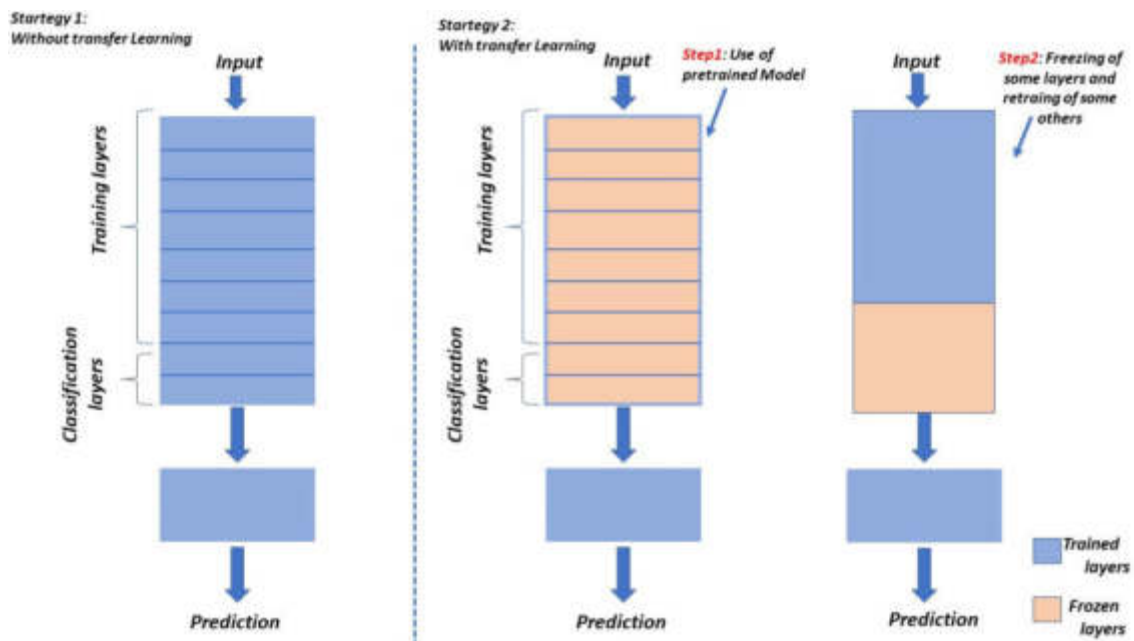


Figure 3.14 Deep transfer learning approach

Identification Of Nosema Cells Using Microscopic Images

ImageNet is a database of images freely accessible (under conditions) online. This database contains 14 million images divided into 1000 categories. Since 2010, a machine learning competition has been ongoing, dedicated to assessing the most effective image processing algorithms using the ImageNet dataset. The name of this competition is ILSVRC. Since 2012, the year of the first convolutional deep neural network (AlexNet), all the winners have been using Deep Learning. Testing the new neural network architectures on the ImageNet dataset is customary. This is precisely what Microsoft accomplished with their architecture known as ResNet (He, K. & al.). ResNet networks perform very well on ImageNet (>93%). There are several variations of ResNet(s) depending on their depth. The teams that created ResNet made their work and results generally available. This allows us to benefit from it to do transfer learning.

Hence, ResNet allows everyone to leverage its capabilities for image classification without requiring millions of images or extensive computational efforts.

For simplicity, replace the last layer(s) of the ResNet network with a layer dedicated to your problem and train the network on your data while keeping (in part) the weights calculated by ResNet. ResNet is one of many architectures that can benefit from it. Many others exist, such as AlexNet, Xception, VGG16, VGG19, ... DenseNet, NASNet and all trained-on ImageNet.

3.5.3.3 Application of transfer learning in the real world

The deep-learning-based approaches such as (Long, Cao, Wang, & Jordan, 2015), (Sun & Saenko, 2016), (Ganin & Lempitsky, 2015), and (Ganin & al., 2016) are applied to solving image classification problems, Alzheimer detection by fine-tuning AlexNet architecture (Maqsood & al., 2019) and (Marcus, Fotenos, Csernansky, Moris, & Buckner, 2010). Also, they are widely applied to resolve problems in several domains like:

Medical applications: In (Shin & al., 2016) have refined the pre-trained deep neural network to solve computer-aided detection problems. In (Byra, & al., 2020) used transfer learning to help assess knee osteoarthritis. In (Tang, Du, Huang, Wang, & Zhang, 2019) active learning and domain adaptation technologies were combined for the classification of various medical data. Also, in (Zeng & al., 2019) transfer learning was used to automatically describe a patient's diagnosis.

Identification Of Nosema Cells Using Microscopic Images

Bioinformatics Applications: Transfer learning can be applied to facilitate biological sequence analysis by understanding the behavior of one organism and transferring it to the others organism like in (Schweikert, Ratsch, Widmer, & Scholkopf, 2008), it can also help on problems of organism classification like in (Huang, Smola, Gretton, Borgwardt, & Schölkopf, 2006) and (daumé III, 2007). In addition, transfer learning tool are widely used in gene expression analysis and association predictions between genes and phenotypes like in (Petegrosso, Park, Hwang, & Kuang, 2016), (Huang & Kuang, 2010), (Xu, Xiang, & Yang, 2010) and (Singh & Gordon, 2008).

Transportation applications: Transfer learning is applied in the field of transport in order to understand images of traffic scenes. in (Di & al., 2018) a solution has been proposed to solve the problem related to traffic images taken from a certain location and which often suffer from variations due to different weather and light conditions. Transfer learning is also applied to the task of modeling driver behavior. For example, in (Lu & al., 2020) an approach has been proposed to adapt the driver model in lane change scenarios. In (Liu, Lasang, Pranata, Shen, & Zhang, 2019) applied transfer learning to recognize driver poses. In (Wang, Zheng, Huang, & Ding, 2018) authors adopted a regularization technique using transfer learning for vehicle type recognition. Transfer learning can also be used for the detection of abnormal vehicle movements as in (Gopalakrishnan, Khaitan, Choudhary, & Agrawal, 2017) and (Bansod & Nandedkar, 2019).

A diverse array of applications has employed transfer learning to address prevailing issues, and we have aimed to highlight the most significant among them. In the context of identifying Nosema images, or more precisely, classifying images as either Nosema or non-Nosema, the selected architectures were AlexNet, VGG16, and VGG19. For these three architectures we will use the DS1 image database, we will fine-tune each model and then retrain it on our DS1, and finally show and discuss the results.

3.5.3.3.1 Fine-tuning AlexNet transfer learning model

3.5.3.3.1.1 Concepts

AlexNet, which was first proposed by Alex Krizhevsky & al. in the 2012 ImageNet Large Scale Visual Recognition Challenge (Krizhevsky, A. & al, 2017). It is a simple CNN

Identification Of Nosema Cells Using Microscopic Images

architecture that consists mainly of five convolutional layers: the first four layers are followed by the pooling layer and the fifth layer is followed by three fully connected layers (FCN). Figure 3.15 Describes the Architecture of AlexNet model.

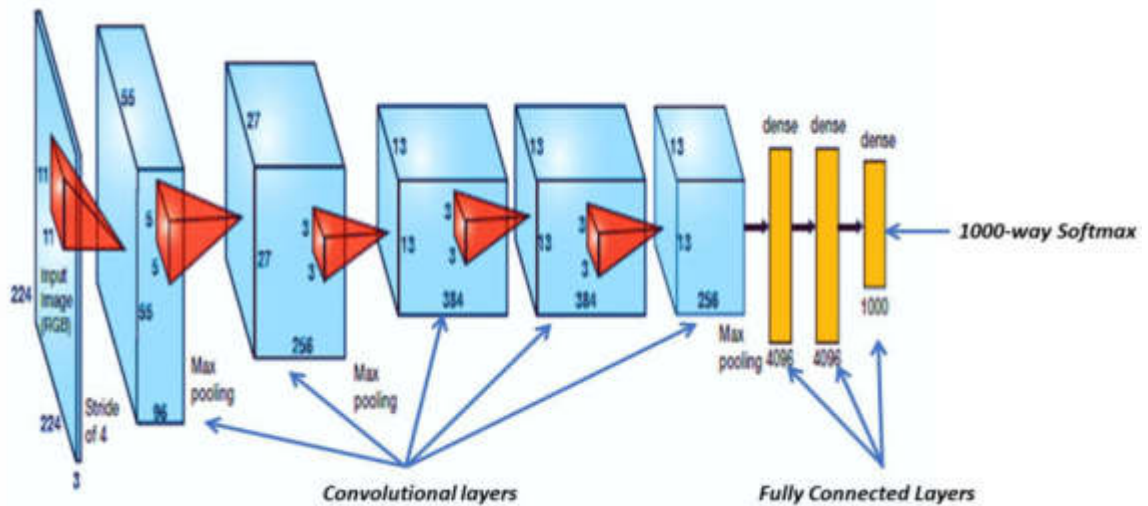


Figure 3.15 AlexNet Architecture

The non-linearity layer of ReLU is from the following equation:

$$f(x) = \max(x, 0) \quad (3.17)$$

It is a half-wave rectifier function, which can significantly accelerate the learning phase and avoid overlearning. The abandonment regularization technique consists of the stall that stochastically defines several input neurons or hidden neurons to zero to reduce the co-adaptations of neurons, which are typically used in fully connected layers of the AlexNet architecture. The ReLU non-linearity layer and the abandonment regularization technique are the reasons for AlexNet's success.

Identification Of Nosema Cells Using Microscopic Images

3.5.3.3.1.2 Experimental methodology for fine-tuned AlexNet model

AlexNet's model has 25 layers, includes over a million photos, and can categorize 1000 categories. To train this model on our dataset of images, the following steps were adhered to:

- 1-Partition of the input data into separate sets for training and validation. The dataset was divided into learning and validation sections based on four cross-validation folders.
- 2-The input data is organized into two labeled folders: the Nosema cell images class and the non-Nosema objects images class.
- 3-RGB images are automatically resized to 277×277 in the model augmentation phase since AlexNet only accepts this dimension of images.
- 4-The AlexNet pre-trained model's last three layers have been replaced: layer 23 with a fully connected layer, layer 24 with a softmax layer, and layer 25 with a classification output layer.
- 5-The last classification layer has been modified to identify two image classes, the Nosema class, and the non-Nosema class, instead of 1000 classes.
- 6-Finally, following the regularization of training options, a series of experiments were conducted to attain the optimal outcome.

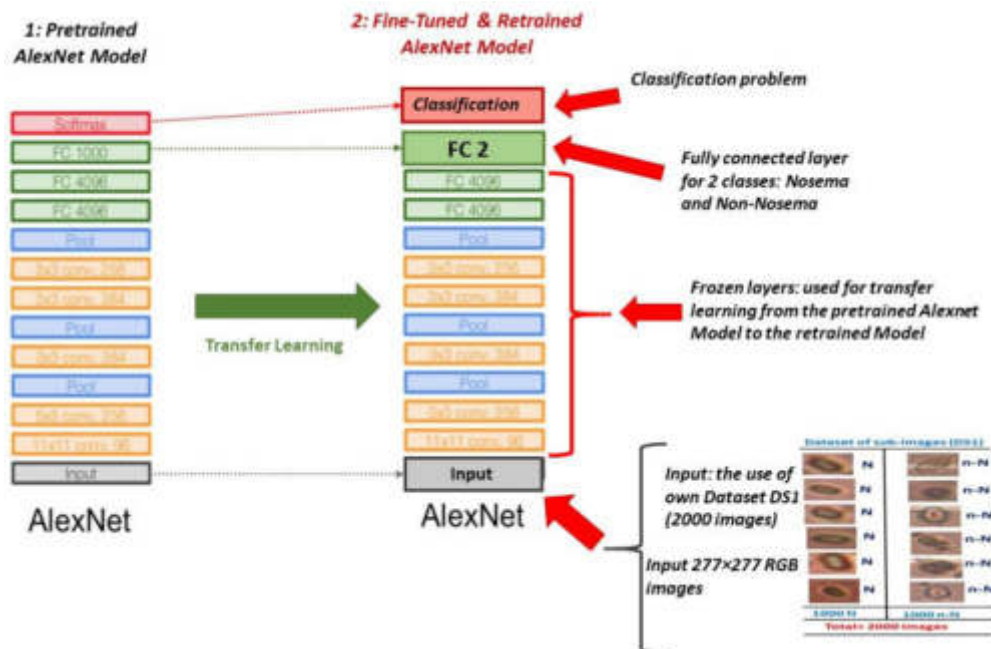


Figure 3.16 Fine-tuned AlexNet Model for DS1 images classification

Identification Of Nosema Cells Using Microscopic Images

Table 3-4 below illustrates the training options finally chosen to train AlexNet according to our images:

Table 3-4: *Experimental setting for retrained AlexNet model*

Model	Parameters	Setting Values
AlexNet	Learning algorithm	Sgdm
	Initial Learning Rate	0.001
	Mini-batchsize	64
	Maximum epochs	20

3.5.3.3.2 Fine-tuning VGG16 and VGG19 transfer learning models

K. Simonyan and A. Zisserman proposed VGG16 from the University of Oxford in the paper "Very Deep Convolutional Networks for Large-Scale Image Recognition." The model achieves 92.70% top-5 test accuracy in ImageNet. VGG-16 and VGG-19 are convolutional neural networks trained on more than one million images in the ImageNet database. Both networks possess the ability to classify images across 1,000 object classes. Furthermore, they share an image input size of 224 by 224 pixels. The concept of the VGG19 is the same as that of the VGG16, except that the VGG16 network has a depth of 16 layers, and the VGG19 has 19 layers. However, the two x-arrays of convolutional neurons are used to analyze the image object. The following image illustrates the general architecture of the VGG16 network. The VGG19 network follows a similar architecture, except for featuring three additional convolutional layers compared to VGG16.

Identification Of Nosema Cells Using Microscopic Images

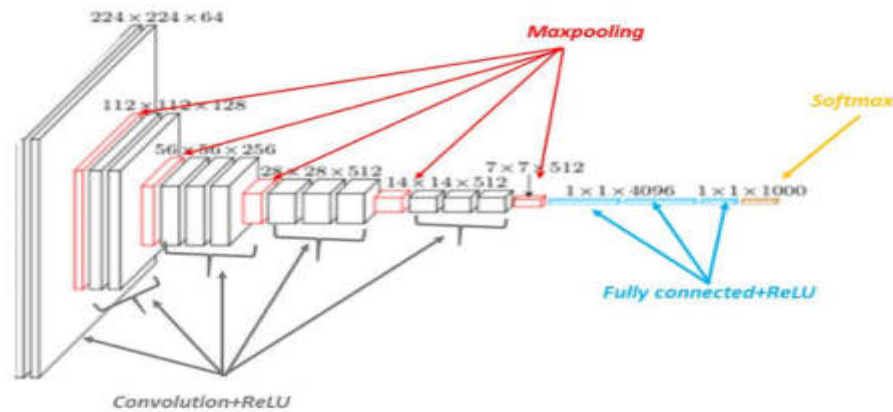


Figure 3.17 VGG16 Architecture

The fine-tuning procedures for both models mirror those of AlexNet, albeit with variations in terms of the input image types and the specific layers to be modified:

1-Partition the input data into two parts. The dataset was divided into learning and validation sections based on four cross-validation folders.

2-The input data is organized in two labeled folders: one for the images class of Nosema cells and the other for the images class of non-Nosema objects.

3-RGB or gray images are automatically resized to 224×224 in the model augmentation phase since VGG16 and VGG19 only accept this dimension of images.

4-For VGG16, the network contains a total of 41; layers numbers 39, 40, and 41 have been replaced by a fully connected layer that supports classification between two classes (Nosema classes and non-Nosema classes) and a classification output layer.

5-For VGG19, which contains a total of 47 layers, layer 45 has been replaced by a fully connected layer to classify two classes of objects, and layer number 47 (the softmax layer) has been replaced by a classification layer.

6-Finally, several experiments were carried out after the regularization of the training options to obtain the optimal result.

The following two figures (Figure 3.18 and Figure 3.19) describe the two models after their modifications.

Identification Of Nosema Cells Using Microscopic Images

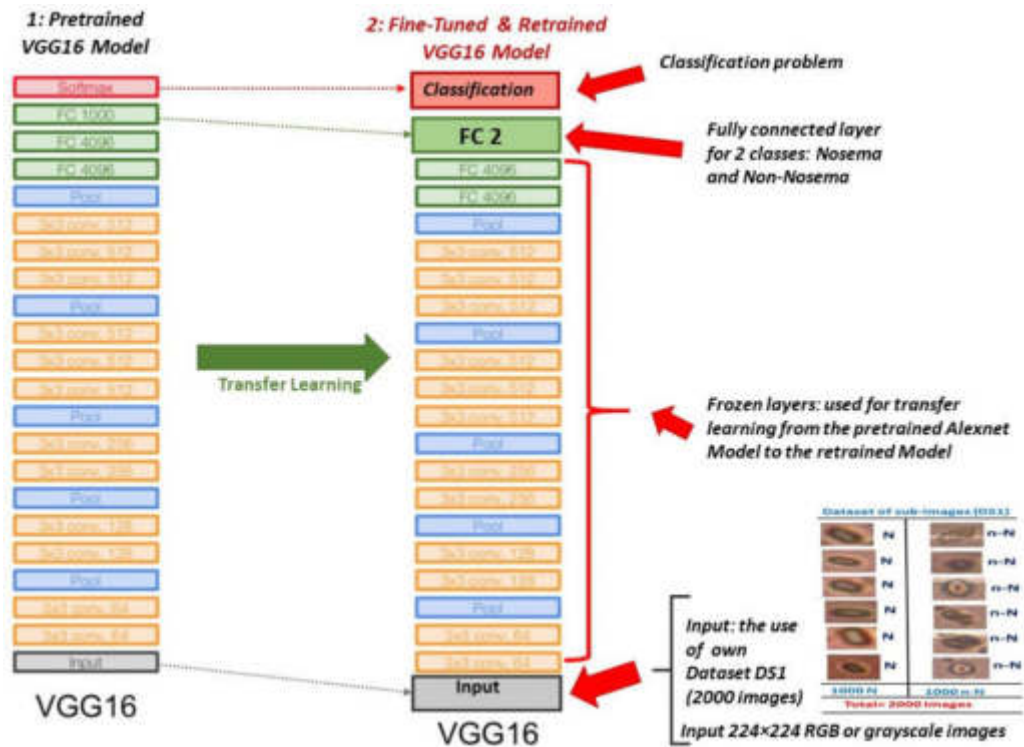


Figure 3.18 The Fine-Tuned VGG16 Model for Nosema Recognition

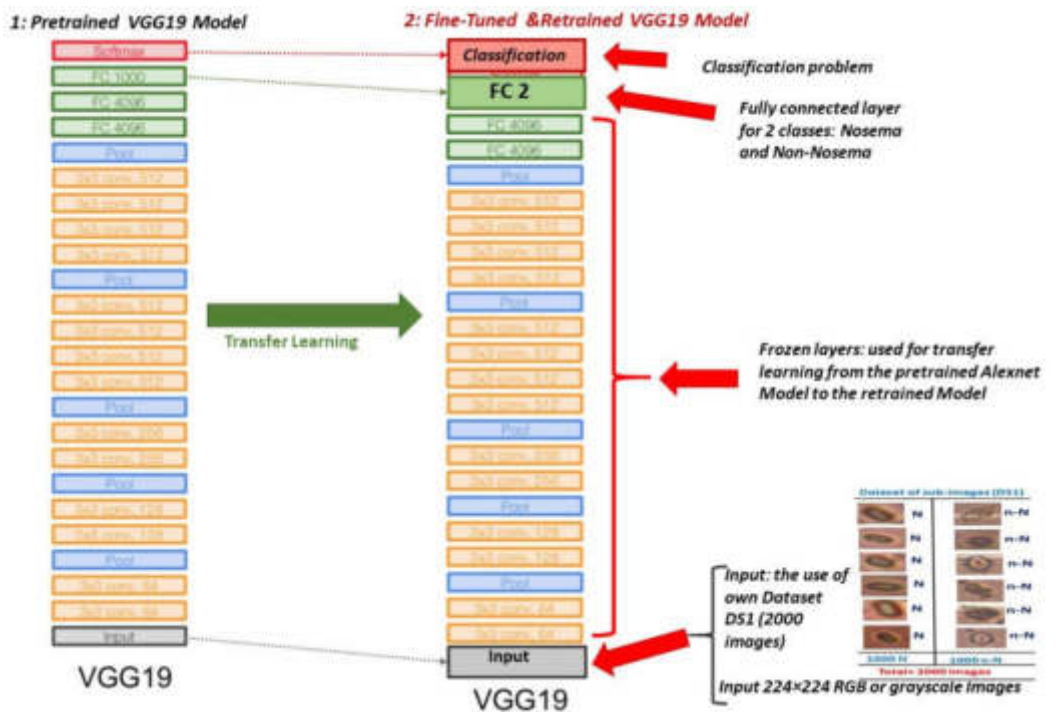


Figure 3.19 The Fine-Tuned VGG19 Model for Nosema Recognition

Table 3-5 below describes the choice of training parameters of two models.

Identification Of Nosema Cells Using Microscopic Images

Table 3-5: Experiment for VGG16 and VGG19 fine-tuned models

Model	Parameters	Setting Values
VGG-16 and VGG-19	Learning algorithm	Adam
	Initial Learning rate	0.0004
	Mini-batch size	10
	Maximum epochs	25
	Validation Frequency	3
	Validation Information	Test-Images

3.6 Recognition result

Next, the detailed description of our classification approach is in the preceding part; the next section will disclose the results of its application on the DS1 and DS2 datasets.

This chapter aims to compare the outcomes of traditional approaches to classification methods with those provided by sophisticated transfer learning techniques. The presentation begins with the results of applying ANN and SVM based on the computed characteristics of DS1 and the results of CNN and the re-trained models AlexNet, VGG16, and VGG19 based on DS2 pictures. The results of the authorized classification techniques will then be shown and examined.

3.6.1. Results of classification with ANN and SVM: The use of DS1

The use of the DS2 characteristics database for object classification was made using two strategies. The first technique involves testing the 15 geometric, static, and textural characteristics without considering the four yellow color features generated by the GLCM, whereas the second consists of trying all 19 characteristics. This procedure aims to demonstrate the significant presence of a yellow hue within Nosema cells. This validates the rationale behind calculating the GLM features for this specific color from the outset. The results of the two classifiers, ANN and SVM, are presented in Table 3-6 below.

Table 3-6: Best recognition results given by ANN and SVM

Number of Features	Classifier	Accuracy	Observation
15 Features	ANN	79.00%	For 1400 neurons in the hidden layer
	SVM	81.00%	Using kernel RBF
19 Features	ANN	83.20%	For 1400 neurons in the hidden layer
	SVM	83.50%	Using kernel RBF

Identification Of Nosema Cells Using Microscopic Images

It is worth noting that the results produced by combining all of the estimated characteristics (19 features) outperform those obtained by the 15 features. Furthermore, around 1400 neurons in the neural network's buried layer provide the best results for all studies. Indeed, the precision of the outcome is improved by utilizing GLCM properties of the yellow hue.

Figure 3.20 depicts the ANN's most excellent accuracy in a confusion matrix (Dghim, Travieso-González, Dutta, & Hernández, 2020).

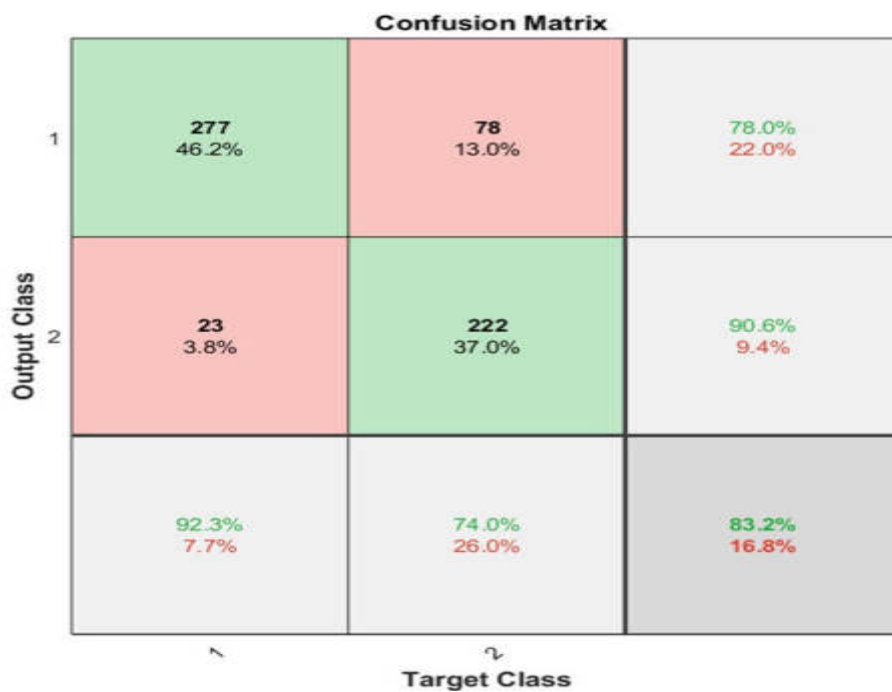


Figure 3.20 Best result accuracy given by the implemented ANN

3.6.2. Results of classification with CNN and transfer learning: the use of DS2

3.6.2.1. CNN result

CNNs had an accuracy rate of 92.50%. It outperforms the ANN and SVM techniques. The first block differentiates this type of neural network since it works as a feature extractor. It does this by incorporating convolutional filtering algorithms with template matching.

Identification Of Nosema Cells Using Microscopic Images

The first layer filters the image with numerous convolution kernels and creates "feature maps" normalized through an activation function (see Figure 3.21).

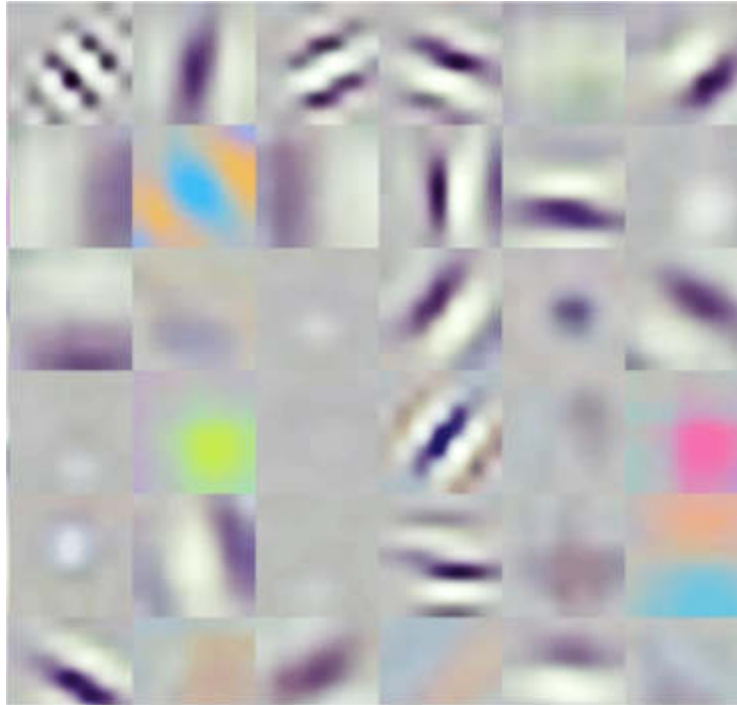


Figure 3.21 Example of the output of the first layer

This operation can be repeated as many times as necessary: the feature maps obtained with new kernels are filtered, providing new feature maps for normalization and resizing. These can then be filtered further, resulting in a recurrent cycle. Finally, the latest feature map values are concatenated into a vector. This vector determines the first block's output and the second block's input.

The second block lacks distinguishing CNN characteristics: It is usually found near the end of all neural networks used for classification. The values of the input vector are changed (through numerous linear combinations and activation functions) to generate a new output vector. This final vector has as many components as classes; the element i represents the probability that the image belongs to class i . As a result, each element is between 0 and 1, and the total is 1. The last layer of this block (and hence of the network) computes these probabilities as an activation function using a logistic function (binary classification) or a SoftMax function (multi-class classification).

Identification Of Nosema Cells Using Microscopic Images

The parameters of the layers, like those of ordinary neural networks, are determined using gradient backpropagation; cross-entropy is reduced during the training phase. However, in the case of CNNs, these parameters are particular to picture properties.

3.6.2.2. Transfer learning results

3.6.2.2.1. Result for AlexNet

The findings achieved after applying the transfer learning methods to categorize two sorts of objects or Nosema object recognition, are presented in the table below. Table 3-7 provides the most significant findings, i.e., those with the highest occurrences, which are as follows: 50%, 60%, 70%, and 80% for training and the others for testing.

Table 3-7: Best classifications results for AlexNet fine-tuned classifier

Trained Data	Validation Data	Accuracy	Epochs Number
0.5	0.5	84.58%	6
0.6	0.4	83.98%	6
0.7	0.3	86.98%	6
0.8	0.2	85.28%	6

The experiment using 70% training data and 30% validation data, and a number of epochs equal to 6 yields the best accuracy result, as shown in table 3-7. The number of epochs was increased in the following experiment. However, six epochs consistently delivered the best accuracy.

3.6.2.2.2. Results for VGG16 and VGG19

The findings of the retrained VGG16 and VGG19 models for the three most significant trials are shown in Tables 3-8. The best accuracy attained by a VGG16 fine-tuned model is 96.25% when the data is divided into 80% for training and 20% for testing, as shown below.

Table 3-8: Best classifications results for VGG16 and VGG19 fine-tuned classifiers

Experiments	Epochs	Accuracy	
		VGG-16	VGG-19
0.7	6	76.29%	71.95%
	6	92.50%	93.00%
08	12	94.50%	82.00%
	20	96.25%	92.32%
	25	93.00%	93.50%
0.9	6	88.00%	77.00%

Identification Of Nosema Cells Using Microscopic Images

These findings are depicted in the figures below:

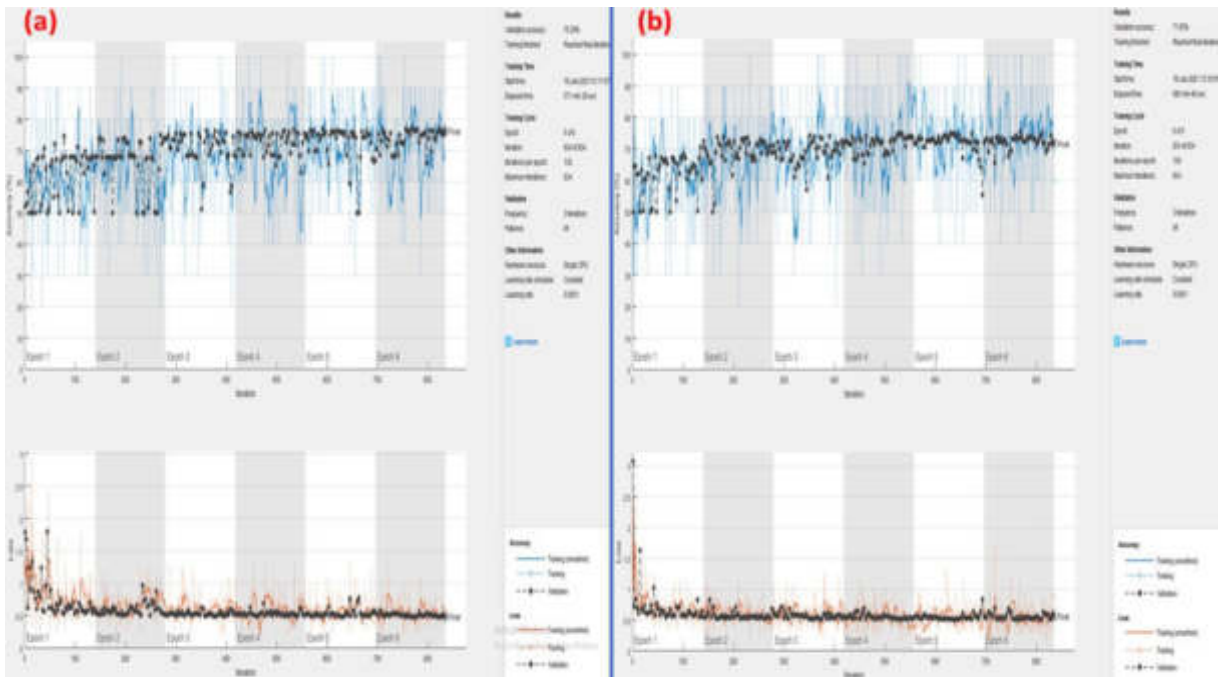


Figure 3.22 Best simulation results for VGG16 (a) and VGG19 (b): 70% of data for training and 30% of data for validation with 6 epochs.

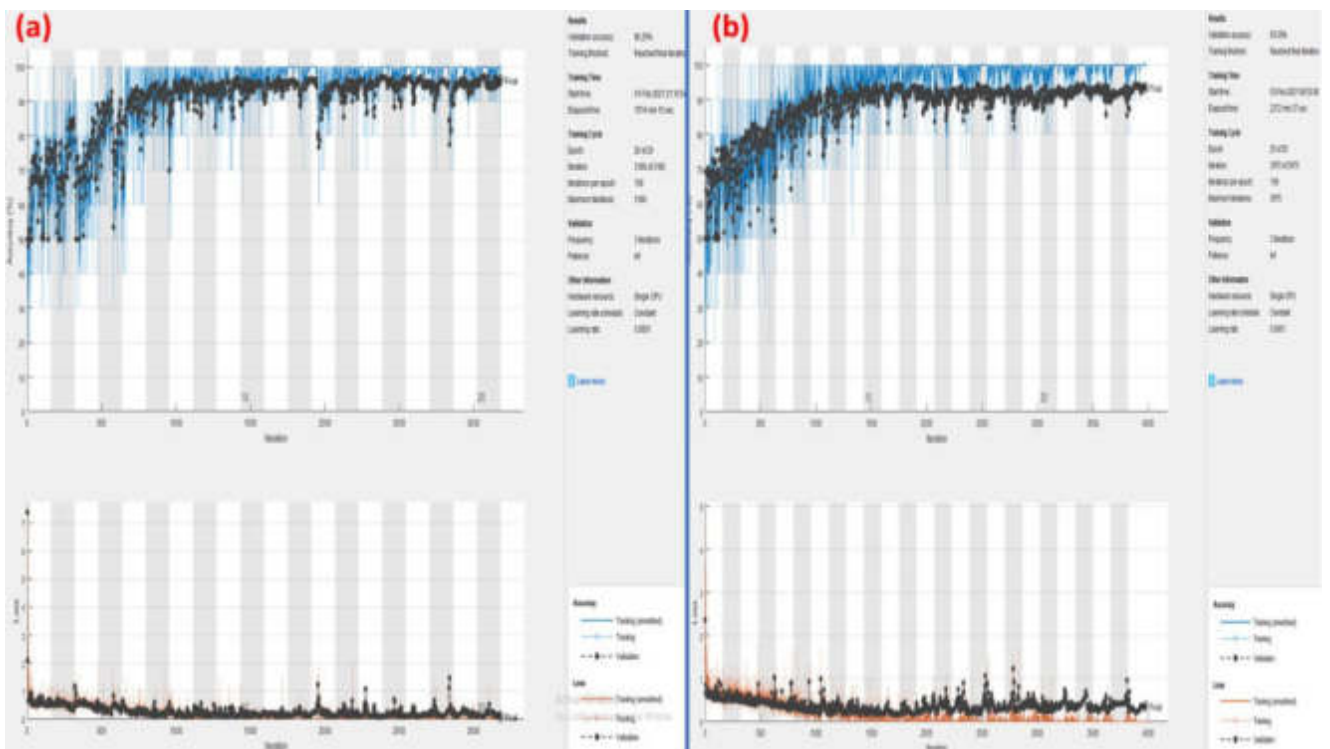


Figure 3.23 Best simulation result of VGG16 (a) and VGG19 (b): for 80% for training and 20% for validation and with 20 epochs for VGG16 and 25 epochs for VGG19.

Identification Of Nosema Cells Using Microscopic Images

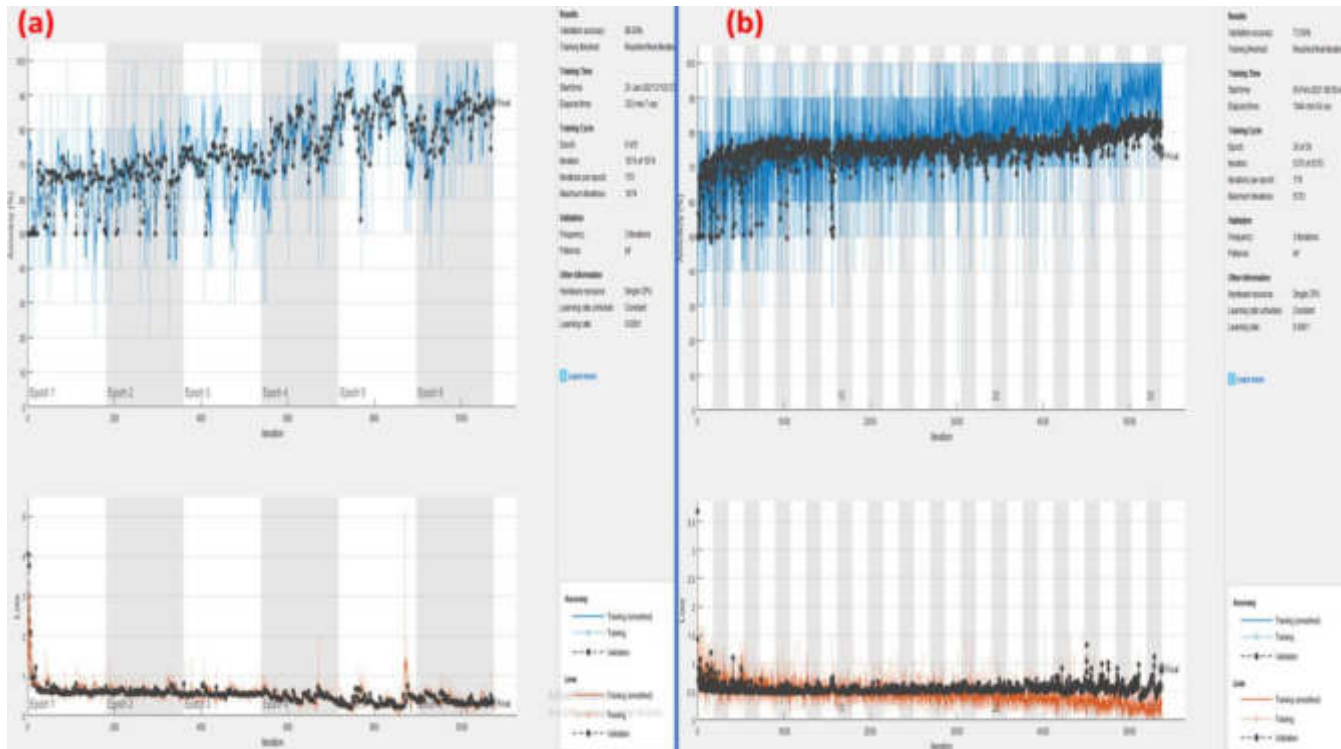


Figure 3.24 Best simulation result of VGG16 (a) and VGG19 (b): for 90% for training and 10% for validation, with 6 epochs for VGG16 and 30 epochs for VGG19

As indicated in Table 3-8, VGG16 demonstrated competence in picture classification between Nosema and non-Nosema images with a success accuracy of 96.25% (see Figure 3.25).

Identification Of Nosema Cells Using Microscopic Images

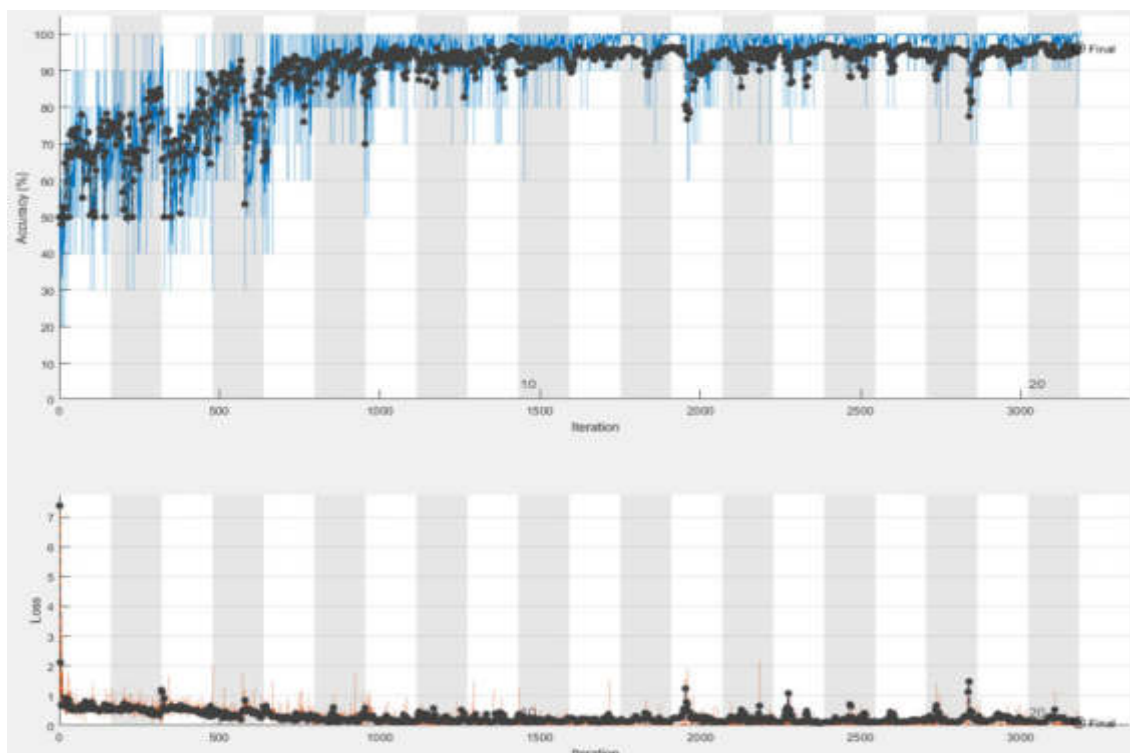


Figure 3.25 Best success accuracy (96.25%) given by VGG16 fine-tuned model

3.7 Discussion

In addition, we have included contemporary research in the bibliography that uses chemical simulations and powerful technical devices to identify bee illnesses or disturbances inside bee colonies. In this section, we evaluate our provided method and compare it to earlier efforts in the literature that exclusively employed image processing and computer vision techniques to identify and recognize *Nosema* spores.

Table 3-9: Comparison of proposed method with existed method in the literature using different image processing tools (%)

Authors	Year	Methods	Dataset	Accuracy
Alvarez-Ramos, Niño, & Santos, 2013	2013	Nosema classification : SIFT+SVM	-	-
Patricio-Nicolas, Mauro-German, Sergio-Damián,	2016	Nosema counting predefined functions in the OpenCV Library	12 microscopic images	92.00%

Identification Of Nosema Cells Using Microscopic Images

Paola-Verónica, & Hector-Luis, 2016				
Prendas-Rojas, Figueroa-Mata, Ramírez-Montero, Calderón-Fallas, Ramírez- Bogantes, & Travieso-González, 2018	2018	Nosema detection and counting: Binary and mathematical morphologies	375 microscopic images	84.00%
Proposed Method (Dghim, Travieso-Gonzales, Dutta, & Hernández, 2020)	2020	Nosema recognition: Binary and mathematical morphologies + ANN	185 microscopic images	91.10%
Proposed Method	2021	Nosema recognition: Binary and mathematical morphologies + ANN+ SVM+ CNN+ AlexNet+VGG16+VGG19	2000 microscopic images	96.25%

This part is dedicated to evaluating the implemented approach and carrying out various comparisons with those previously described in the literature.

The comparison of the methodologies used in this study to cutting-edge approaches highlights their effectiveness. As seen in the table above, the findings described in this PhD document surpass those reported in the literature. This is explained by the suggested model's ability to extract characteristics from microscopic images of Nosema illness and the performance of the classifiers utilized.

In (Alvarez-Ramos, Niño, & Santos, 2013) employed images in which the spores were accentuated against the background. This approach demands a substantial level of quality in the photographs, in addition the number of used images and the success accuracy rate were not mentioned. In (Patricio-Nicolas, Mauro-German, Sergio-Damián, Paola-Verónica, & Hector-Luis, 2016), authors relied on a small dataset of microscopic images (only 12 images) and extract a few numbers of features to identify and count Nosema spores, with this amount it gives the impression that it is only a training process,

Identification Of Nosema Cells Using Microscopic Images

if so, a high accuracy is misleading 92%. Compared to our method in (Dghim, Travieso-González, Dutta, & Hernández, 2020) in which we relied on 85 typical images obtained from the microscope, in them it is clearly noticed that there is a lot of noise and extracted 9 features that we used later with an ANN classifier to recognize Nosema cells, and we obtained a success accuracy of 91.10%. In (Prendas-Rojas, Figueroa-Mata, Ramírez-Montero, Calderón-Fallas, Ramírez- Bogantes, & Travieso-González, 2018), authors extracted three principals features to characterize Nosema cells and worked on 375 images to test their method; the accuracy was 84%. When compared to the three previous studies, this accuracy appears commendable, particularly considering the limited number of utilized microscopic images (more than the three previous works). Through this, we conclude that the number of the images in the dataset makes a big difference in the success accuracy of the method, as well as the exactitude, the precision and the choice of calculated features that describe the Nosema cell surely contribute to the amelioration of this accuracy.

The presented method consists of two main parts. The first part is the study of microscopic images and the extraction of the most relevant characteristics that can describe a Nosema cell. The second part is the use of different kinds of classification systems to recognize the Nosema cells. Some of those classifiers used the extracted features to the recognition process like ANN and SVM while the other deep learning and transfer learning classifiers used microscopic images of Nosema cells, these classifiers are an implemented method CNN, AlexNet, VGG16, and VGG19 pretrained models. In contrast to prior literature, our approach demonstrated richness, diversity, and distinctiveness across multiple facets: from the computed cell features and employed classifiers to the chosen datasets and the attained success accuracy, which surpassed the literature's figure (96.25%). Moreover, this reaffirms the efficacy of deep learning tools in the recognition of Nosema images, as posited in the Hypothesis within the thesis introduction section.

The next section delves into fine-tuned models to conduct more experiments for Nosema recognition. These experiments use a new environment of work with Python 3.7.9 amd64, and a machine equipped with an i7-9700/8GB, and a GPU processor. MATLAB was initially utilized for image processing to highlight its strengths in this

Identification Of Nosema Cells Using Microscopic Images

sector. As the project continues, Python will be used for machine learning tasks because of its large libraries and frameworks that are well-suited for complex computational tasks. We will use data augmentation techniques in this phase, and the dataset will be increased to contain thousands of photographs. Python's versatility and the availability of image augmentation tools make it an excellent choice for this stage of the study, allowing us to improve the dataset's resilience and variety for more successful machine learning model training.

The new experiment uses many and various fine-tuning models involving an increasing number of epochs to improve the recognition accuracy of Nosema as much as possible. In fact, the first part of experiments is done simply by fine tuning the pretrained models and the second phase is done by exploiting the efficiency of data augmentation to increase the accuracy of recognition.

3.8 Fine-tuned models without data augmentation

3.8.1 Methodology

In the previous sections of this chapter, the models AlexNet, VGG16, and VGG19 were employed to initiate transfer learning. This initial endeavor was aimed at assessing the efficacy of these models in recognizing disease cells and juxtaposing their performance against other machine learning techniques (ANN and SVM) and deep learning techniques (CNN). Transfer learning models have shown their high efficiency compared to different classifiers and have achieved an accuracy of 96.25% in Nosema cell recognition. Despite reaching the highest accuracy reported in the literature, we were excited to conduct more experiments using several transfer learning models to get a better result. As such, the concept involves manipulating the number of epochs, mainly since we previously relied on a limited number of them, that was, at most, 30. Additionally, leveraging a GPU processor is crucial to expedite simulation time and achieve outstanding image display, responsiveness, and visual smoothness outcomes.

In this experiment, we fine-tuned around 19 transfer learning models, which are EfficientNetB0, EfficientNetB1, EfficientNetB2, EfficientNetB3, EfficientNetB4, EfficientNetB5, EfficientNetB6, EfficientNetB7, and Inception. ResNetV2, InceptionV3, MobileNet, MobileNetV2, ResNet50, ResNet50v2, ResNet101, ResNet152V2, VGG16,

Identification Of Nosema Cells Using Microscopic Images

VGG19, and Xception. Prior to each experiment, a specific training dataset is designated for training the model. Additionally, a validation dataset might be employed to ascertain the model's aptness and pinpoint optimal classifier hyperparameters. Lastly, a set of tests allows us to get an idea of the real performance of the model. In this case, the chosen approach ideally involves a ten-cross-validation strategy. Out of these, eight folds exist for training and 2 for testing. The models are initialized with pre-trained ImageNet weights, and we fine-tuned them with our dataset, DS1, which contained 2000 images each of Nosema and non-Nosema. All the pre-trained models will be used as feature extractors. To fine-tune the pre-trained models, for every one of them, the last predicting layer will be placed by our own predicting layer of two classes, Nosema and non-Nosema, using a sigmoid activation function. The weights are used as feature extractors and are frozen and not updated during the training. The fine-tuned models have the same architecture as shown in Figure 3.26.

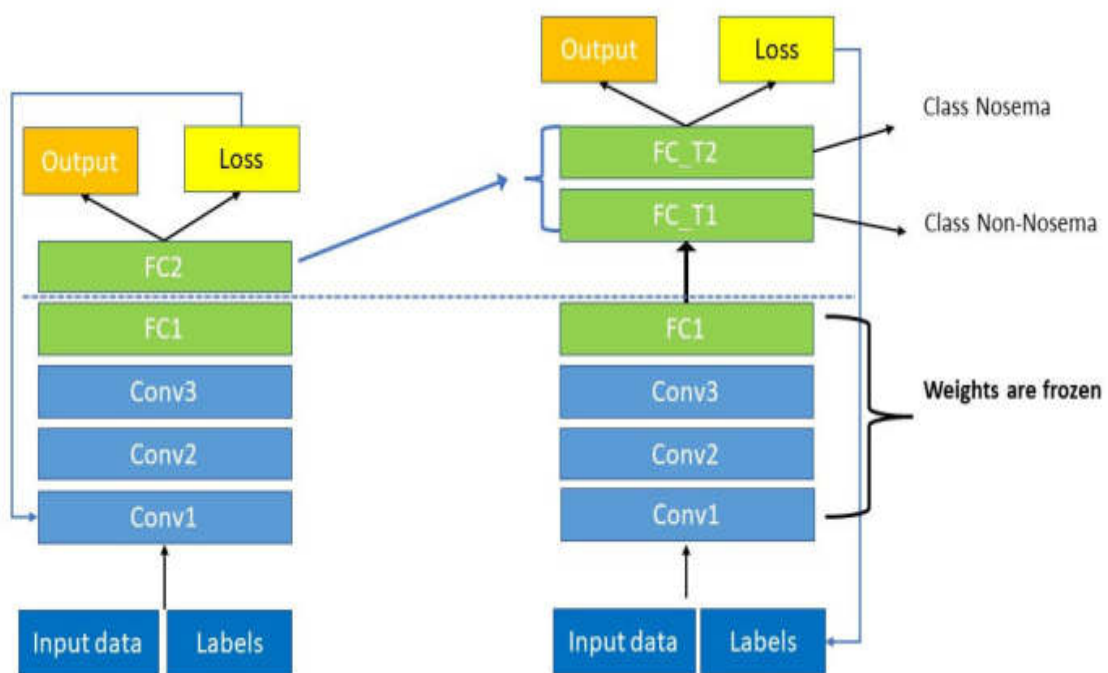


Figure 3.26 Pipeline of fine-tuned models

The information Images are standardized to a common size of 200 by 200 pixels and include three RGB channels (Red, Green, and Blue). The first nine normalized images with labels are shown in Figure 3.27.

Identification Of Nosema Cells Using Microscopic Images

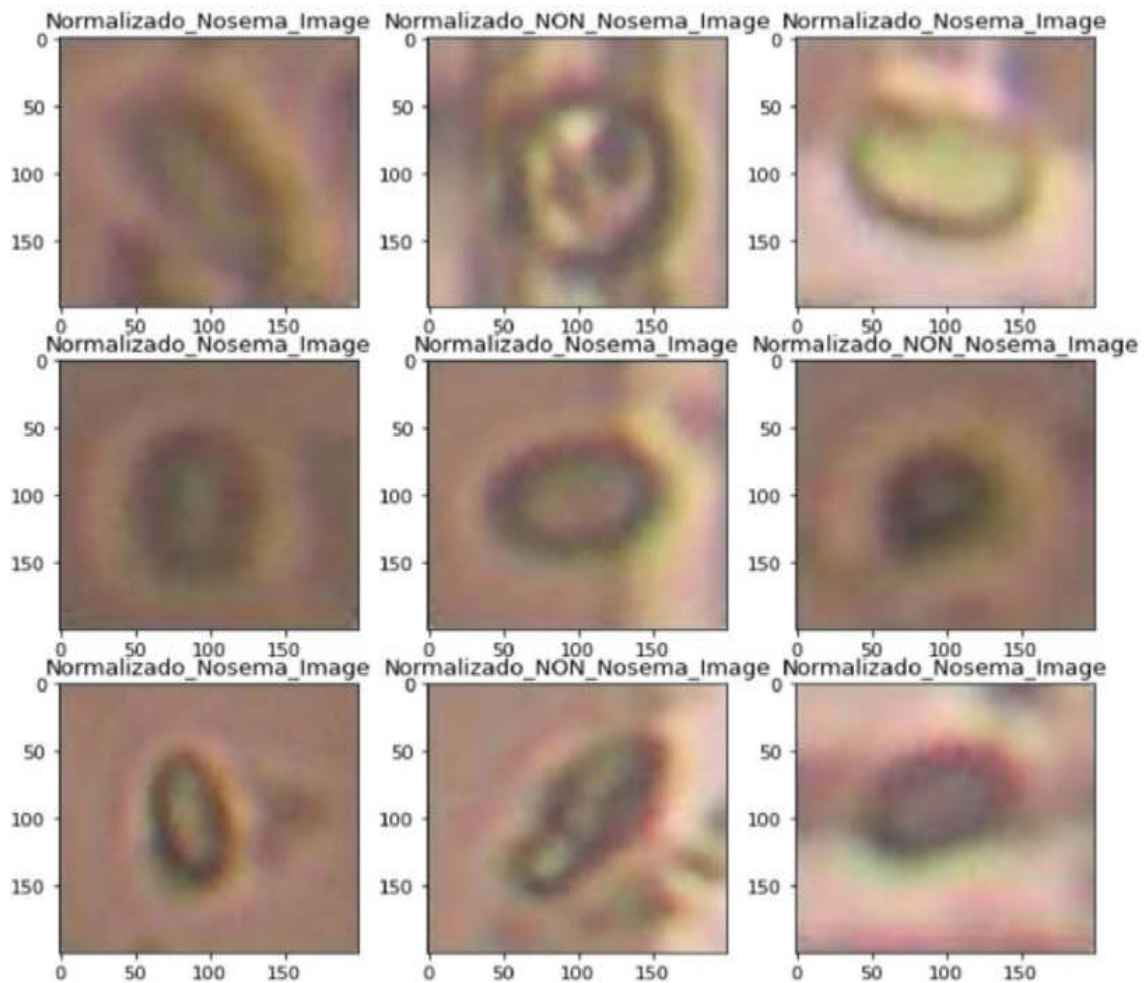


Figure 3.27 Prepared Input Images for fine-tuned models

The parameters of each model must then be set, as is customary. Furthermore, the number of epochs must be determined. The accepted approach in our setting is as follows:

1-Start training the models with 50 epochs. It should be noted that convergence might take up to 50 epochs, depending on the learning rate used. If image augmentation layers are not used, validation accuracy may be as low as 60%.

2-After training, discard the models that reach an accuracy less than 96.25% (the maximum accuracy in the prior tests) and keep the others.

3-Run a second experiment with conserved models for a total of 100 epochs.

4- Throughout the experiment, certain models were halted before reaching 100 epochs. This decision was based on their consistent decline in accuracy over a span of 12 epochs, coupled with their failure to surpass the 96.25% benchmark. Continuing their training in such cases would have been inefficient and time-consuming.

Identification Of Nosema Cells Using Microscopic Images

5- Ultimately, only the models with the highest performance across the 100 epochs will be used for the following experiment. In fact, it should be mentioned that all models begin to decrease before completing the 100 epochs, which is why we did not do another experiment with more than 100 epochs.

3.8.2 Experiment results

The accuracies are given by a 5-fold cross-validation strategy. This approach involves randomly dividing the set of observations into five groups, or folds, of approximately equal size. The first fold is treated as a validation set, and the method is fit on the remaining 5-1 folds. Every particular result of a particular folder was given in the form of an accuracy model, a loss model, and a confusion matrix, which show the exact precision of the folder. After that, the mean accuracy was calculated to have the final precision of the fine-tuned model.

Like said in the methodology, the 19 models were first trained during 50 epochs. Next, the 7 models in Table 3.10 below were eliminated because of their low accuracies or because they continued to decrease after 50 epochs. All models approve different frozen weights. The best mean accuracy result during 50 epochs of training was 93,88%, and it was given by the pretrained model EfficientNetB5. Note that some of them have stopped before achieving 50 epochs. Table below can show the results of this experiment.

Table 3-10: Experiment results for fine-tuned models with 50 epochs

Fine-Tuned Model	Epochs	Frozen weights	Mean accuracy %
EfficientNetB4	50	17.673.823	93.28 ±1,83
EfficientNetB5	50	28.513.527	93.88±1.59
EfficientNetB6	50	40.960.143	93.28±1.74
InceptionResnetV2	20	54.336.736	60.07±3.58
InceptionV3	40	21.802.784	73.74±1.77
Xception	30	20.861.480	81.91±6.39
ResNet152V2	20	58.331.648	60.82±2.76

Identification Of Nosema Cells Using Microscopic Images

In the next of this subsection the results of fine-tuned models on 100 epochs will be shown. Note that some of them have stopped before achieving 100 epochs.

Table 3-11: Experiment results of fine-tuned models with 100 epochs

Fine-tuned Model	Epochs	Frozen Weights	Mean Accuracy %
EfficientNetB0	100	4.049.571	95.84±0.87
EfficientNetB1	90	6.575.239	96.29±0.86
EfficientNetB2	100	7.768.569	95.59±1.19
EfficientNetB3	80	42.658.176	94.89±0.66
EfficientNetB7	60	64.097.687	93.63±0.65
ResNet50	70	23.587.712	95.84±1.32
ResNet50V2	60	58.370.944	96.59±1.06
ResNet101	70	42.658.176	95.94±0.51
MobileNet	90	3.228.864	95.04±0.66
MobileNetV2	90	2.257.984	96.34±0.64
VGG16	100	14.714.688	97.64±0.75
VGG19	100	20.024.384	96.79±0.58

Table 3-11 shows that the VGG16 fine-tuned model has the highest precise accuracy of Nosema identification at 97.64%. It must be stated that we have increased the accuracy of recognizing Nosema cells by 1.39% (previously 96.25%).

The third step of this experiment involves applying augmentation data to the model that provides the greatest recognition accuracy (VGG16) in order to measure the skills of the latter in the improvement of the prediction of the fine-tuned model.

3.9 Fine-tuning VGG16 with Data augmentation

Deep neural networks' robustness is highly related to the image number computed in the datasets. This is due to the fact that the training process involves dealing with millions of parameters. This way during the training, it becomes imperative to acquaint the system with an exponential number of parameters, which must be matched by a

Identification Of Nosema Cells Using Microscopic Images

proportional number of examples, if it is not the case, the network will learn more than what is supposed and generate the over-fitting problem. In the case of very deep architectures like VGGNet and GoogLeNet, the problem is more complicated, and the number of parameters is very large. On the other hand, many applications need very deep architectures to increase the number of extracted features and cross the deepest component or propriety describing this pattern. In this study, the efficiency of data augmentation is utilized to address this challenge, a strategy that is commonly employed in the existing literature, as seen in (Pezoulas, Grigoriadis, Gkois, Tachos, Smole, Bosnić, ...Fotiadis, 2021), (Lee, Lee, Hong, Bae, Lim, & Kim 2021), and (Zhang, Bao, Sun, Li, Li, Qian, & Zhou, 2022) many architectures used this metric and approved their efficiency to overcome the over-fitting problem. This technique consists of the transformation of the training set (varied size, angles, contrast...etc.) with the purpose to increase the generalization and improve the ability of the model to recognize different versions of the same image. In this work, the data augmentation technique was utilized as a crucial approach to enhance the training dataset's size and enhance the efficiency of the proposed method. The objective is to assess the impact of data augmentation on the development of AI (artificial intelligence) models by improving the performance of transfer learning models in disease recognition (Chaitanya, Karani, Baumgartner, Erdil, Becker, Donati, & Konukoglu, 2021).

The Nosema images underwent various degrees of rotation using a specific Python code. The images were randomly rotated at angles of 20, 30, 60, and 180 degrees, utilizing the rotation range parameter. Subsequently, the augmented dataset of images was used for training purposes. A 5-fold cross-validation methodology was applied, and the training was done during 100 epochs. VGG16 is fine-tuned as previously.

As a result, the proposed method achieved a mean accuracy of 99.35% showing an improvement of 1.71% compared to the fine-tuned VGG16 without augmentation data. Moreover, the highest precision given by the VGG16 fine-tuned model was 99,70% with the particular 2-fold using a +30 ° rotation of the images showing an improvement of 3.45% compared to the first experiment did previously. The next tables and figures show the detailed result.

Identification Of Nosema Cells Using Microscopic Images

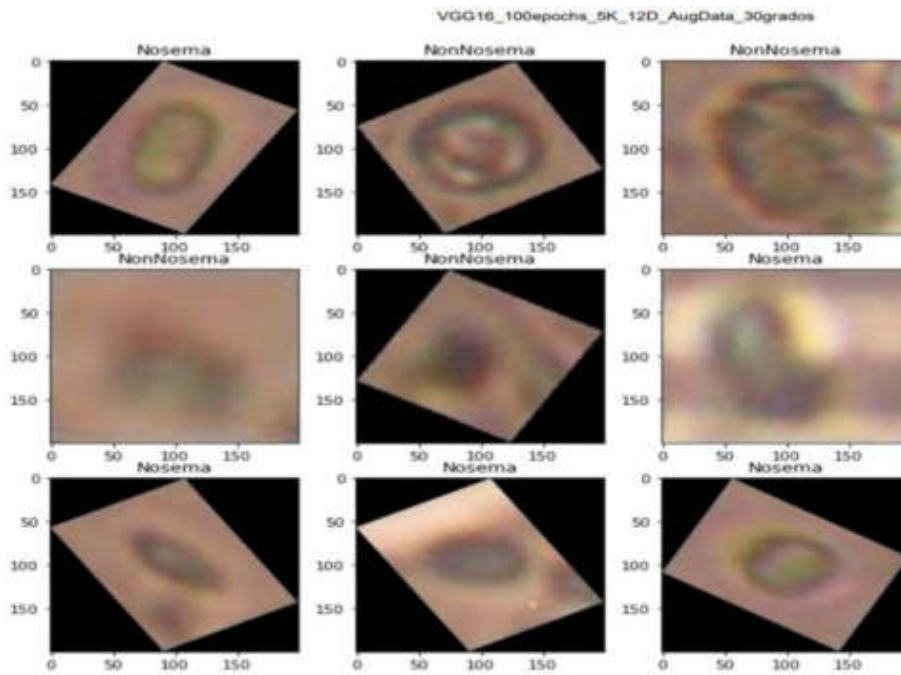


Figure 3.28 9 first augmented images with 30-degree rotation

VGG16_100epochs_5K_12D_AugData_30grados

```

Esta es la carpeta K-Fold 2
Esta es la repetición 0
> Train len: 19161 , Test len: 4791
> X_train shape: (19161, 200, 200, 3) , Y_train shape: (19161, 1)
> X_test shape: (4791, 200, 200, 3) , Y_test shape: (4791, 1)
Model: "model"

```

Layer (type)	Output Shape	Param #
input_2 (InputLayer)	[(None, 200, 200, 3)]	0
vgg16 (Functional)	(None, 6, 6, 512)	14714688
global_average_pooling2d (G1	(None, 512)	0
dropout (Dropout)	(None, 512)	0
dense (Dense)	(None, 2)	1026

```

Total params: 14,715,714
Trainable params: 1,026
Non-trainable params: 14,714,688

```

Figure 3.29 Experiment setting for VGG16

Identification Of Nosema Cells Using Microscopic Images

Table 3-12: Experiment results for fine-tuned VGG16 model with Augmentation Data

VGG16 fine-tuned model using Augmentation Data	Rotation	Mean Accuracy during 100 epochs %
	+20	98.57±0.27
	+30	99.35±0.14
	+60	99.25±0.12
	+180	97.89±0.09

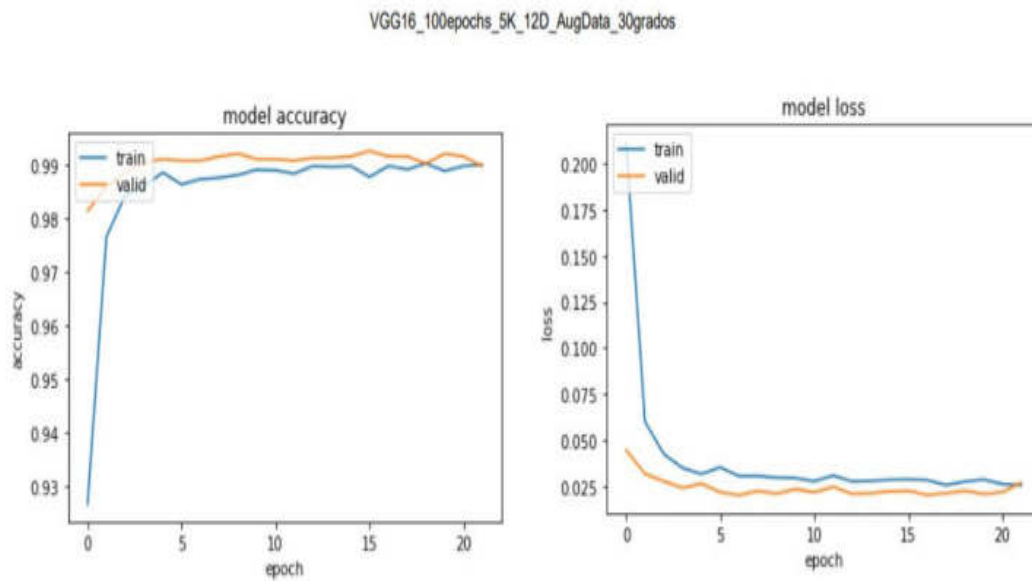


Figure 3.30 Accuracy and loss models for best precision given with 2-fold cross validation strategy.

Identification Of Nosema Cells Using Microscopic Images

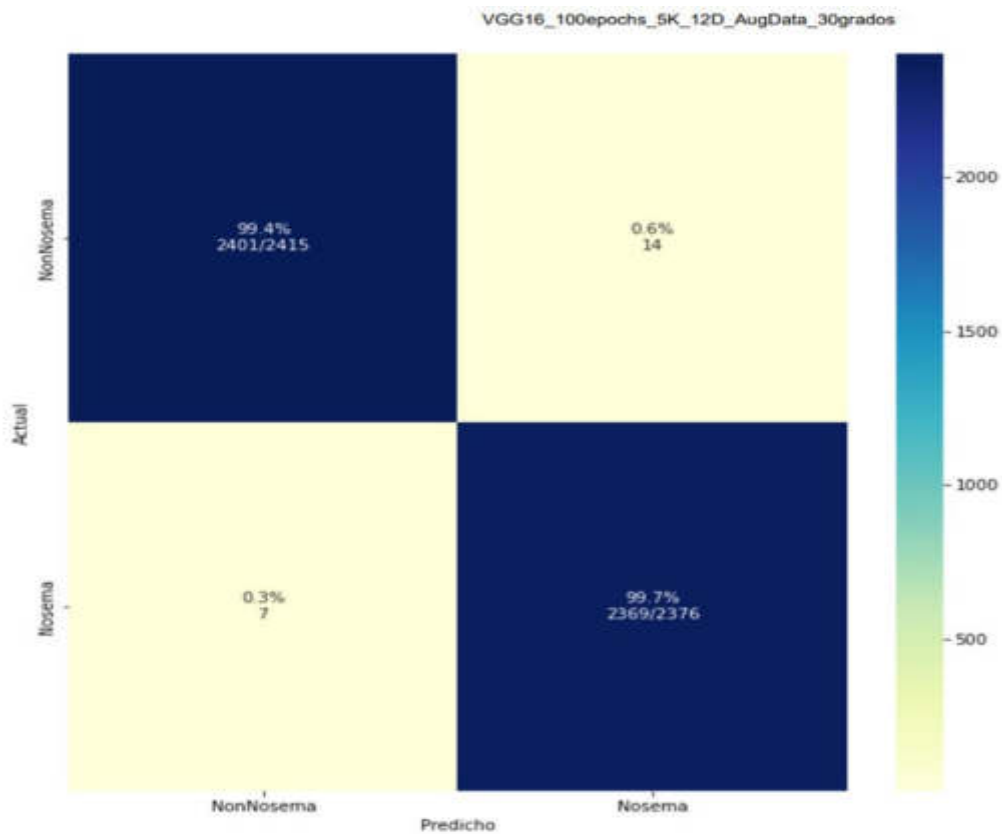


Figure 3.31 Confusion matrix for best accuracy (99.70%) given by VGG16 with Augmentation Data.

The experiments demonstrate that data augmentation method improves the classification performance. As a result, the proposed method enabled VGG16 to achieve 99.70% accuracy, showing an increase in recognition performance improvement by 3.45% compared to its first experiment (see table 3.4) like shown in table and figure below. This leads us to conclude that several factors can affect the work of a transfer learning model, and this thesis presents many factors such as the number of images in the dataset, the choice of parameters setting of the model, the choice of epochs number during the training, and especially the use of the data augmentation method. Moreover, the most important of all is to solve a recognition or identification problem and achieving the optimal outcome needs exploring different architectures and conducting numerous experiments on the dataset.

Identification Of Nosema Cells Using Microscopic Images

Table 3-13: Comparison between proposed methods

VGG16	Proposed method 2021	Proposed method 2022
Performance without Augmentation Data	20 epochs	100 epochs
	96.25% (particular file accuracy)	97.64% (mean accuracy)
Performance with Augmentation Data	-	99.35% (mean accuracy) 99.70% (particular file accuracy)

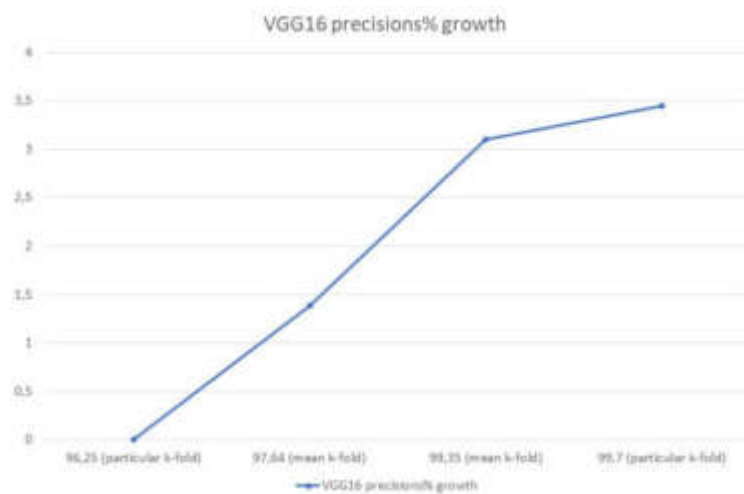


Figure 3.32 The increment of VGG16 precision accuracy from the first to the last experiment

From 20,000 images, there are only 7 Nosema images and 14 non-Nosema images that have been misclassified as shown in the confusion matrix above (Figure 3.31), and this is essentially related to the quality of the used images in this doctoral thesis. This problem was mentioned and studied in chapter 2. Let's see an example of a Nosema image which has been classified as non-Nosema image in Figure 3.33.

Identification Of Nosema Cells Using Microscopic Images

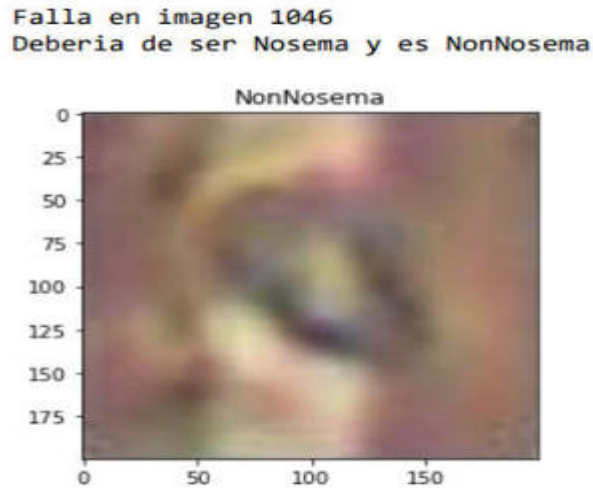


Figure 3.33 An example of a misclassified Nosema image

The image is a Nosema cell superimposed on the counting grid. Its location gives it a very different shape from a normal cell because of the color of the grid, despite this, the identification result is close to 100%. Our challenge was identification of Nosema cells despite the defective and noisy quality of the used images.

3.10 Conclusion

The application of AI in the real world makes systems easier and smarter. For instance, it enhances the comprehension of disease systems, enhances the reproducibility of diagnoses, and can even substitute experts in certain repetitive tasks, thus undeniably benefiting various domains. In this area, disease analysis becomes a very interesting research domain in AI, looking for understanding the symptoms, doing the diagnosis automatically and rapidly take a decision. In these axes, we presented our contribution by trying to answer the questions related to the recognition of Nosema in the microscopic images.

In this chapter, the recognition method is presented. The contribution in this domain is delineated through three algorithms. The initial algorithm entails the extraction of features from the Nosema cell, which are subsequently fed into ANN and SVM classifiers to facilitate cell recognition based on the extracted features. In the second one, the images of Nosema cells and other objects in the digital images are used in deep learning and transfer learning models to recognize the disease. Lastly, in the third one a data augmentation method was implemented to enhance the functionality of the model.

Identification Of Nosema Cells Using Microscopic Images

In this work, the process of calculating Nosema features and their application in supervised recognition has been outlined. Additionally, various classifier models have been discussed to showcase the effectiveness of the approach and the noteworthy outcomes achieved. Especially for the use of transfer learning with augmentation data to do the recognition task.

Identification Of Nosema Cells Using Microscopic Images

4 Chapter IV: Automatic Algorithm for Nosema Identification & Counting

4.1 Introduction

Nosema was recognized in earlier chapters by analyzing individual cell images, collecting the cell's properties, and using them in the classification procedure. Individual cell photos were also used to retrain several Nosema detection methods. The previous two approaches identified sick cells from other things by using their individual cropped sub-pictures, which were cropped from the original microscopic images (Nosema and non-Nosema items). Based on the information put within the VGG16 model in the previous chapter, this chapter tries a fresh approach. Indeed, the work in this chapter is entirely automated; the methods for automatic recognition and counting of cells inside microscopic pictures based on VGG16-constructed information will be shown and detailed in this chapter. To be more exact, the cells will be detected and gathered within the main microscopic image to establish the disease stage. A computerized program will count the infected cells in the microscopic picture and classify them as very mild, mild, moderate, semi-strong, or strong. This established strategy, along with the accurate diagnostic, assists in streamlining the infection level.

The experiments in this chapter make use of a Python 3.7.9 amd64 environment and a system outfitted with an i7-9700/8GB and a GPU processor.

4.2 The automatic algorithm

One of the main problems that can appear when developing a computer vision system is being able to choose the appropriate processing techniques to extract the necessary information ([Gonzalez & Woods, 2008](#)) and achieve the stated objective. As a result, various techniques built upon distinct automated systems developed within the same domain were evaluated ([Alvarez-Ramos, Nino, & Santos, 2013](#)).

Chapter 3 described the usage of numerous classifier models to demonstrate the efficacy of this work's proposed technique and its highly interesting findings particularly

Identification Of Nosema Cells Using Microscopic Images

regarding the use of transfer learning with augmentation data to perform the cells recognition task. As shown previously, the trials undertaken allowed the fine-tuned VGG16 model to achieve 99.70% identification accuracy of Nosema cells.

In this chapter, the automatic algorithm makes use of the VGG16's expertise and results to identify the needed items in microscopic images. In other words, the main role of this algorithm is to perform object detection on an input image using a sliding window approach and a pre-trained model (VGG16). This section of the work is implemented with Python. Python was chosen because of its library richness, allowing to push the language's limits and undertake ambitious and hard projects in various application fields. In a scientific study, for example, the biopython library makes it easier to process and interpret biological data. The pyGame library is utilized in the area of video games to construct 2D or 3D video games. Python modules, therefore, contribute to the language's two key strengths: simplicity of use and diversity. In figure 4.1 there's an overview of the implemented methodology followed. The steps of this method will be detailed in this chapter.

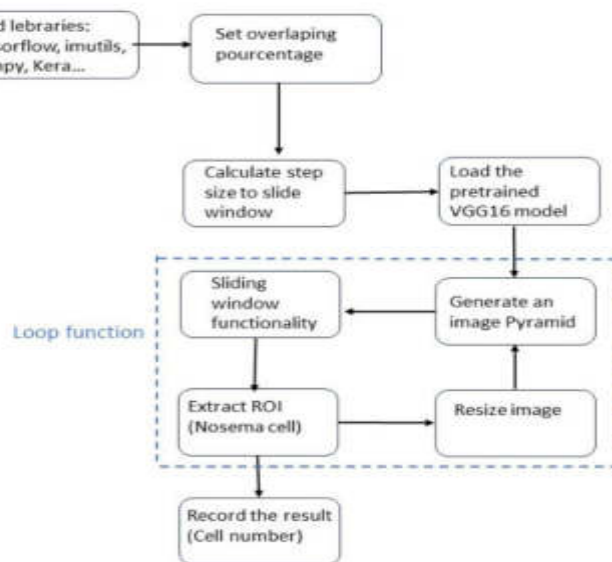


Figure 4.1 Pipeline of the proposed algorithm for the automatic detection.

In the subsections below there's a step-by-step explanation of the automatic algorithm implementation and functionalities.

Identification Of Nosema Cells Using Microscopic Images

4.2.1 Used libraries

The algorithm accepts an RGB microscopic image as input and produces an output a file containing images of the identified cells. Additionally, a text file is generated, providing the count of cells identified in each sliding window. The algorithm starts by calling the necessary libraries and the required packages.

```
1  #%%
2  import cv2
3  import imutils
4  import numpy as np
5  import tensorflow as tf
6  import os
7  import datetime
8
9
```

Figure 4.2 Used libraries

A brief description of the used libraries and their functions are detailed below:

- **TensorFlow:** is a deep learning package that was created by the Google Brain team ([Mattman, 2021](#)). It offers a versatile and effective framework for developing various machine learning models, particularly neural networks. TensorFlow provides automated differentiation, GPU support for rapid computing, distributed training, and platform-independent deployment.
- **Keras (tf.keras):** is a popular deep learning library option because it is tightly linked with TensorFlow ([Géron, 2022](#)), which is well-known for its dependability in production deployments. TensorFlow also includes tools for production deployment and management, debugging and visualization, and running models on embedded devices and browsers. Keras is utilized by Google, Netflix, Uber, and NVIDIA in the technology business. We picked tf.keras as our primary tool for this project since it is a library focused to expediting the building of deep learning models, and also it is used to upload our model VGG16.
- **Cv2:** is a Computer Vision Library, often known as OpenCV, that will be used to execute image processing tasks.
- **Numpy:** is a package that allows to work with multidimensional arrays and matrices.

Identification Of Nosema Cells Using Microscopic Images

- **Datetime:** is a built-in Python module that contains classes for manipulating dates and timings. It enables to work with dates, times, and time intervals, making it easy to execute time and date calculations.
- **Imutils:** is a set of functions that make it easier to interact with OpenCV, a famous computer vision library. It offers a set of simple and straightforward tools for performing typical image processing tasks and operations. Imutils' primary functions include the ability to resize pictures, rotate images, translate images, conduct color conversions, and operate with contours and bounding boxes.
- **OS:** is a Python built-in module that allows to interface with the operating system and execute actions on directories, files, and system data. Some of the most important functions of Os include the ability to create, delete, and navigate directories, operate with files (reading, writing, and deleting), and access environment variables.

Both **imutils** and **OS** are strong packages that complement other libraries such as OpenCV and TensorFlow, making it easier to work with pictures and handle files and directories in Python applications.

4.2.2 Variables configuration

The next step involves configuring the required parameters for object detection method:

Windows= [(30,30), (30,30)]: represents the size of a window for object detection. The windows are 30x30 pixels in size. Additionally, there are two window sizes available. A series of trials tested the available window sizes to determine the dimension and see which size yielded the best Nosema number.

Overlap percentages = [0, 0]: creates a two-valued list named overlap percentages. During the object detection procedure, each number reflects the proportion of overlap between adjacent sliding panes. Both values are set to zero in this case, indicating that there is no overlap between windows. Based on a specified window size and an overlap percentage, the step size for sliding windows is calculated. The function is as follows:

Overlap = (window size * overlap percentage) / 100: This calculates the amount of overlap based on the specified percentage of overlap and the width of the window. The overlap is calculated as a fraction of the window width, so it's divided by 100.

Identification Of Nosema Cells Using Microscopic Images

Step = window size - overlap: This computes the step size by subtracting the overlap from the window's width. Step size is an integer value. The step determines how much the sliding window will move horizontally and vertically between consecutive positions during object detection or feature extraction processes.

The filename template of the input image used for object recognition is 'Image.JPG'. The last variable is **name-trained-model = 'modelo1 rep 0'**: represents the filename or identifier of the pre-trained model that will be used for object detection.

In summary, this code snippet initializes various parameters for object detection. It sets up the window sizes, overlap percentages, the filename of the image template, and the identifier of the pre-trained model to be used in the subsequent parts of the algorithm.

4.2.3 Load the pretrained model: VGG16

A function was implemented to load the pre-trained VGG16 model: using a **tf.keras** command called **tf.keras.models.load_model()**, this function takes one parameter **file_name**, which represents the file name of the pre-trained model to be loaded. The function uses a default value of **'modelo1 rep 0.h5'** if no filename is provided when the function is called. Inside the function, a new variable name is created by concatenating the value of **file_name** with the file extension **'.h5'**. The **'.h5'** extension is typically used for saving Keras models in HDF5 format. The described function loads the model architecture, model weights, and optimizer state from the specified file. The loaded model is assigned to a new variable called **new_model**. The function then calls **new_model.summary()**, which prints a summary of the model architecture to the console. The summary includes information about the layers in the model, the number of parameters, and the output shape of each layer. Finally, the function returns the **new_model**, which is the pre-trained model loaded from the specified filename.

To summarize, this function is a useful tool that loads a pre-trained Keras/TensorFlow model from a file and returns the loaded model object. Moreover, this tool allows one to reuse and train the pre-trained model again, or to utilize it for inference on new data.

In this method, transfer learning is conducted. Transfer learning means that the VGG16 pre-trained model is loaded using tensorflow/keras and a final layer is added that performs classification to this model. If the classification is accurate, a new training of

Identification Of Nosema Cells Using Microscopic Images

the model is performed, but just on the last layer created (to fit the images); during this training, all elements of the pre-trained model are not trained anymore; they are in feature extraction mode.

4.2.4 Pyramid Function

The function pyramid involves three parameters: **image**, which is the input image, **scale**, which is the scaling factor for resizing the image, and **minSize**, which is the minimum size threshold for stopping the pyramid generation. Below there are the steps followed to create a pyramid image:

1-The function starts by yielding the original image as the first element in the pyramid. This is done to include the original image scale in the pyramid.

2-The function enters an infinite loop while remaining True.

3-Inside the loop, the **width w** of the image is calculated by dividing the original **width (image.shape[1])** by the scale parameter. This resizes the image to a smaller size at each iteration of the loop.

4-The **imutils.resize function** is called to resize the image to the calculated width w.

5-The **imutils.resize** function is a convenient method from the imutils library that resizes the image while maintaining its aspect ratio.

6-The function checks if the resized image's **height (image.shape[0])** is less than the **minSize[1]** or if its **width (image.shape[1])** is less than the **minSize[0]**. If either condition is true, it means the image has become too small to continue generating the pyramid, and the loop is broken.

7-If the conditions in step 5 are not met, the current resized image is yielded as the next element in the pyramid.

8-The loop continues, and the process of resizing and yielding the image is repeated until the conditions in step 6 are met, and the loop is exited.

In summary, the pyramid function generates an image pyramid from the input image. It starts with the original image and then iteratively resizes the image at different scales by the specified scale factor. The process continues until the image becomes smaller than the specified **minSize**, and the pyramid generation stops. The resulting pyramid contains multiple scales of the input image, which is useful for applying multi-scale object detection or processing tasks.

Identification Of Nosema Cells Using Microscopic Images

4.2.5 Sliding window function

The Python method sliding window creates sliding windows over an input image that have a certain size. Sliding windows travel sequentially over the picture, collecting various sections of interest, and are used for localized processing, such as object detection or feature extraction.

1-The function `sliding_window` requires three inputs: **image**, the input picture, **stepSize**, the step size or stride of the sliding window, and **windowSize**, a tuple indicating the sliding window's size (height, width).

2-Two nested loops are used at the function's beginning. The inner loop iterates over the image's horizontal coordinates (**x**), while the outer loop iterates over the image's vertical places (**y**).

3-The values for **y** and **x** are generated using the range function. The range for **y** has a step size of **stepSize** and extends from **0** to the image's height (**image.shape[0]**). Similar to **y**, the range for **x** has a step size of **stepSize** and ranges from **0** to the image's width (**image.shape[1]**).

4-A sliding window generator is made using the yield statement inside the stacked loops. For each point (**x**, **y**) in the picture, the generator produces a tuple (**x**, **y**, **window**) after iterating over it.

5-The window is extracted from the image using slicing. The slicing notation **image[y:y + windowSize[1], x:x + windowSize[0]]** extracts a subregion from the image starting at position (**y**, **x**) and with the size specified by **windowSize**.

6-As long as there are valid positions in the image, the generator keeps producing sliding windows for those points.

Figure 4.3 shows the movement of the sliding window in the same microscopic image, and Figure 4.4 shows some details.

Identification Of Nosema Cells Using Microscopic Images

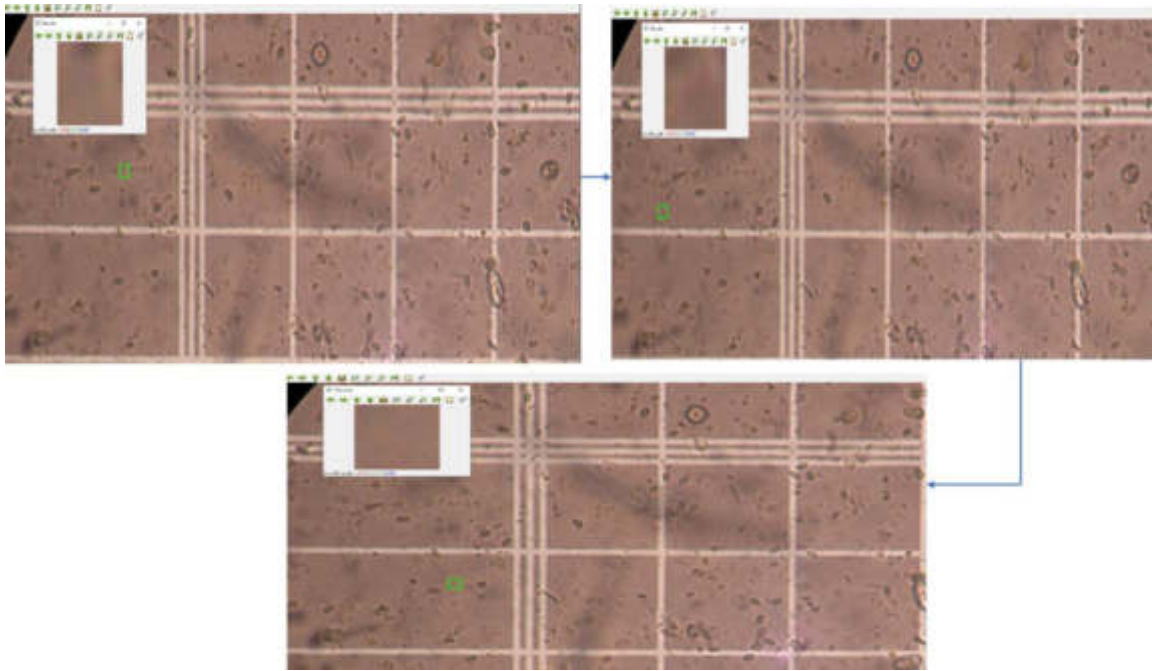


Figure 4.3 Sliding window in green color moving through the microscopic image

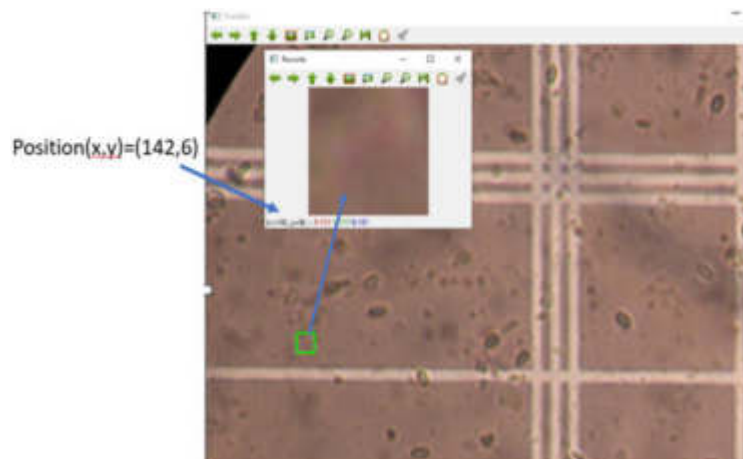


Figure 4.4 Sliding window Details

In summary, the `sliding_window` function constructs a series of sliding windows that travel over the input picture at a predetermined step size. The function iterates over all potential places for the sliding windows using nested loops, returning a set of integers comprising the position (x, y) and the matching window data taken from the image at each point. This generator may be used to perform localized operations on distinct parts of a picture, such as object recognition, feature extraction, or other activities that involve inspecting numerous sections of the input image.

Identification Of Nosema Cells Using Microscopic Images

4.2.6 Record Results

The code initiates by opening a file in **append mode** to record the output of the image processing and object detection activities. It then reads an image from a file and loads a pre-trained model. Following this, a directory is created with a **timestamped** name to store the results, and another file is opened in **append mode** to record the output of the image processing and object detection processes (see Figure 4.5).

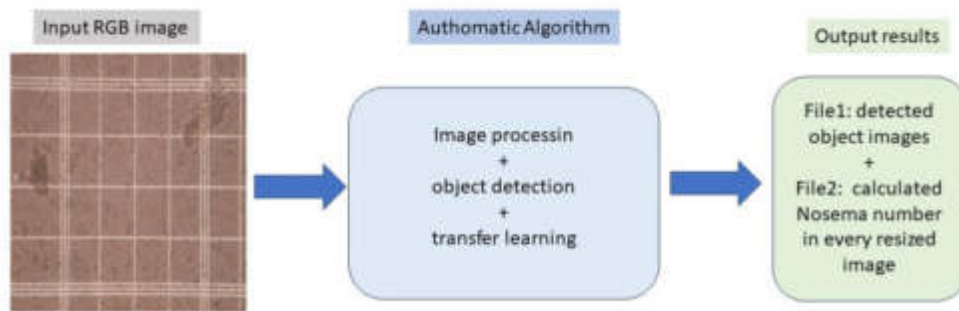


Figure 4.5 Record results description

4.3 Results and discussion

4.3.1 Experimental results

As stated in the introduction to the thesis paper, the used dataset is initially divided into 5 files initially labeled by the experts based on the degree of infection. A clean microscopic picture is required for the "very mild" infection category. The mild level contains [5-30[spores, moderate has [30-80[, semi-strong has [80-120[, and strong has more than 120 spores in a single microscopic image.

Several algorithm tests were performed on many microscopic pictures of various infection levels. Consequently, we assessed the algorithm based on the number of spores or cells present in each microscopic picture. As an example, the outcomes of small images from each level are presented Below.

Identification Of Nosema Cells Using Microscopic Images

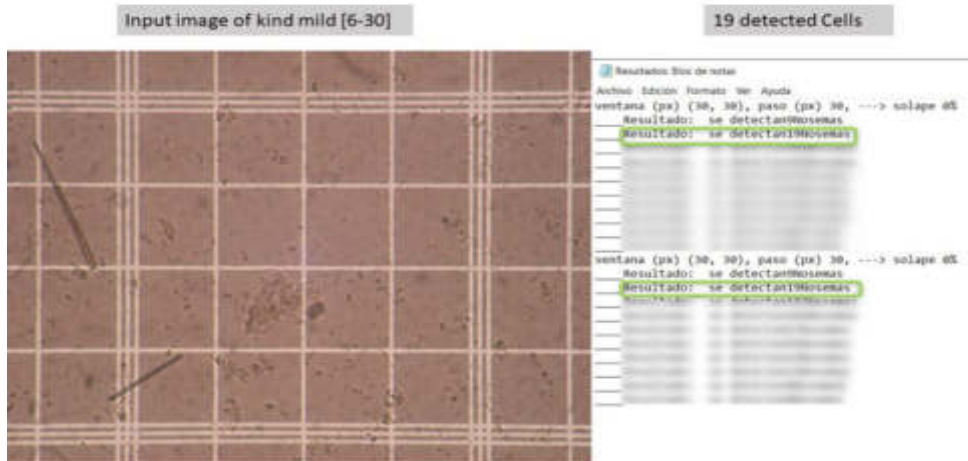


Figure 4.6 Detection and counting results on an input image of mild level

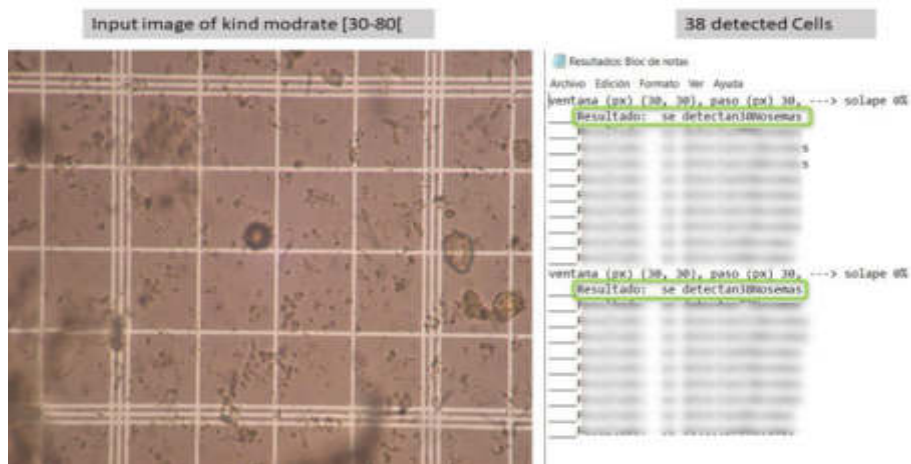


Figure 4.7 Detection and result on an input image of moderate level

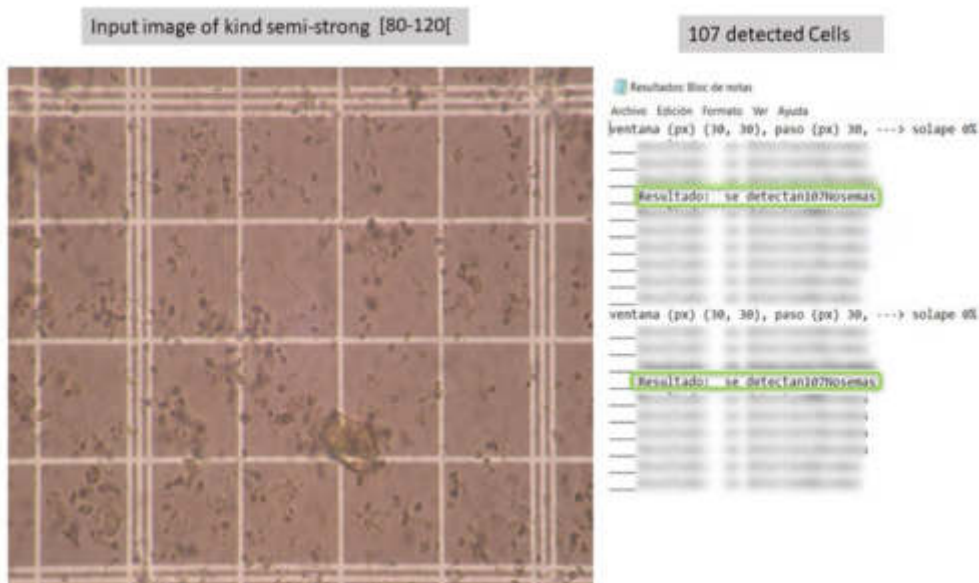


Figure 4.8 Detection and counting result on an input image of semi-strong level

Identification Of Nosema Cells Using Microscopic Images

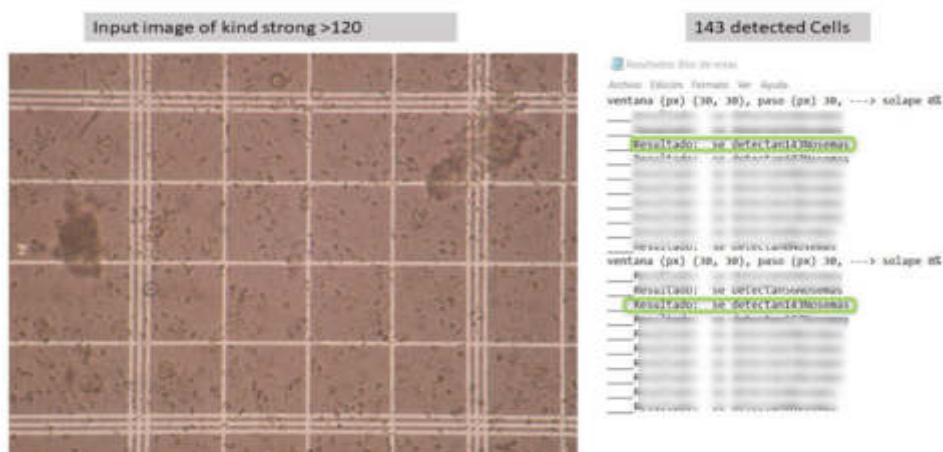


Figure 4.9 Detection and counting result on an input image of strong level

Table 4.1 shows the results of the automated counting algorithm on around twenty randomly chosen images for the experiment.

Table 4-1: Experiment results for the Automatic Algorithm

Image label/ infection level	Manuel Counting	Automatic Counting	Level confirmation	%Absolut error	%Success
Centr194.JPG/Strong	143	143	confirmed	0	100
centr178.JPG/Moderate	38	38	confirmed	0	100
Inf der201.JPG/Semi-strong	87	87	confirmed	0	100
Sup der185.JPG/Semi-strong	94	94	confirmed	0	100
1- Sup lz231.JPG/Strong	161	160	confirmed	0.62	99.38
Centr240.JPG/Moderate	50	50	confirmed	0	100
4-Inf izq292.JPG/Mild	22	22	confirmed	0	100
4-Inf izq243.JPG/Moderate	51	51	confirmed	0	100
Centro254.JPG/Semi-strong	92	92	confirmed	0	100
Inf izq278.JPG/Strong	164	165	confirmed	0.60	99.40
Sup der213.JPG/Moderate	73	73	confirmed	0	100
2- Inf izq184.JPG/Semi-strong	107	107	confirmed	0	100
Centro213.JPG/Semi-strong	91	91	confirmed	0	100
Sup der201.JPG/Semi-Strong	95	95	confirmed	0	100
4- Supder255.JPG/Semi-strong	85	85	confirmed	0	100

Identification Of Nosema Cells Using Microscopic Images

5- Centr184.JPG/Semi-strong	118	118	confirmed	0	100
5- Centro292.JPG/Mild	19	19	confirmed	0	100
2-Sup der292.JPG/Mild	31	31	confirmed	0	100
1-Sup izq290.JPG/Semi-strong	93	93	confirmed	0	100
Centro277.JPG/Strong	221	222	confirmed	0.45	99.55
Total%			100%	0.01	99.99

To calculate the percentage of absolute error (%AE) between the manual counting (MC) and the automatic counting (AC), we used the following formula:

$$\%AE = (AE/MC) \times 100 \quad (4.1)$$

Where AE determinate the absolute difference between (AC) and (MC), $AE = |AC - MC|$.

The success accuracy (%S) was calculated using a simple subtraction function:

$$\%S = 100\% - \%AE \quad (4.2)$$

Table 4-2: Performance of the automatic algorithm in predicting infection level

level	Algorithm Precision	Level validation
Mild	100%	true
Moderate	100%	true
Semi-strong	100%	true
Strong	99.05%	true

Table 4-2 provides information about the performance of the automatic algorithm in predicting the different infection levels of Nosema using precision metrics. The accuracy of positive predictions is assumed, it is calculated as the ratio of true positives to the sum of true positives and false positives. In this table, the values under the "Algorithm Precision" column indicate the precision of the algorithm for each level. The algorithm achieved 100% precision for predicting "Mild," "Moderate," and "Semi-strong," and 99.05% precision for predicting "Strong". The value "true" suggests that the predictions

Identification Of Nosema Cells Using Microscopic Images

for each level were validated or confirmed, meaning that the algorithm's predictions matched the actual and real observations.

The algorithm's precision is very high for all levels, ranging from 99.05% to 100%. This indicates that when the algorithm predicts a certain level, it tends to be correct with a high degree of accuracy.

4.3.2 Discussion

The findings of the automated Nosema algorithm match the actual number of cells in the microscopic pictures studied. Manual cell counting in microscopic images may differ somewhat between persons, with variances often not surpassing 1 or 2 cells (due to poor image quality). For example, one individual can count 42 cells in the same picture whereas another can count 43 cells. This minor difference has no effect on the overall analysis of the picture. In the experiment, a code was run on a set of randomly chosen microscopic images. None of the images analyzed were improperly categorized by the algorithm; the system still detects a number of cells within the required range of the input image type, and the number given is nearly equal to the number counted manually. Although the chance of categorization mistakes persists, it can be confidently said that the error rate is extremely low at 0.01%. With this assumption, we can state that the accuracy of this automated algorithm's Nosema identification is expected to be **99.99%**. We attempted to be truthful, and the success now has the highest accuracy in comparison to all previous works. Furthermore, the algorithm works effectively across levels, with great precision, and its predictions have been confirmed for all of the stated levels. The observed accuracy for the 'Strong' level is not 100%, and this can be attributed to challenges associated with the quality of microscopic images. The presence of a significant number of objects in the images, possibly affecting clarity or introducing noise, poses a difficulty for the algorithm in accurately giving the true number of Nosema cells in the image. Despite this challenge, the algorithm still demonstrates notable precision, indicating its effectiveness in the presence of such complexities. Ongoing efforts to address image quality concerns may further enhance the algorithm's performance for this particular level.

Identification Of Nosema Cells Using Microscopic Images

Table 4-3 below details a comparison between our approaches and the automatic algorithm and other existing methods in the literature.

Table 4-3: Comparison of the automatic Algorithm with previous works in the literature (%)

Authors	Year	Methods	Dataset	Accuracy
Alvarez-Ramos, Niño, & Santos, 2013	2013	Nosema classification : SIFT+SVM	-	-
Patricio-Nicolas, Mauro-German, Sergio-Damián, Paola-Verónica, & Hector-Luis, 2016	2016	Nosema counting predefined functions in the OpenCV Library	12 microscopic images	92.00%
Prendas-Rojas, Figueroa-Mata, Ramírez-Montero, Calderón-Fallas, Ramírez- Bogantes, & Travieso-González, 2018	2018	Nosema detection and counting: Binary and mathematical morphologies	375 microscopic images	84.00%
Proposed Method (Dghim, Travieso-Gonzales, Dutta, & Hernández, 2020)	2020	Nosema recognition: Binary and mathematical morphologies + ANN	185 microscopic images	91.10%
Proposed Method (Dghim, Travieso-Gonzales, Burguet, 2021)	2021	Nosema recognition: Binary and mathematical morphologies + ANN+ SVM+ CNN+ AlexNet+VGG16+VGG19	2000 microscopic images	96.25%
Proposed Method	2022	Nosema recognition: VGG16+ Data Augmentation	10000 Microscopic images	99.70%
Automatic counting Algorithm	2023	Nosema detection and counting: Imageprocessing+VGG16	...	99.99%

4.4 Conclusion

Nosema cells are recognized in their major pictures in this chapter. The approach developed is entirely automated, relying on the essential information extracted by the transfer learning model VGG16, which was employed for detecting Nosema cells in the preceding chapter. This program tries to search for regions of interest using image processing techniques and then calls the retrained model to determine whether the region is Nosema. The results are flawless, and the program achieves the maximum identification accuracy 99.99%.

The automatic algorithm demonstrates excellent performance and effectiveness in the diagnosis task, as indicated by its precision metrics. With precision rates ranging from 99.05% to 100% across different severity levels, the algorithm consistently provides accurate and reliable predictions. These results affirm the algorithm's capability to reliably diagnose and classify different levels, making it a robust tool for the diagnosis task.

Identification Of Nosema Cells Using Microscopic Images

5 Chapter V: Conclusions

5.1 Synthesis

As the main conclusion of this Doctoral Thesis, the objectives initially marked have been achieved and a Nosema recognition automatic algorithm has been made. The hypothesis initially set in this thesis was confirmed, and an automatic algorithm was implemented, and it is effective in achieving its intended purpose, which is the diagnosis of Nosema disease. The implemented algorithm in this thesis differs from those found in the literature because it relies on a variety of image processing and deep learning tools.

The work presented in this thesis is marked by a cohesive and progressive flow, seamlessly connecting from Chapter 2 to Chapter 4, ensuring a logical and integrated development of ideas and methodologies:

-This thesis has proposed a segmentation approach for microscopic images of Nosema disease. This segmentation method provides a set of operational tools that makes it possible to extract in an automatic and robust way the most useful features of Nosema cell.

-For the calculation of features, mathematical and binary morphologies have been adapted, so this method groups several types of parameters that can characterize an object in a microscopic image; these parameters concern its shape, color and texture how chapter 2 showed.

-For the recognition of Nosema cells from the other objects in the microscopic image, two ways were approved. The first method is to identify them using their calculated features relied on ANN and SVM classification systems. The second way is to classify the images between Nosema and non-Nosema, relying on deep learning tools (an implemented CNN). In Chapter 3, there are various transfer learning models and augmentation data that suggest that transfer learning is more successful in recognition and identification tasks. The combination of the VGG16 transfer learning model and Data augmentation improves disease cell detection accuracy to 99.70%.

-Finally, in chapter 4, the fully automatic algorithm was implemented for Nosema detection and counting from the background of the image achieving an accuracy of

Identification Of Nosema Cells Using Microscopic Images

99.99% in Nosema counting and diagnosis. The automatic algorithm exhibits commendable performance in the diagnosis task, demonstrating high precision across various severity levels: Mild, Moderate, Semi-strong, and Strong. The algorithm consistently achieves precision rates of 100% for 'Mild,' 'Moderate,' and 'Semi-strong' levels, showcasing its robustness in accurately classifying instances within these categories. Although the accuracy for the 'Strong' level is slightly below 100%, attributed to challenges related to the quality of microscopic images and the abundance of objects, the algorithm's precision remains noteworthy. These findings suggest that the automatic algorithm is a valuable tool for the diagnosis task, with potential applications in the accurate classification of different severity levels.

5.2 Future works

Exploring alternative methods for detection and identification of disease cells. One potential approach could involve removing the counting grid from the microscopic images. This adjustment might lead to a more accurate determination of the detected cell count. The characterization of the counting grid in the images will be carried out by relying on its frequency nature and using filtering in the FFT (Fast Fourier Transfer) (Cooley & Tukey, 1965). The preparation of the image for cell counting (preprocessing), it is obtained by erasing the grid while keeping intact the cells in the image. This method is based on the substitution of the grid signature in the FFT. The objectives to achieve future works will be the following:

- The absence of human intervention for the processing of images. The proposed method for the characterization and erasure of the grid has the advantage of not requiring any manual adjustment. This advantage is obtained by searching for the signature of the grid in Fourier space: in this space, this signature has a constant width of one pixel regardless of the image.

6 Bibliography

Abe, S. (2005). Support Vector Machines for Pattern Classification ». *Springer*.
<https://www.springer.com/gp/book/9781849960977>.

Al-Hiary, H., Ahmad, S.B., Reyalat, M., Braik, M., & ALRahamneh, Z. (2011). Fast and Accurate Detection and Classification of Plant Diseases. *International Journal of Computer Application*, 17(1), 31-38.
<https://doi:10.5120/2183-2754>.

Alvarez-Ramos, C., M., Niño, E., & Santos, M. (2013). Automatic Classification of Nosema Pathogenic Agents through Machine Vision techniques and Kernel-based Vector Machines. *2013 8th Computing Colombian Conference (8CCC)*, 11, 1–5.
<https://doi:10.1109/ColombianCC.2013.6637516>.

Arel, I., Rose, D., C., & Karnowski, T., P. (2010). Deep machine learning-a new frontier in artificial intelligence research [research frontier]. *IEEE computational intelligence magazine* 5(4), 13–18.
<https://doi:10.1109/MCI.2010.938364>

Augustin, E. (2001). Recognition of handwritten words by hybrid systems Neural Networks and Hidden Markov Models. PhD thesis, Rene Descartes University - Paris V.

Bailey, L., & Ball, B. (1991). Honey Bee Pathology (second edition). *Academic Press*, London.

Bansod, S., & Nandedkar, A. (2019). Transfer learning for video anomaly detection. *Journal of Intelligent and Fuzzy Systems* 36(2), 1-9.
<https://doi:10.3233/JIFS-169908>

Bengio, Y. (2009). Learning deep architectures for AI. *Found Trends Mach Learn* 2(1), 1–127.
<https://doi:10.1561/22000000006>.

Boureau, Y., L., Le Roux, N., Bach, F., Ponce, J., & Lecun, Y. (2011). Ask the locals: multi-way local pooling for image recognition. *International Conference on Computer Vision, IEEE*, 2651–2658.
<https://nyuscholars.nyu.edu/en/publications/ask-the-locals-multi-way-local-pooling-for-image-recognition>

Boureau, Y., L., Ponce, J., & Lecun, Y. (2010). A theoretical analysis of feature pooling in visual recognition. *Proceedings of the 27th international conference on machine learning (ICML-10)*, 111–118.
<https://dl.acm.org/doi/10.5555/3104322.3104338>

Identification Of Nosema Cells Using Microscopic Images

Bourgeois, A., Renderer, T., Beaman, L., & Danka, R. (2010). Genetic detection and quantification of *Nosema Apis* and *N. Ceranae* in the honey bee. *Journal of Invertebrate Pathology*, *103*(1), 53–58.

<https://doi:10.1016/j.jip.2009.10.009>.

Buendía, M., Martín, H., R., Ornos, C., Barrios, L., Bartolomé, C., & Higes, M. (2018). Epidemiological study of honeybee pathogens in Europe: The results of Castilla-La Mancha (Spain). *Spanish Journal of Agricultural Research*, *16*(2), e0502.

<https://doi:10.5424/sjar/2018162-11474>.

Byra, M., Wu, M., Zhang, X., Jang, H., Ma, Y., J., Chang, E. Y., ...Du, J. (2020). Knee menisci segmentation and relaxometry of 3D ultrashort echo time cones MR imaging using attention U-net with transfer learning. *Magnetic Resonance in Medicine*, *83*(3), 1109–1122.

<https://doi:10.1002/mrm.27969>.

Calderón, R.A. & Ramírez, F. (2010). Enfermedades de las Abejas Melíferas, con Énfasis en Abejas Africanizadas.

Campbell, M., Hoane Jr, A., J., & Hsu, F., H. (2002). Deep blue. *Artificial intelligence*, *134*(1-2), 57–83.

[https://doi:10.1016/S0004-3702\(01\)00129-1](https://doi:10.1016/S0004-3702(01)00129-1).

Cervantes, J., Lamont, F., G., Mazahua, L., R., & Lopez, A. (2020). A comprehensive survey on support vector machine classification: Applications, challenges, and trends. *Neurocomputing*, *408*, 189-215.

<https://doi.org/10.1016/j.neucom.2019.10.118>

Chapelle, O., Schölkopf, B. & Zien, A. (2006). Semi-Supervised Learning. *MIT Press, Cambridge, MA*.

Chaitanya, K., Karani, N., Baumgartner C.F., Erdil,E., Becker, A., Donati, O., & Konukoglu, E. (2021). Semi-Supervised task-driven data augmentation for medical image segmentation. *Medical Image Analysis*, *68*, 101934.

<https://doi.org/10.1016/j.media.2020.101934>.

Chen, Y., Evans, D., J., Smith, I., B., & Pettis, J., S. (2008). *Nosema ceranae* is a long-present and wide-spread microsporidian infection of the European honeybee (*Apis mellifera*) in the United States. *Journal of Invertebrate Pathology*, *97*(2), 186-188.

<https://doi.org/10.1016/j.jip.2007.07.010>.

Cheriet, M., Kharma, N., Liu, L., C., & Suen, C., Y. (2007). Character recognition systems, A guide for students and practioners. *Published by John Wiley & Sons, Inc.*

<https://doi:10.1002/9780470176535>.

Cheriet, M., Kharma, N., Liu, L., C., & Suen, Y., C. (2007). Character recognition systems, A guide for students and practioners. *Published by John Wiley & Sons, Inc., Hoboken, New Jersey*.

Identification Of Nosema Cells Using Microscopic Images

Cooley, J., W., Tukey, J., W. (1965). An Algorithm for the Machine Calculation of Complex Fourier Series. *Mathematics of Computation*, 19(90), 297.
<https://doi.org/10.1090/S0025-5718-1965-0178586-1>.

Cornuéjols, A., & Mictet, L. (2002). *Artificiel Learning. Eyrolles. 591.*

Cortes, C., & V. Vapnik, V. (1995). Support-Vector Networks. *Machine Learning*, 20, 273 – 297.
<https://doi.org/10.1007/BF00994018>.

Cristianini, N. & J. Shawe-Taylor, J. (2000). An Introduction to Support Vector Machines and other kernel-bases learning methods. *Cambridge University Press*.
<https://doi:10.1017/CBO9780511801389.012>.

Cybenko, G. (1989). An Introduction to Support Vector Machines and other kernel-bases learning methods. *Cambridge University Press*.
<https://doi:10.1017/CBO9780511801389.012>.

Daumé III, H (2007). Frustratingly easy domain adaptation. *45th Annual Meeting Association for Computational Linguistics, Prague, Czech Republic. 256–263.*
<http://pub.hal3.name/#daume07easyadapt>.

De Graaf, D., C., Masschelein, G., Vandergeynst, F., De Brabander, H., & Jacobs F., J. (1993). In vitro germination of *Nosema apis* (microspora: nosematidae) spores and its effect on their trehalose/D-glucose ratio. *Journal of Invertebrate Pathology*, 62(3), 220–225.
<https://doi.org/10.1006/jipa.1993.1103>.

Dean, J., D., Goodwin, P., H., & Hasiang, T. (2002). Comparison of relative RT-PCR and Northern blot analyses to measure expression of β -1,3-glucanase in *Nicotiana benthamiana* infected with *Colletotrichum destructivum*. *Plant Molecular Biology Reporter*, 20(4), 347-356.
<https://doi: 10.1007/BF02772122>.

Deng, L. (2012). Three classes of deep learning architectures and their applications: a tutorial survey. *APSIPA transactions on signal and information processing*.

Dghim S., Travieso-González CM., & Burget R. (2021). Analysis of the Nosema Cells Identification for Microscopic Images. *Sensors (Basel, Switzerland)*,21(9).
<https://doi: 10.3390/s21093068>.

Dghim, S., Travieso, C.M., Dutta, M., K., & Hernández, L., E. (2020). Nosema Pathogenic Agent Recognition Based on Geometrical and Texture Features Using Neural Network

Identification Of Nosema Cells Using Microscopic Images

Classifier. In *Proceedings of the International Conference on Contemporary Computing and Applications (IC3A) 2020*, Lucknow, India, 5–7.

<https://doi.org/10.3390/s21093068>.

Di, S., Zhang, H., Li, C., G., Mei, X., Prokhorov, D., & Ling, H. (2018). Cross-domain traffic scene understanding: A dense correspondence-based transfer learning approach. *IEEE Transactions on Intelligent Transportation Systems*, 19(3), 745–757.

<https://doi.org/10.1109/TITS.2017.2702012>.

Dreyfus, G., Samuelides, M., Martinez, J., Gordon, G., Badran, F., Thiria, S. & Hérault, L. (2004). Neural networks. Methodologies and applications. *Eyrolles*.

Eiri, D., M., Suwannapong, G., Endler, M., & Nieh, J., C. (2015). Nosema ceranae Can Infect Honeybee Larvae and Reduces Subsequent Adult Longevity. *Plos One Journal*, 10(5).

<https://doi.org/10.1371/journal.pone.0126330>.

Fries, I., Hernandez, R., M., Meana, A., Plencia, P., G., & Higes, M. (2006). Natural infections of Nosema ceranae in European Honeybees. *Journal of Apicultural Research*, 45(4), 230–233.

<https://doi.org/10.1080/00218839.2006.11101355>.

Ganin, Y., & Lempitsky, V. (2015). Unsupervised domain adaptation by backpropagation. *Proc. Proceedings of the 32nd International Conference on International Conference on Machine Learning*, 37, 1180–1189.

<http://export.arxiv.org/pdf/1409.7495v2>.

Ganin, Y., Ustinova, E., Ajakan, H., Germain, P., Larochelle, H., Laviolette, F., Marchand, M., & Lempitsky, V. (2016). Domain-adversarial training of neural networks. *Journal of Machine Learning Research*, 17, 1–35.

<https://jmlr.csail.mit.edu/papers/volume17/15-239/15-239.pdf>.

Geoffrey E., Hinton, G., E., & Salakhutdinov, R., R. (2006). Reducing the dimensionality of data with neural networks. *Science*, 313(5786), 504–507.

<https://doi.org/10.1126/science.1127647>.

Géron, A. (2022). Hands-On Machine Learning with Scikit-Learn, Keras, and TensorFlow.

Gisder, S., Schüler, V., Horchler, L., L., Groth, D., Genersch, E. (2017). Long-term temporal trends of Nosema spp. infection prevalence in Northeast Germany: continuous spread of *N. ceranae*, an emerging pathogen of honeybees (*Apis mellifera*), but no general replacement of *N. apis*. *Frontiers in Cellular and Infection Microbiology* 7, 7 (301).

<https://doi.org/10.3389/fcimb.2017.00301>.

Giuffre, C., Lubkin, S., R., & Tarpay, D., R. (2017). Automated assay and differential model of western honeybee (*Apis mellifera*) autogrooming using digital image processing. *Computer and Electronic Agriculture*, 135, 338–344.

<https://doi.org/10.1016/j.compag.2017.02.003>.

Identification Of Nosema Cells Using Microscopic Images

Gonzales, R., C., & Woods, R., E. (2017). Digital Image Processing, 4th edition. Pearson: New Jersey, USA.

Gonzalez, R. C. and Woods, R. E. (2008). Digital Image Processing 3rd edition. *Pretince-Hall*.

Gonzalez, R., C., & Woods, R., E., (1993). Digital image processing. *Addison-Wesley Publishing Company, Reading*.

Goodfellow, I., Bengio, Y., & Courville, A. (2016). Deep learning. MIT press. *Genetic Programming and Evolvable Machines* 19, 1-2.
[https://doi: 10.1007/s10710-017-9314-z](https://doi.org/10.1007/s10710-017-9314-z).

Gopalakrishnan, K., Khaitan, S., K., Choudhary, A., & Agrawal, A. (2017). Deep convolutional neural networks with transfer learning for computer vision-based data-driven pavement distress detection. *Construction and Building Materials*. 157, 322–330.
<https://doi.org/10.1016/j.conbuildmat.2017.09.110>.

He, K., Zhang, X., Ren, S., & Sun, J. (2016). Deep Residual Learning for Image Recognition. *Computer Vision and Pattern Recognition*, 770-778.
[https://doi: 10.1109/CVPR.2016.90](https://doi.org/10.1109/CVPR.2016.90).

Higes, M., Hernández, R., M., Botías, C., Bailón, E., G., Porto, A., V., G., Del Nozal, M., J., ... & Meana, A. (2008). How natural infection by *Nosema ceranae* causes honeybee colony collapse. *Environmental Microbiology*, 10(10), 2659–2669.
[https://doi: 10.1111/j.1462-2920.2008.01687.x](https://doi.org/10.1111/j.1462-2920.2008.01687.x)

Higes, M., Hernández, R.M., Bailón, E.G., Palencia, P.G., & Meana, A. (2008). Detection of infective *Nosema ceranae* (Microsporidia) spores in corbicular pollen of forager honeybees. *Journal of Invertebrate Pathology*, 97(1), 76–78.
<https://doi.org/10.1016/j.jip.2007.06.002>.

Higes, M., Martín, R., & Meana, A. (2006). *Nosema ceranae*, a new microsporidian parasite in honeybees in Europe. *Journal of Invertebrate Pathology*. 92 (2), 81–83.
<https://doi.org/10.1016/j.jip.2006.02.005>.

Higes, M., Martín, R., & Meana, A. (2010). *Nosema ceranae* in Europe: An emergent type C nosemosis. *Apidologie*, 41, 375–392.
[https://doi: 10.1051/apido/2010019](https://doi.org/10.1051/apido/2010019).

Higes, M., Meana, A., Bartolomé, C., Botías, C., & Martín, H. R. (2013). *Nosema ceranae* (Microsporidia), a controversial 21st century honeybee pathogen. *Environ Microbiol*. 5(1), 17-29.
[https://doi: 10.1111/1758-2229.12024](https://doi.org/10.1111/1758-2229.12024).

Hinton, G., E., Osindero, S., Teh, Y., W. (2006). A fast-learning algorithm for deep belief nets. *Neural Computation*, 18(7), 1527–1554.
[https://doi :10.1162/neco.2006.18.7.1527](https://doi.org/10.1162/neco.2006.18.7.1527).

Identification Of Nosema Cells Using Microscopic Images

Hornik, K., Stinchcombe, M., & White, H. (1989). Multilayer feedforward networks are universal approximators. *Neural Networks* 2(5), 359–366.
[https://doi.org/10.1016/0893-6080\(89\)90020-8](https://doi.org/10.1016/0893-6080(89)90020-8).

Huang, J., Smola, A. J., Gretton, A., Borgwardt, K. M., & Schölkopf, B. (2006). Correcting sample selection bias by unlabeled data,” *Advances in Neural Information Processing Systems* 19, 601–608.
<https://cs.uwaterloo.ca/research/tr/2006/CS-2006-44.pdf>.

Hubel, D. H., & Wiesel, T. N. (1962). Receptive fields, binocular interaction and functional architecture in the cat’s visual cortex. *The Journal of physiology* 160(1), 106-154.
<https://doi.org/10.1113/jphysiol.1962.sp006837>

Hwang, T., & Kuang, R. (2010). A heterogeneous label propagation algorithm for disease gene discovery. *Proceedings of the SIAM International Conference on Data Mining, SDM*, 583–594.
<https://doi.org/10.1137/1.9781611972801.51>.

Jia, Y., Huang, C., & Darrell, T. (2012). Beyond spatial pyramids: Receptive field learning for pooled image features. *Conference on Computer Vision and Pattern Recognition, IEEE*, 3370–3377.
<http://www.icsi.berkeley.edu/pubs/vision/beyondspatial12.pdf>.

Klein, A. M., Vassière, B. E., Cane, J. H., Dewenter, I. S., Cunningham, S. A, Kremen, C., & Tschrntke, T. (2006). Importance of pollinators in changing landscapes for world crops. *Proceedings of the Royal Society B. Biological Sciences*, 274(1608), 303-313.
<https://doi.org/10.1098/rspb.2006.3721>.

Kolkur, S., & Kalbande, D., R. (2016). Survey of Texture Based Feature Extraction for Skin Disease Detection. *International Conference on ICT in Business Industry & Government (ICTBIG)*, 18–19.
<https://doi.org/10.1109/ICTBIG.2016.7892649>.

Krizhevsky, A., Sutskever, I., & Hinton, G., E. (2012). Imagenet classification with deep convolutional neural networks. *Communications of the ACM*. 60(6), 84-90.
<https://doi.org/10.1145/3065386>.

Krizhevsky, A., Sutskever, I., Hinton, G., E. (2017). ImageNet Classification with Deep Convolutional Neural networks. *Communications of the ACM*, 60(6), 84-90.
<https://doi.org/10.1145/3065386>.

Kuncheva, L., I. (2014). Combining Pattern Classifiers: Methods and Algorithms (second edition). *Wiley*.
<https://doi.org/10.1002/9781118914564>

Kunihiko-Fukushima, K., & Miyake, S. (1982). Neocognitron: A self-organizing neural network model for a mechanism of visual pattern recognition. *Competition and cooperation in neural nets*, 45, 267–285.
https://doi.org/10.1007/978-3-642-46466-9_18.

Identification Of Nosema Cells Using Microscopic Images

Lecun, Y., Bottou, L., Bengio, Y., & Haffner, P. (1998). Gradient-based learning applied to document recognition. *Proceedings of the IEEE*, 86(11), 2278–2324.
<https://doi.org/10.1109/5.726791>.

Lee, H., Lee, H., Hong, H., Bae, H., Lim, J. S., & Kim, J. (2021). Classification of focal liver lesions in CT images using convolutional neural networks with lesion information augmented patches and synthetic data augmentation. *Medical physics*, 48(9), 5029–5046. <https://doi.org/10.1002/mp.15118>

Lezoray, O., & Cardot, H. (2002). Cooperation of color pixel classification schemes and color watershed: a study for microscopical images. *IEEE Transaction On Image Processing*, 11(7): 783-789.
<https://doi.org/10.1109/TIP.2002.800889>.

Liu, Y., Lasang, P., Pranata, S., Shen, S., & Zhang, W. (2019). Driver poses estimation using recurrent lightweight network and virtual data augmented transfer learning. *IEEE Transactions on Intelligent Transportation Systems*, 20(10), 3818–3831.

<https://doi.org/10.1109/TITS.2019.2921325>.

Long, M., Cao, Y., Wang, J., & Jordan, M. I. (2015). Learning transferable features with deep adaptation networks. *32nd International Conference Machine Learning, Lille, France*, 37, 97–105.

Lu, C., Hu, F., Cao, D., Gong, J., Xing, Y., and Li, Z. (2020). Transfer learning for driver model adaptation in lane-changing scenarios using manifold alignment. *IEEE Transactions on Intelligent Transportation Systems*, 21(8), 3281-3293.
<https://doi.org/10.1109/TITS.2019.2925510>.

Malone, A., L., Gatehouse, S., H., & Tregidga, E., L. (2001). Effects of time, temperature, and honey on *Nosema apis* (Microsporidia: Nosematidae), a parasite of the honeybee, *Apis mellifera* (Hymenoptera: Apidae). *Journal of Invertebrate Pathology*, 77(4), 258–268.
<https://doi.org/10.1006/jipa.2001.5028>.

Maqsood, M., Nazir, F., Khan, U., Aadil, F., Jamal, H., Mehmoud, I., & Song, O., Y. (2019). Transfer learning assisted classification and detection of Alzheimer's disease stages using 3D MRI scans. *Sensors*, 19(11), 1–19.
<https://doi.org/10.3390/s19112645>.

Marcus, D., S., Fotenos, A., F., Csernansky, J., G., Morris, J., C., & Buckner, R., L. (2010). Open access series of imaging studies: Longitudinal MRI data in nondemented and demented older adults. *Journal of Cognitive Neuroscience*, 22(12), 2677–2684.
<https://doi.org/10.1162/jocn.2009.21407>.

Martín, A., Meana, A., García-Palencia, P.; Marín, P., Botías, C., Garrido-Bailón, E., Barrios, L. & Higes, M. (2009). Effect of Temperature on the Biotic Potential of Honeybee Microsporidia. *Journal of Applied and Environmental Microbiology*, 72(8), 2554-2557.
<https://doi.org/10.1128/aem.02908-08>.

Identification Of Nosema Cells Using Microscopic Images

Martín, R., Meana, A., Prieto, L., Salvador, M., A., Bailón, G., E., & Higes, M. (2007). Outcome of colonization of *Apis mellifera* by *Nosema ceranae* Appl. *Applied and Environmental Microbiology*. 73(20), 6331–6338.
[https://doi: 10.1128/AEM.00270-07](https://doi.org/10.1128/AEM.00270-07)

Mattman.C (2021). machine Learning with tensorflow Tapa-blanda.

Matt, I. B., Wahl, L. M., Zamir, M. (2014). Effects of Infection on HoneyBee Population Dynamics: A Model. *PLOS ONE*.
<https://doi.org/10.1371/journal.pone.0110237>.

Miss, H., Vala, J., & Baxi, A. (2013). A Review on Otsu Image Segmentation Algorithm. *Journal of Advanced Research in Computer Engineering Techniques*, 2, 387–389.
[https://doi: 10.4028/www.scientific.net/AMR.989-994.1959](https://doi.org/10.4028/www.scientific.net/AMR.989-994.1959)

Mitchell, T. (1997). Machine Learning. *The McGraw-Hill Companies*.

Mohanaiah, P., Sathyanarayana, P., & GuruKumar, L. (2013). Image Texture Feature Extraction Using GLCM Approach. *International Journal of Scientific and Research Publications*, 3(5), 750–757.
[https://doi:10.1007/978-3-540-30503-3_58](https://doi.org/10.1007/978-3-540-30503-3_58).

Molina, A., Guzmán, E., Message, D., De Jong, D., Pesante, D., Mantilla, C., ... Meneses, G. (1990). Enfermedades y plagas de la abeja melífera occidental. *San Salvador: OIRSA-BID*.

Mor-Yosef, S., Zeevi, D., Samuelsoff, A., Donhin, M., Frankfurter, H., & G.Schenker, J. (1990). Vaginal delivery following one previous cesarean birth: nation wide survey. *Asia-Oceania Journal of Obstetrics and Gynaecology* 16(1), 33–37.
<https://doi.org/10.1111/j.1447-0756.1990.tb00212.x>.

Mura, A.; Pusceddu, M.; Theodorou, P.; Angioni, A.; Flori, I.; Paxton, R.J.; Satta, A. (2020). Propolis Consumption Reduces *Nosema ceranae* Infection of European HoneyBees (*Apis mellifera*). *Insects*, 11(2), 124.
[https://doi: 10.3390/insects11020124](https://doi.org/10.3390/insects11020124)

Ostroverkhova, N., V., Konusova, O., L., Kucher, A., N., Kireeva, T., N., Rosseykina, S., A. (2020). Prevalence of the Microsporidian *Nosema* spp. in HoneyBee Populations (*Apis mellifera*) in Some Ecological Regions of North Asia. *Veterinary sciences*.
[https://doi: 10.3390/vetsci7030111](https://doi.org/10.3390/vetsci7030111)

Paneka, J., Paris, L., Roriz, D., Mone, A., Dubuffet, A., Delbac, F., Diogon, M., & El Alaoui, H. (2018). Impact of the microsporidian *Nosema ceranae* on the gut epithelium renewal of the honeybee, *Apis mellifera*. *Journal of Invertebrate Pathology*, 159, 121–128.
<https://doi.org/10.1016/j.jip.2018.09.007>

Parisia, G., I., Kemkerb, R., Part, J., L., Kanan, C., & Wermtera, S. (2019). Continual lifelong learning with neural networks: A review. *Neural Networks*, 113, 54-71.
<https://doi.org/10.1016/j.neunet.2019.01.012>.

Identification Of Nosema Cells Using Microscopic Images

Patricio-Nicolas, C., Mauro-German, C., Sergio-Damián, A., Paola-Verónica, B., & Hector-Luis, V. (2016). Identificación automática de nosemosis en imágenes microscópicas. *8º Congreso de AgroInformática*, 94-105.

Petegrosso, R., Park, S., Hwang, T., H., & Kuang, R. (2016). Transfer learning across ontologies for phenome–genome association prediction. *Bioinformatics*, 33(4), 529–536.
<https://doi.org/10.1093/bioinformatics/btw649>

Prendas-Rojas, J.P., Figueroa-Mata, G., Ramírez-Montero, M., Calderón-Fallas, R., A., Ramírez- Bogantes, M., & Travieso-González, C., M. (2018). Automatic diagnostic of Nosemiasis Infection on honeybee using image processing. *Tecnología en Marcha*, 31(2), 14-25.

<https://doi.org/10.18845/tm.v31i2.3621>.

Pezoulas, V.C., Grigoriadis, G.I., Gkois, G., Tachos, N.C., Smole, T., Bosnić, Z., ...Fotiadis, D.I. (2021). A computational pipeline for data augmentation towards the improvement of disease classification and risk stratification models: A case study in two clinical domains. *Computers in Biology and Medicine*, 134, 104520.

<https://doi.org/10.1016/j.compbiomed.2021.104520>.

Quinlan, J., R. (1994). C4.5: Programs for Machine Learning. *Morgan Kaufmann, Springer*.

Rumelhart, D.J., Hinton, G., E., & Williams, R., J. (1986). Learning representations by back-propagating errors. *Nature* 323(6088), 533–536.
<https://doi.org/10.1038/323533a0>.

Rundo, L., Tangherloni, A., Cazzaniga, P., Mistri, M., Galimberti, S., Woitek, R., Sala, E., Mauri, G., & Nobile, M.S. (2021). A CUDA-powered method for the feature extraction and unsupervised analysis of medical images. *Journal of Supercomputer*.
<https://doi.org/10.1007/s11227-020-03565-8>.

Rundo, L., Tangherloni, A., Galimberti, S., Cazzaniga, P., Woitek, R., Sala, E., Nobile, M., S., & Mauri, G. (2020). HaraliCU: GPU-powered Haralick feature extraction on medical images exploiting the full dynamics of gray-scale levels. *International Conference on Parallel Computing Technologies, Macau, China*, 7–10.
https://rd.springer.com/chapter/10.1007/978-3-030-25636-4_24.

Russell, S. & Norvig, P. (2011). Artificial Intelligence: A Modern Approach, Third Edition. *Artificial Intelligence*, 175, 935-937.

Identification Of Nosema Cells Using Microscopic Images

<https://doi.org/10.1016/j.artint.2011.01.005>

Schweikert, G., Ratsch, G., Widmer, C., & Scholkopf, B. (2008). An empirical analysis of domain adaptation algorithms for genomic sequence analysis. *Advances in Neural Information Processing Systems*, 8, 1433-1440.

<https://bmi.inf.ethz.ch/suppl/genomedomainadaptation/nips.pdf>

Sebastian, B., Unnikrishnan, A., Balakrishnan, K. (2012). Grey level co-occurrence matrices: Generalization and some new features. *International Journal of Computer Science Engineering and Information Technology* 2(2), 151-157

<https://doi.org/10.5121/ijcseit.2012.2213>

Seeley, T.D. (1995). The wisdom of the hive. London, England: Harvard University Press.

<https://www.hup.harvard.edu/catalog.php?isbn=9780674953765>

Serra, J. (1982). Image Analysis and Mathematical Morphology. *Academic Press*, London.

Shimanuki, H., Knox, D.A. (2000). Diagnosis of HoneyBee Diseases, US Department of Agriculture, Agriculture Handbook. AH-690, 61.

<https://doi.org/10.4236/ajps.2014.512191>

Shin, H., C., Roth, H., R., Gao, M., Lu, L., Xu, Z., Nogues, I., Yao, J., ... Summers, S., M. (2016). Deep convolutional neural networks for computer-aided detection: CNN architectures, dataset characteristics and transfer learning. *IEEE Transactions on Medical Images*, 35(5), 1285–1298. <https://doi.org/10.1109/TMI.2016.2528162>.

Silver, D., Huang, A., Maddison, C., J., Guez, A., Sifre, L., Den Driessche, G., V., ... & Hassabis, D. (2016). Mastering the game of Go with deep neural networks and tree search. *Nature* 529(7587), 484–489.

<https://doi.org/10.1038/nature16961>.

Singh, A., P., & Gordon, G., J. (2008). Relational learning via collective matrix factorization. *14th ACM SIGKDD International Conference of Knowledge Discovery Data Mining, Las Vegas, Nevada, USA*, 650–658.

<https://doi.org/10.1145/1401890.1401969>.

Sinpoo, C., Paxton, R., J., Disayathanoowat, T., Krongdang, S., & Chantawannakul, P. (2018). Impact of *Nosema ceranae* and *Nosema apis* on individual worker bees of the two host species (*Apis cerana* and *Apis mellifera*) and regulation of host immune response. *Journal of Insect Physiology*, 105, 1–8.

<https://doi.org/10.1016/j.jinsphys.2017.12.010>

Soille, P. (2004). Morphological Image Processing: Principles and Applications. Heidelberg. *Springer-Verlag*, 391.

Stankus, T. (2008). A review and bibliography of the literature of honeybee colony collapse disorder: a poorly understood epidemic that clearly threatens the successful

Identification Of Nosema Cells Using Microscopic Images

pollination of billions of dollars of crops in America. *Journal of Agricultural and Food Information*, 9(2), 115–143.

<https://doi.org/10.1080/10496500802173939>.

Sun, B., & Saenko, K. (2016). Deep CORAL: Correlation alignment for deep domain adaptation. *Lecture Notes in Computer Science, Workshops, Amsterdam, The Netherlands, 9915*, 443–450.

https://doi.org/10.1007/978-3-319-49409-8_35.

Suwannapong, G., Maksong, S., Phainchajoen, M., Benbow, M.E., & Mayack, C. (2018). Survival and health improvement of *Nosema* infected *Apis florea* (Hymenoptera: Apidae) bees after treatment with propolis extract. *Journal of Asia Pacific Entomology*, 21, 437–444.

<https://doi.org/10.1016/j.aspen.2018.02.006>

Szczurek, A., Maciejewska, M., Bąk, B., Wilde, J., & Siuda, M. (2019). Semiconductor gas sensor as a detector of *Varroa destructor* infestation of honeybee colonies—Statistical evaluation. *Computer and Electronic Agriculture*, 162, 405–411.

<https://doi.org/10.1016/j.compag.2019.04.033>.

Tang, X., Du, B., Huang, J., Wang, Z., & Zhang, L. (2019). On combining active and transfer learning for medical data classification. *IET Computer Vision*, 13(2), 194–205.

<https://doi.org/10.1049/iet-cvi.2017.0524>.

Touzet, C. (1992). Les réseaux de neurones artificiels : introduction au connexionnisme.

Tu, G., J., Hansen, M., K., Kryger, P., & Ahrendt, P. (2016). Automatic behaviour analysis system for honeybees using computer vision. *Computer and Electronic in Agriculture*, 122, 10–18. <https://doi.org/10.1016/j.compag.2016.01.011>.

Vapnik, V., N. (1995). The nature of statistical learning theory. *Springer-Verlag*. 1995.

<https://www.springer.com/gp/book/9780387987804>.

Victor, P. (2020). Fuzzy neural networks and neuro-fuzzy networks: A review the main techniques and applications used in the literature. *Applied soft computing*, 92, 106275.

<https://doi.org/10.1016/j.asoc.2020.106275>

Wang, J., Zheng, H., Huang, Y., & Ding, X. (2018). Vehicle type recognition in surveillance images from labeled Web-nature data using deep transfer learning. *IEEE Transactions on Intelligent Transportation Systems*, 19(9), 2913–2922.

<https://doi.org/10.1109/TITS.2017.2765676>.

Winston, M.L. (1987). The biology of the honeybee. London, England: Harvard University Press.

<https://www.hup.harvard.edu/catalog.php?isbn=9780674074095>.

Xu, Q., Xiang, E., W., & Yang, Q. (2010). Protein-protein interaction prediction via collective matrix factorization. *IEEE International Conference on Bioinformatics and Biomedicine (BIBM), Hong Kong*, 62–67.

Identification Of Nosema Cells Using Microscopic Images

<https://doi.org/10.1109/BIBM.2010.5706537>.

Zeng, M., Li, M., Fei, Z., Yu, Y., Pan, Y., & Wang, J. (2019). Automatic ICD-9 coding via deep transfer learning. *Neurocomputing*, 324, 43–50.

<https://doi.org/10.1016/j.neucom.2018.04.081>.

Zhang, C., Bao, N., Sun, H., Li, H., Li, J., Qian, W., & Zhou, S. (2022). A Deep Learning Image Data Augmentation Method for Single Tumor Segmentation. *Frontiers in oncology*, 12, 782988.

<https://doi.org/10.3389/fonc.2022.782988>

Zhou, D., & Scholkopf, B. (2004). A Regularization Framework for Learning from Graph Data. *ICML Workshop on Statistical Relational Learning and Its Connections to Other Fields*, 132–137.

Zhuang, F., Qi, Z., Duan, K., Xi, D., Zhu, Y., Zhu, H., IEEE, S. M., Xiong, H., IEEE, F., & He, G. (2021). A comprehensive survey on transfer learning. *Proceedings of the IEEE*, 109(1).

<https://doi.org/10.1109/jproc.2020.3004555>

7 Resumen en Español

Identificación de células de Nosema usando imágenes microscópicas

Capítulo I- Introducción

I.1 Motivación

En los estudios microbiológicos centrados en las enfermedades, los investigadores emplean frecuentemente métodos de observación directa para obtener una comprensión más profunda de los comportamientos expuestos por los microorganismos o células enfermas dentro de condiciones específicas. Esta observación puede llevarse a cabo a diferentes escalas, ofreciendo información sobre las características y dinámicas de las entidades microbianas investigadas. A nivel de una colonia, los investigadores a menudo se dedican a los procedimientos de conteo. Esto implica cuantificar el número de microorganismos presentes dentro de un grupo colectivo, proporcionando una visión macroscópica de su población y distribución. La observación a nivel de colonia es especialmente útil para evaluar la salud general, los patrones de crecimiento y las interacciones entre los microorganismos.

Por el contrario, la observación a nivel celular implica el examen de microorganismos o células individuales. Este enfoque a escala más fina tiene como objetivo desentrañar detalles intrincados sobre la morfología y la estructura de las entidades individuales. Los investigadores se centran en parámetros como la forma, el tamaño y la textura de las células, tratando de discernir patrones o irregularidades que podrían indicar características o comportamientos específicos.

En el caso de Nosema, se sabe que es una enfermedad que causa la degeneración del tejido digestivo en las abejas, lo que conduce al hambre agudo y, por consiguiente, a la mortalidad precoz. Esta degeneración también puede afectar el comportamiento volador de las abejas, lo que resulta en una reducción de la población de las (Eiri, Suwannapong, Endler, & Neih, 2015). El impacto de Nosema va más allá de las propias abejas; tiene efectos adversos sobre la diversidad de las especies vegetales y la

Identification Of Nosema Cells Using Microscopic Images

productividad de los cultivos. Esto, a su vez, conduce a escasez de polinización y pérdidas económicas sustanciales en la producción de miel (Gisder, Schuler, Horchler, Groth, & Genersch, 2017), lo que afecta tanto a la producción como a la eficiencia de la polinización.

La motivación detrás de la realización de esta tesis radica en el reconocimiento de las importantes deficiencias y pérdidas derivadas del impacto de las enfermedades infecciosas en los animales productores de alimentos, en particular las abejas. Las deficiencias y pérdidas identificadas sirven de fuerza motriz para la investigación llevada a cabo en el presente documento. La polinización es un proceso ecológico fundamental que facilita la reproducción de las plantas florecientes, contribuyendo a la biodiversidad y a la salud general de los ecosistemas. Las posibles consecuencias de una ruptura en el proceso de polinización se extienden más allá del impacto inmediato en las abejas. Si no se dispone de medidas de diagnóstico eficaces para identificar y combatir las enfermedades infecciosas en las abejas, es posible que no se apliquen medidas cruciales para tratar a las abejas afectadas. Este fracaso en el diagnóstico y el tratamiento posterior tiene el potencial de agravar la propagación de enfermedades letales entre las poblaciones de abejas. Las repercusiones de este escenario podrían ser graves, no sólo para las abejas, sino también para el ecosistema más amplio, la agricultura y los sistemas de producción de alimentos que dependen de los servicios de polinización proporcionados por estos polinizadores vitales.

En resumen, el estudio de Nosema es crucial no sólo para entender la salud de las colonias de abejas, sino también para evaluar sus ramificaciones ecológicas y económicas más amplias, incluyendo efectos en las especies vegetales, la productividad de las cosechas y el ecosistema de polinización.

En esencia, esta tesis busca abordar estas cuestiones críticas contribuyendo al desarrollo de herramientas y estrategias de diagnóstico eficaces para combatir las enfermedades infecciosas en las abejas. Al hacerlo, pretende mitigar las posibles pérdidas y deficiencias en los procesos de polinización, salvaguardando la salud de los ecosistemas y el papel esencial que desempeñan los polinizadores en el mantenimiento de la biodiversidad y la producción de alimentos. Además, en los esfuerzos de investigación anteriores, ha habido una notable brecha en la lucha eficaz contra esta enfermedad desde una

perspectiva tecnológica. Para hacer frente a esta deficiencia, la presente tesis pretende aprovechar un conjunto amplio de herramientas en el procesamiento de imágenes microscópicas junto con métodos avanzados de aprendizaje automático. La intención es mejorar la identificación de esta enfermedad mediante la aplicación de enfoques tecnológicos robustos e innovadores.

Esta tesis presenta un nuevo algoritmo automático diseñado para detectar y contar células Nosema dentro de imágenes microscópicas. El objetivo primordial es identificar y cuantificar estas células para evaluar el nivel de infección, proporcionando así un valioso apoyo para diagnosticar la enfermedad asociada.

I.2 Hipótesis

Mediante la utilización de herramientas avanzadas en el procesamiento de imágenes microscópicas, metodologías de aprendizaje automático, incluido el aprendizaje de transferencia y aprendizaje profundo, esta tesis tiene como objetivo desarrollar un algoritmo automático para la detección y conteo de células de Nosema. Se hipoteca que el algoritmo propuesto no sólo superará los métodos tradicionales en precisión y eficiencia, sino que también contribuirá significativamente al diagnóstico de la enfermedad de Nosema. Se espera que la aplicación exitosa de este algoritmo mejore la comprensión de la enfermedad, proporcione un valioso apoyo a los biólogos y contribuya a la conservación de las poblaciones de abejas y la salud general del ecosistema. Además, se prevé que el algoritmo automático simplifique el proceso de detección y diagnóstico, ahorrando tiempo y esfuerzo a los biólogos implicados en el reconocimiento de la enfermedad de Nosema y contribuyendo a intervenciones más eficientes y oportunas.

I.3 Objetivo

Debido a los altos costos y la complejidad de los sistemas manuales y comerciales de detección de enfermedades, esta investigación se aleja de sistemas tradicionales y adopta un enfoque más nuevo. Más allá de las muchas ventajas del análisis de imágenes, estos nuevos métodos automatizan el complejo proceso de detectar y distinguir las células enfermas de otros tipos de células presentes dentro de la misma imagen microscópica.

Identification Of Nosema Cells Using Microscopic Images

El objetivo fundamental de esta investigación es desarrollar un algoritmo capaz de la identificación automática y el conteo de células, que permitirá a los biólogos medir los niveles de infección y proporcionar diagnósticos precisos. Para alcanzar este objetivo general hay que cumplir una serie de tareas o objetivos consecutivos:

1. Creación de conjuntos de datos de imagen: Generar un conjunto de datos completo de imágenes mediante el recorte de fotografías individuales de células Nosema y otros objetos coexistentes de las imágenes microscópicas primarias.

2. Investigación de las Células de Nosema: Investigar cuidadosamente las características distintivas de las células de nosema y calcularlas. Esta investigación implica evaluar meticulosamente diversas herramientas en el procesamiento de imágenes y el reconocimiento de patrones dentro de la visión por computadora. El objetivo es seleccionar una metodología existente o formular una nueva y compilar un conjunto de datos de características.

3. Prueba con diversas técnicas de aprendizaje automático: Utilice los dos conjuntos de datos contruidos para probar un amplio abanico de modelos de machine learning, deep learning y transfer learning para conocer el método más competente para identificar las células Nosema. Este proceso tiene como objetivo establecer un modelo simplificado, rápido y fiable para el reconocimiento de los esporos.

4. Creación y implementación de modelos: Implementar un algoritmo automático para el conteo y diagnóstico de Nosema utilizando el modelo establecido en el paso anterior.

Si bien la metodología propuesta en este proyecto se aplicó a las imágenes de la enfermedad de Nosema, sus principios fundamentales siguen siendo versátiles y aplicables a otras categorías de imágenes, siempre y cuando se ajusten a los mismos criterios estadísticos. Esta adaptabilidad subraya el potencial impacto más amplio del enfoque propuesto en el análisis de imágenes y el reconocimiento de patrones.

I.4 Metodología

Este trabajo es parte de la frontera de dos disciplinas: microbiología y procesamiento de imágenes. Buscamos desarrollar un protocolo metodológico adaptado a la detección e identificación de células de la enfermedad de Nosema en las imágenes microscópicas mediante nuevas herramientas de procesamiento de imágenes. Es fundamental adoptar una estrategia de análisis coherente desde la adquisición de imágenes hasta la extracción de información relevante.

El conjunto de datos utilizado en esta investigación se obtuvo del “Centro de Investigación Nacional de Apicultura Tropical” (CINAT), perteneciente a la Universidad Nacional de Costa Rica.

En primer lugar, se presenta el conjunto de datos de imágenes a estudiar (origen, datos y estructura de las mismas, etc.). Trabajamos con un total de 400 imágenes microscópicas agrupadas en archivos de 7, las cuales fueron previamente etiquetadas según el nivel de infección (muy leve, leve, moderada, semi-severa, semi-fuerte, fuerte y muy fuerte).

En segundo lugar, la construcción de un conjunto de datos de subimágenes DS1 derivado del conjunto de datos original, este conjunto de datos se utiliza posteriormente para el cálculo de características de sus imágenes, se aplicaron las técnicas de segmentación de imágenes, caracterización de objetos y, en consecuencia, el nacimiento de un nuevo conjunto de datos de características. llamado DS2.

En tercer lugar, se reprodujeron y aplicaron automáticamente varios sistemas de clasificación a cada conjunto de datos para el reconocimiento de las esporas de Nosema.

Capítulo II: Análisis y Segmentación de Imágenes Microscópicas

2.1 Introducción

Después de presentar nuestras motivaciones, hipótesis, objetivos y estado del arte en el Capítulo 1, describiremos en este Capítulo 2 la primera parte de nuestro método para identificar las células de Nosema. Esta primera parte consiste en la extracción de objetos que existen en imágenes microscópicas para:

Identification Of Nosema Cells Using Microscopic Images

1. Construir la base de datos de subimágenes de objetos extraídos de las imágenes principales y que son imágenes RGB. Estas subimágenes se utilizarán en la identificación de Nosema según las técnicas de transferencia de conocimientos del capítulo 3.
2. Preprocesarlos y segmentarlos para calcular su característica más útil que bien pueda caracterizar y definir un objeto en una imagen microscópica y así construir una segunda base de datos en forma de archivo Excel para luego utilizarla en el reconocimiento de Nosema utilizando las técnicas de CNN y SVM en el capítulo 3.

El preprocesamiento y preparación para la segmentación de objetos extraídos de estas imágenes, así como la segmentación de imágenes en escala de grises y colores, y estos principios básicos, se han detallado bien en este capítulo. Estos últimos están condicionados por criterios de brillo y textura de las imágenes microscópicas estudiadas. Así, proponemos en el contexto de esta tesis un algoritmo de segmentación autoadaptable al contexto de la imagen que utilizamos en esta tesis. La originalidad de este algoritmo es que tiene capacidades de genericidad, flexibilidad y adaptabilidad a la variabilidad de contextos.

2.2 Creación de DS1 (el primer Base de Datos) a partir de subimágenes extraídas de imágenes microscópicas

En base a los problemas detallados más adelante, concluimos que, si hacemos el procesamiento de la imagen microscópica completa, muchas de las células de Nosema desaparecerán o serán consideradas como ruido en la imagen, y también objetos que tengan una forma cercana a la de Nosema. serán consideradas como células de Nosema. Es por eso que decidimos estudiar primero las características de estas células recortando la imagen de la célula de la imagen digital (ver figura 7.1).

Identification Of Nosema Cells Using Microscopic Images

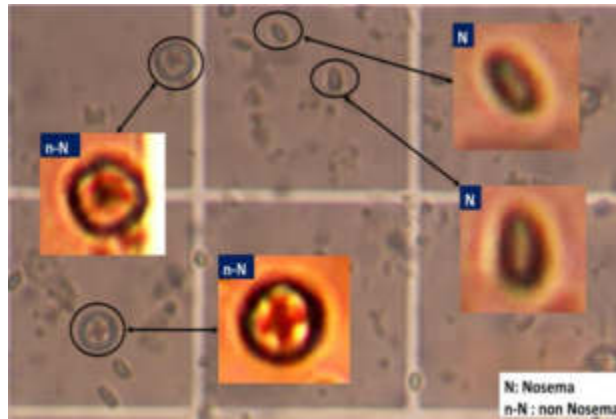


Figura 7.1 Ejemplo de extracción de conjunto de datos para células de Nosema y otros objetos que existen en las imágenes microscópicas

Se selecciona la región de interés (ROI), por lo que para ello se ha desarrollado un sencillo algoritmo semiautomático para capturar la imagen de la celda, indicando y recortando nuestro ROI, y luego, se preprocesa automáticamente para detectar la forma de la célula. Dado que nuestras imágenes están cargadas por muchos objetos y se puede decir que son muy borrosas y ruidosas, seleccionamos la celda de Nosema, recortando una imagen de Nosema que está claramente aislada de otros objetos y asegurándonos de que solo se extraiga la fuente potencial de información para el estudiar, preferiblemente; un área, lo más pequeña posible, donde haya una celda aislada (ver Figura 7.2). Por lo tanto, cada subimagen de células de Nosema contiene solo una celda clara. El mismo trabajo se aplica a los objetos que no se consideran células de Nosema. Sobre la base de los pasos descritos anteriormente, se creó una base de datos DS1 que contiene un total de 2000 imágenes de muestra. DS1 consta de 1000 muestras de imágenes de células de Nosema y 1000 imágenes, que no se consideran células de Nosema (es decir, cualquier otro objeto existente en imágenes microscópicas). La Figura A.2 a continuación describe el proceso de construcción de DS1.

Identification Of Nosema Cells Using Microscopic Images

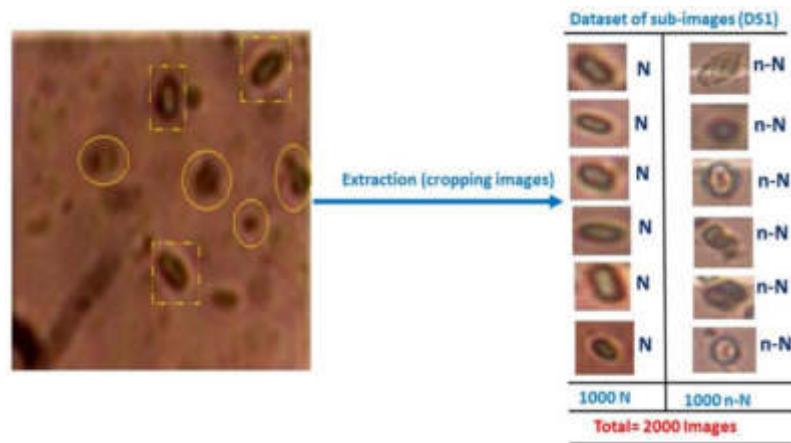


Figura 7.2 Construcción de la base de datos de imágenes: contiene tanto los tipos de objetos Nosema (N) como el nombre Nosema (n-N)

2.3 Segmentación automática y extracción de características: Creación de un conjunto de datos DS2 de características extraídas:

Es necesaria una etapa de preprocesamiento antes de la extracción de las características. El punto inicial es una imagen RGB. El primer paso es convertir la imagen de RGB a una imagen en escala de grises. El segundo paso consiste en la binarización de la imagen mediante la creación de umbrales mediante el método Otsu. En el tercer paso, la operación de relleno por inundación se usó en píxeles de fondo de la imagen binaria de entrada para llenar el agujero del objeto desde sus ubicaciones específicas y luego ignorar todos los objetos más pequeños existentes en la imagen del objeto deseado. Como paso final, el perímetro del objeto se mejora mediante el método de dilatación. Entonces, la forma deseada del objeto se obtiene calculando la diferencia entre las dos imágenes, antes y después de la mejora del perímetro. El resultado del paso final es una imagen de forma, que se extrajo de la subimagen del conjunto de datos (ver Figura 7.3).

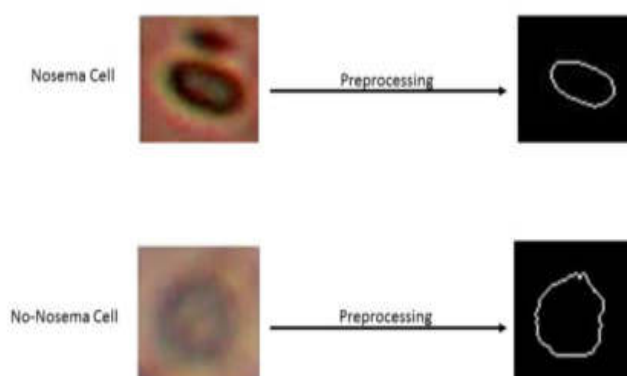


Figura 7.3. Resultados de la forma de dos ejemplos antes y después del preprocesamiento. La primera muestra es Nosema y la segunda es un objeto no Nosema.

De la imagen de la forma, se extrajeron en total 9 características. Describen la estructura de la celda de Nosema y constan de 6 características geométricas y 3 estadísticas. Además, a partir de las subimágenes extraídas, se calcularon 6 características de textura y 4 características de color de matrices de co-ocurrencia de nivel de gris (GLCM).

Una vez extraídas las características de los diferentes objetos, se genera el conjunto de datos de características: consta de 19 características para 2000 objetos, es decir, un valor de 38000 dividido en partes iguales entre dos tipos de objetos: uno para las características calculadas de los objetos de interés. (Células de Nosema), y el otro para otro objeto existente en las imágenes microscópicas. Esta parte del trabajo fue significativamente exigente desde el punto de vista informático, ya que la extracción de 2000 subimágenes, así como el cálculo de 19 funciones para cada imagen, costó muchos días de cálculos, utilizando una CPU, en particular, PcCom Basic Elite Pro Intel Core i7-9700. / 8GB / 240SSD.

Capítulo III: Reconocimiento de Nosema

3.1 Introducción

En este capítulo, explicaremos nuestro enfoque para identificar las células de Nosema o diferenciarlas de los objetos que existen con ellas en la misma imagen microscópica. Aparece una noción de clase de celda, que intuitivamente, requiere saber si los métodos clásicos de clasificación de formas pueden caracterizar las celdas, y dar un buen resultado, luego compararlas con los métodos más recientes de clasificación de objetos. Aquí, nos enfocamos en el uso de herramientas de aprendizaje ANN y SVM como métodos de clasificación clásicos, herramientas de aprendizaje profundo de CNN y herramientas de transferencia de conocimiento como AlexNet, VGG-16 y VGG-19 como métodos modernos en la clasificación de objetos. Para el primer tipo de métodos utilizaremos los vectores de características extraídos de los objetos estudiados y para el segundo tipo de métodos utilizaremos las imágenes RGB de los objetos estudiados. La elección de las arquitecturas Transfer Learning se basó en una prueba de muchos tipos

de arquitecturas y las que dieron los mejores resultados fueron elegidas para ser estudiadas en esta tesis.

En este capítulo hemos señalado que el reconocimiento de una celda se puede realizar por varios métodos, pero, a modo de comparación, mostraremos cuál es el método de identificación más útil.

3.2 Estrategia 1: Reconocimiento de esporas de Nosema con procesamiento de imágenes y aprendizaje automático

En este capítulo, se utilizaron redes neuronales para la detección automática de enfermedades Nosema en abejas. Las redes neuronales demostraron su calidad en muchas aplicaciones del mundo real, así como para tareas de clasificación. Por lo general, una red neuronal se compone de dos partes que constituyen el conjunto de funcionalidades de aprendizaje utilizadas para entrenar el modelo NN, mientras que un conjunto de funciones de prueba se utiliza para verificar la corrección del modelo NN entrenado. Se debe configurar el diseño de red adecuado, incluido el tipo de red, el método de aprendizaje y con una o dos capas ocultas. En la fase de aprendizaje, los pesos de conexión siempre se actualizaron hasta que alcanzaron el número de iteración definido o el error aceptable. Por lo tanto, la capacidad del modelo ANN para responder con precisión se aseguró utilizando el criterio del error cuadrático medio (MSE) para enfatizar la validez del modelo entre la entrada y la salida de la red. Además, la red calcula las salidas y ajusta automáticamente los pesos para reducir errores y reconocer los objetos.

Para el experimento, el conjunto de datos se dividió en una parte de aprendizaje del modelo y otra parte de prueba y validación. Durante el enfoque propuesto, se llevaron a cabo dos tipos de experimentos: en el primero, el modelo se probó con solo las 15 características geométricas, estadísticas y de textura sin contar las características de color amarillo calculadas con el GLCM. El segundo experimento se implementó concatenando las 19 características. Además, estos dos experimentos se realizaron para demostrar la fuerte presencia de color amarillo en la célula de Nosema. Los experimentos se realizaron aplicando una precisión diferente de la división de datos entre los datos para el entrenamiento y los datos para las pruebas. El experimento se

realizó con varias arquitecturas de redes neuronales diferentes; en particular, se ha experimentado con el número de neuronas en la capa oculta. Cada prueba se repitió al menos 30 veces para obtener el valor óptimo de precisión en el reconocimiento del éxito. En primer lugar, el programa se probó con una cantidad de neuronas igual a la cantidad de características de entrada extraídas de las imágenes (15 o 19) en las que se agrega el peso de forma aleatoria, y después de eso, se aumentó la cantidad de neuronas en el oculto. capa por 50 en cada nuevo experimento.

3.3 Estrategia 2: Reconocimiento de esporas de Nosema mediante enfoques de aprendizaje profundo

Experimento 1

Otro enfoque para trabajar con aprendizaje profundo es utilizar una red neuronal profunda previamente entrenada. Para el primer enfoque, la ventaja es su estructura; Se utiliza un modelo de una red neuronal profunda ya existente mediante la aplicación de algunos cambios simples. En el último caso, se utiliza un conjunto de datos limitado y el conocimiento se transfiere de este modelo a una nueva tarea. También se dice que transfiere las características aprendidas de una CNN previamente entrenada a un nuevo problema con un conjunto de datos limitado. El aprendizaje de transferencia implica formar una CNN con datos de origen etiquetados disponibles (llamado alumno de origen) y luego extraer las capas internas que representan una representación genérica de entidades de nivel medio para un alumno de CNN de destino. Se agrega una capa de adaptación al alumno de CNN de destino para corregir las diferentes distribuciones condicionales entre los dominios de origen y destino. Los experimentos se realizan sobre la clasificación de la imagen del objeto, donde la precisión media se mide como una medida de rendimiento. El primer experimento se realizó utilizando el conjunto de datos Pascal VOC 2007 como objetivo e ImageNet 2012 como fuente. El segundo experimento se realizó utilizando el base de datos Pascal VOC 2012 como objetivo de ImageNet 2012 como fuente. Las pruebas han demostrado con éxito la capacidad de transferir información de un alumno de CNN a otro. Los modelos preajustados utilizados en este trabajo son AlexNet, VGG16 y VGG19. En comparación con publicaciones anteriores encontradas en la literatura, nuestro método fue rico, variado y diferente en términos

Identification Of Nosema Cells Using Microscopic Images

de las características calculadas de la celda, los clasificadores utilizados, los conjuntos de datos adoptados y la precisión de éxito obtenida que es mayor que la encontrada en la literatura. (96,25%). Por otro lado, esto confirma el mérito de las herramientas de aprendizaje profundo en el reconocimiento de imágenes de Nosema, que se asume en la Hipótesis en la sección de introducción de esta tesis.

Experimento 2

En el segundo, nos interesamos en modelos ajustados para realizar más experimentos para el reconocimiento de Nosema. Estos experimentos utilizan un nuevo entorno de trabajo con Python 3.7.9 amd64 y una máquina equipada con un i7-9700/8GB y un procesador GPU.

El objetivo de este experimento es utilizar muchos y varios modelos de ajuste fino que implican un número cada vez mayor de épocas para mejorar la precisión de reconocimiento de Nosema tanto como sea posible. De hecho, la primera parte de los experimentos se realiza simplemente ajustando los modelos previamente entrenados y la segunda fase se realiza explotando la eficiencia del aumento de datos para aumentar la precisión del reconocimiento. En este experimento, ajustamos alrededor de 19 modelos de transferencia de aprendizaje que son: EfficientNetB0, EfficientNetB1, EfficientNetB2, EfficientNetB3, EfficientNetB4, EfficientNetB5, EfficientNetB6, EfficientNetB7, InceptionResNetV2, InceptionV3, MobileNet, MobileNetV2, ResNet50, ResNet50v2, ResNet101, ResNet152V2, VGG16, VGG19 y Xception.

La metodología aprobada es la siguiente:

1- Comenzó con el Entrenamiento de los modelos durante 50 épocas. Tenga en cuenta que la convergencia puede tardar hasta 50 épocas dependiendo de la elección de la tasa de aprendizaje. Si no se aplicaron capas de aumento de imagen, la precisión de validación solo puede alcanzar ~60%.

2- Después del entrenamiento, elimine los modelos que tengan una precisión inferior al 96,25% (que es la precisión más alta en los experimentos anteriores) y conserve los demás.

Identification Of Nosema Cells Using Microscopic Images

3- Realizar un segundo experimento entrenando los modelos conservados aprobando un número de épocas igual a 100.

4- Durante el experimento, hubo modelos que decidimos detener su entrenamiento antes de alcanzar las 100 épocas porque continúan disminuyendo sus precisiones a lo largo de 12 épocas y al mismo tiempo, no superaron el 96,25%, por lo que será inusual para continuar su formación y perder el tiempo.

5- finalmente, solo se conserva el modelo que tiene mayor ocurrencia en las 100 épocas. De hecho, cabe mencionar que todos los modelos comienzan a decrecer antes de completar las 100 épocas, por eso no hicimos otro experimento con más de 100 épocas.

Experimento 3

En este trabajo, empleamos la técnica de aumento de datos como una tarea importante para aumentar los datos de entrenamiento y mejorar la eficiencia del trabajo propuesto. Intentaremos evaluar el impacto del aumento de datos en el desarrollo de modelos de IA (inteligencia artificial) mejorando el rendimiento de los modelos de aprendizaje de transferencia en el reconocimiento de enfermedades. los datos de aumento se aplicarán al modelo que dará la mejor precisión. La transformación aplicada a las imágenes de Nosema fue de diferentes grados de rotación con un código Python particular. Rotamos las imágenes aleatoriamente 20, 30, 60 y 180 grados usando el parámetro de rango de rotación. Más tarde, el nuevo conjunto de datos de imágenes fue llamado para entrenamiento. Se aplicó una metodología de validación cruzada de 5 veces y el entrenamiento se realizó durante 100 épocas.

3.4 Resultados

Nuestro objetivo es comparar los resultados entre los enfoques tradicionales de clasificación y los enfoques más desarrollados de Transferencia de aprendizaje. Comenzamos presentando los resultados de la aplicación de ANN y SVM en base a las características calculadas DS1, y los resultados de la aplicación de CNN y los modelos reentrenados AlexNet, VGG16 y VGG19 basados en imágenes DS2. Luego, examinaremos y discutiremos los resultados de los métodos de clasificación aprobados

Identification Of Nosema Cells Using Microscopic Images

en esta tesis. Luego mostramos nuestra idea para nuestro artículo que se está preparando para conteos de células de Nosema en imágenes microscópicas.

Una segunda sección definirá nuestro método de segmentación celular a partir de sus antecedentes.

Resultado experimento 1

Las tablas siguientes muestran los resultados dados tras la aplicación de los clasificadores.

Tabla 7.1: Mejores resultados dados por ANN y SVM.

Número de características	Clasificador	Precisión	Observación
15 Features	ANN	79.00%	Para 1400 neuronas en la capa oculta
	SVM	81.00%	Usando el núcleo RBF
19 Features	ANN	83.20%	Para 1400 neuronas en la capa oculta
	SVM	83.50%	Usando el núcleo RBF

Tabla 7.2: Mejores resultados de clasificaciones para el clasificador optimizado AlexNet.

Experimento (datos entrenados, el resto para validación)	Precisión	Número de épocas
0.5	84.58%	6
0.6	83.98%	6
0.7	86.98%	6
0.8	85.28%	6

Tabla 7.3: Mejores resultados de clasificación para clasificadores ajustados VGG16 y VGG19

Experimentos	Épocas	Precisión	
		VGG-16	VGG-19
0.7	6	76.29%	71.95%
	6	92.50%	93.00%
08	12	94.50%	82.00%
	20	96.25%	92.32%
	25	93.00%	93.50%
0.9	6	88.00%	77.00%

Identification Of Nosema Cells Using Microscopic Images

se puede concluir que ya sea el conjunto de datos más grande o el conjunto de datos más pequeño, el nivel de aprendizaje de la red con modelos de aprendizaje por transferencia es obviamente mejor que los modelos tradicionales, especialmente las ANN se examinan en este estudio y SVM que acercó los resultados. Además, se observa una clara tasa de convergencia del modelo de transferencia VGG-16 y VGG-19 al nivel de los resultados proporcionados. Además, estos modelos de transferencia son un poco más rápidos que ANN y SVM, al menos en este caso. CNN ha demostrado su eficacia en este problema de reconocer o clasificar las células de Nosema como modelo de aprendizaje profundo. CNN era casi comparable a VGG-19. Por otro lado, hay que decir que las opciones de formación de las RNA, así como los algoritmos de aprendizaje por transferencia, marcan la diferencia en los resultados.

Frente a AlexNet, VGG-16, VGG-19 y CNN han demostrado su fuerte efectividad en este trabajo en la clasificación de patrones, celdas y objetos.

Para la parte de extracción de características, se evaluaron varias características diferentes de las subimágenes: características geométricas, estadísticas, textura y GLCM extraídas del canal amarillo. Este experimento utilizó una gran base de datos, los resultados dados tanto por la ANN como por la SVM son buenos ya que es la primera vez. La calidad de las imágenes microscópicas utilizadas en este trabajo no siempre ayudó a extraer objetos claros y nítidos. Al calcular los resultados con un número diferente de características (15 y 19), se aprobó la importancia de los datos extraídos por el GLCM en la mejora resultante.

Discusión

Además de las herramientas de procesamiento de imágenes, citamos en la bibliografía algunos trabajos recientes que utilizaron simulaciones químicas y corrientes tecnológicas para detectar enfermedades de las abejas o alteraciones dentro de las colonias de abejas. En esta sección, estamos evaluando nuestro método presentado y comparándolo con los trabajos anteriores encontrados en la literatura que solo usaban las técnicas de procesamiento de imágenes y visión por computadora para detectar, contar o clasificar las esporas de Nosema.

Resultado experimento 2

Identification Of Nosema Cells Using Microscopic Images

Las precisiones vienen dadas por una estrategia de validación cruzada de 5 veces. Este enfoque consiste en dividir aleatoriamente el conjunto de observaciones en 5 grupos, o pliegues, de aproximadamente el mismo tamaño. El primer pliegue se trata como un conjunto de validación y el método se ajusta a los 5-1 pliegues restantes. Cada resultado particular de una carpeta en particular se proporcionó en forma de un modelo de precisión, un modelo de pérdida y una matriz de confusión que muestran la precisión exacta de la carpeta. Después de eso, se calculó la precisión media para tener la precisión final del modelo ajustado. La tabla describe los resultados de 100 épocas.

Tabla 7.4: Resultados de modelos ajustados con 100 épocas

Modelos afinados	Épocas	Pesos Congelados	% De precisión media
EfficientNetB0	100	4.049.571	95.84±0.87
EfficientNetB1	90	6.575.239	96.29±0.86
EfficientNetB2	100	7.768.569	95.59±1.19
EfficientNetB3	80	42.658.176	94.89±0.66
EfficientNetB7	60	64.097.687	93.63±0.65
ResNet50	70	23.587.712	95.84±1.32
ResNet50V2	60	58.370.944	96.59±1.06
ResNet101	70	42.658.176	95.94±0.51
MobileNet	90	3.228.864	95.04±0.66
MobileNetV2	90	2.257.984	96.34±0.64
VGG16	100	14.714.688	97.64±0.75
VGG19	100	20.024.384	96.79±0.58

El modelo ajustado VGG16 ofrece la máxima precisión en el reconocimiento de Nosema. Hay que decir que hemos conseguido aumentar la precisión del reconocimiento de las células de Nosema en un 1,39 % (anteriormente era del 96,25 %). Ahora, la tercera fase de este experimento es aplicar datos de Aumento al modelo que brinda la mejor precisión de reconocimiento (VGG16) para estimar las habilidades de este último en la mejora de la predicción de los modelos ajustados.

Resultado de experimento 3

La transformación aplicada a las imágenes de Nosema fue de diferentes grados de rotación con un código Python particular. Rotamos las imágenes aleatoriamente 20, 30, 60 y 180 grados usando el parámetro de rango de rotación. Más tarde, el nuevo conjunto de datos de imágenes fue llamado para entrenamiento. Se aplicó una metodología de validación cruzada de 5 veces y el entrenamiento se realizó durante 100 épocas. VGG16 está afinado como antes.

Como resultado, el método propuesto logró una precisión media del 99,35 %, lo que muestra una mejora del 1,71 % en comparación con el VGG16 ajustado sin datos de aumento. Además, la precisión más alta proporcionada por el modelo de ajuste fino VGG16 fue del 99,70 % con el particular 2 veces usando una rotación de +30 ° de las imágenes mostrando una mejora del 3,45 % en comparación con el primer experimento realizado anteriormente.

Capítulo IV: Algoritmo automático para la identificación y conteo de Nosema

Resumen

Este capítulo adopta un enfoque nuevo y diferente. De hecho, el trabajo en este capítulo es totalmente automático. Más concretamente, para determinar el estadio de la enfermedad, las células serán identificadas dentro de la imagen microscópica principal y recogidas. Un algoritmo automático contará las células enfermas en la imagen microscópica para clasificarlas como muy suaves, leves, moderadas, semi-fuerte o fuertes. Este enfoque implementado ayuda a racionalizar el proceso de detección.

Los hallazgos del algoritmo automático Nosema coinciden con el número real de células en las imágenes microscópicas estudiadas. El conteo manual de células en imágenes microscópicas puede diferir ligeramente entre las personas, con variaciones que a menudo no superan 1 o 2 células. Por ejemplo, un individuo puede contar 42 células en la misma imagen mientras que otro puede contar 43 células. Esta diferencia menor no tiene efecto en el análisis general de la imagen. En el experimento, se ejecutó un código sobre un conjunto de imágenes microscópicas seleccionadas aleatoriamente. Ninguna de las imágenes analizadas fue categorizada incorrectamente por el algoritmo; el

Identification Of Nosema Cells Using Microscopic Images

sistema todavía detecta un número de células dentro del rango requerido del tipo de imagen de entrada, y el número dado es casi igual al número contado manualmente. Aunque persiste la posibilidad de errores de categorización, se puede decir con confianza que la tasa de error es extremadamente baja en el 0,01%. Con esta suposición, podemos afirmar que la exactitud de la identificación de Nosema de este algoritmo automatizado se espera que sea del 99,99%. Intentamos ser sinceros, y el éxito ahora tiene la mayor precisión en comparación con todas las obras anteriores. Además, el algoritmo funciona eficazmente a través de los niveles, con gran precisión, y sus predicciones se han confirmado para todos los niveles indicados. La precisión observada para el nivel de "fuerza" no es del 100%, y esto se puede atribuir a los retos asociados con la calidad de las imágenes microscópicas. La presencia de un número significativo de objetos en las imágenes, posiblemente afectando la claridad o introduciendo ruido, plantea una dificultad para el algoritmo en dar con precisión el número verdadero de células Nosema en la imagen. A pesar de este desafío, el algoritmo sigue demostrando notable precisión, indicando su eficacia en presencia de tales complejidades. Los esfuerzos en curso para abordar las preocupaciones de calidad de la imagen pueden mejorar aún más el rendimiento del algoritmo para este nivel en particular.

Capítulo V: Conclusiones

Síntesis

Como principal conclusión de esta tesis doctoral, se han logrado los objetivos inicialmente marcados y se ha hecho un algoritmo automático de reconocimiento de Nosema. La hipótesis inicialmente establecida en esta tesis se confirmó, y se implementó un algoritmo automático, y es eficaz en el logro de su propósito previsto, que es el diagnóstico de la enfermedad de Nosema. El algoritmo implementado en esta tesis difiere de los encontrados en la literatura porque se basa en una variedad de procesamiento de imágenes y herramientas de aprendizaje profundo.

El trabajo presentado en esta tesis se caracteriza por un flujo cohesivo y progresivo, conectando sin problemas del capítulo 2 al capítulo 4, asegurando un desarrollo lógico e integrado de ideas y metodologías:

-Esta tesis ha propuesto un enfoque de segmentación para imágenes microscópicas de la enfermedad de Nosema. Este método de segmentación proporciona un conjunto de

Identification Of Nosema Cells Using Microscopic Images

herramientas operativas que permite extraer de forma automática y robusta las características más útiles de la célula Nosema.

-Para el cálculo de las características, se han adaptado morfologías matemáticas y binarias, por lo que este método agrupa varios tipos de parámetros que pueden caracterizar un objeto en una imagen microscópica; estos parámetros se refieren a su forma, color y textura como se mostró en el capítulo 2.

-Para el reconocimiento de las células Nosema de los otros objetos en la imagen microscópica, se aprobaron dos vías. El primer método es identificarlos utilizando sus características calculadas basadas en los sistemas de clasificación ANN y SVM. La segunda forma es clasificar las imágenes entre Nosema y no-Nosema, basándose en herramientas de aprendizaje profundo (CNN). En el Capítulo 3, existen varios modelos de aprendizaje de transferencia y datos de ampliación que sugieren que el aprendizaje en transferencia es más exitoso en las tareas de reconocimiento e identificación. La combinación del modelo de aprendizaje de transferencia VGG16 y la ampliación de datos mejora la precisión de detección de células de enfermedad hasta el 99,70%.

-Finalmente, en el capítulo 4, se implementó el algoritmo totalmente automático para la detección y el conteo de Nosema desde el fondo de la imagen alcanzando una exactitud del 99,99% en la contabilidad y el diagnóstico de los Nosema. El algoritmo automático muestra un rendimiento encomiable en la tarea de diagnóstico, demostrando una alta precisión en varios niveles de severidad: Mild, Moderate, Semi-strong, y Strong. El algoritmo consigue constantemente tasas de precisión del 100% para los niveles 'Mild', 'Moderate' y 'Semi-strong', mostrando su robustez en la clasificación precisa de instancias dentro de estas categorías. Aunque la precisión para el nivel de "fuerza" está ligeramente por debajo del 100%, atribuido a los desafíos relacionados con la calidad de las imágenes microscópicas y la abundancia de objetos, la exactitud del algoritmo sigue siendo notable.

Estos hallazgos sugieren que el algoritmo automático es una herramienta valiosa para la tarea de diagnóstico, con posibles aplicaciones en la clasificación precisa de diferentes niveles de gravedad.

Trabajos futuros

Identification Of Nosema Cells Using Microscopic Images

Exploración de métodos alternativos para la detección e identificación de las células de la enfermedad. Un enfoque potencial podría implicar la eliminación de la red de conteo de las imágenes microscópicas. Este ajuste podría conducir a una determinación más precisa del número de células detectadas. La caracterización de la red de conteo en las imágenes se realizará basándose en su naturaleza de frecuencia y utilizando la filtración en el FFT (Fast Fourier Transfer) (Cooley & Tukey, 1965). La preparación de la imagen para el conteo de células (preprocesamiento), se obtiene borrando la rejilla manteniendo intactas las células en la imagen. Este método se basa en la sustitución de la firma de la red en el FFT. Los objetivos para lograr futuras obras serán los siguientes:

- La ausencia de intervención humana para el procesamiento de imágenes. El método propuesto para la caracterización y el borrado de la red tiene la ventaja de no requerir ningún ajuste manual. Esta ventaja se obtiene buscando la firma de la rejilla en el espacio de Fourier: en este espacio, esta firma tiene una anchura constante de un píxel independientemente de la imagen.